2001

Shell Model Description of Normal Parity Bands in Heavy Deformed Nuclei.

Gabriela Popa
Louisiana State University and Agricultural & Mechanical College

INFORMATION TO USERS

This manuscript has been reproduced from the microfilm master. UMI films the text directly from the original or copy submitted. Thus, some thesis and dissertation copies are in typewriter face, while others may be from any type of computer printer.

The quality of this reproduction is dependent upon the quality of the copy submitted. Broken or indistinct print, colored or poor quality illustrations and photographs, print bleedthrough, substandard margins, and improper alignment can adversely affect reproduction.

In the unlikely event that the author did not send UMI a complete manuscript and there are missing pages, these will be noted. Also, if unauthorized copyright material had to be removed, a note will indicate the deletion.

Oversize materials (e.g., maps, drawings, charts) are reproduced by sectioning the original, beginning at the upper left-hand corner and continuing from left to right in equal sections with small overlaps.

Photographs included in the original manuscript have been reproduced xerographically in this copy. Higher quality 6" x 9" black and white photographic prints are available for any photographs or illustrations appearing in this copy for an additional charge. Contact UMI directly to order.

ProQuest Information and Learning
300 North Zeeb Road, Ann Arbor, MI 48106-1346 USA
800-521-0600

SHELL MODEL DESCRIPTION OF NORMAL PARITY BANDS IN HEAVY DEFORMED NUCLEI

A Dissertation

Submitted to the Graduate Faculty of the
Louisiana State University and
Agricultural and Mechanical College
in partial fulfillment of the
requirements for the degree of
Doctor of Philosophy

in

The Department of Physics and Astronomy

by
Gabriela Popa
Diploma in Physics, Universitatea din Bucureşti, România, 1993
May 2001

To my mother Stefana, my father Marin,

and my husband Aurel

Acknowledgments

At the end of my Ph.D. study program, my thought goes to the people who have encouraged and supported me in my career in Physics. First of all I wish to express my sincere gratitude to my advisor Professor Jerry P. Draayer, whom I met in Predeal, Romania at the"Frontier Topics in Nuclear Physics" Summer School, where he made me an offer to work on my Ph. D. in his research group at Louisiana State University. Not only he led me with enthusiasm and patience toward the completion of this dissertation, but he also gave me the opportunity to learn and work in a different culture and environment, with people from an international community. I have been also given the chance to participate and present my work in many workshops and conferences in the United States and abroad. His comments and the discussions with him strengthened and sharpened my knowledge in nuclear physics. I deeply appreciate for his time and energy that were never exhausted. I also want to thank him and his wife Lois Draayer for their hospitality. The valuable time spent at their house will never be forgotten.

My thanks go also to Professor Jorge G. Hirsch from Instituto de Ciencias Nucleares, Universidad Nacional Autónoma de México, with whom I have worked in the United States and Mexico City, and collaborated on many parts of this dissertation. I also want to thank him and his wife for their warm hospitality.

I would also like to thank Professors R. F. O'Connell, R. Haymaker, E. Zgainer, and Professor L. Escobar from the Department of Experimental Statistics, for their comments and suggestions, and for serving on my dissertation committee. I wish to thank Professor C. Johnson for valuable discussions and for providing a special series of lectures in writing articles in physics, for the graduate students. My thanks go also to the Professors in the Department of Physics with whom I have taken classes, for their dedication and enthusiasm in teaching the Physics subjects. I wish to thank to Mrs. Arnell Jackson, Beverly Rodriguez, Ophelia Dudley, Lanelle Chenevert, and Hortensia Valdes,

not only for their support with all the paper work, administrative, and technical help provided, but also for their friendly and kindly attitude.

I wish to acknowledge financial support from the Department of Physics and Astronomy, the U.S. National Science Foundation, the Louisiana Board of Regents Support Fund, the Conacyt (Mexico) Fund, and the Charles E. Coates Memorial Fund.

Thanks go also to my recent and former colleagues and friends in the Nuclear Theory group and in the Department of Physics and Astronomy who contributed to a good working environment, Dr. Andrei Ludu, Dr. Dirk Troltenier, Dr. Andrey Blochin, Vesselin Gueorguiev, Guergana Stoitcheva, Dr. Ulrich Eichmann, Ionel Stetcu, and Alice Acatrinei. Especially I would like to thank my former office mates Dr. Jutta Escher and Dr. Thomas Beuschel who took me in their homes when I first had come to the United States, offered me their friendship from the very first day we met, and helped with valuable discussions during the years. I also thank my office mates Kristina Sviratcheva and Kalin Drumev for being very understanding and supportive.

To be able to write my dissertation in Physics, I had to go a long way. I wish to thank the people who helped me choose and maintain my path in Physics. I wish to express my thanks to my teachers from elementary school for making me feel special and building my personality. I thank them for stimulating my curiosity and imagination. Special thank goes to my high-school physics-teacher Sorin Badea for special training and extra time he offered me and my classmates who wanted to excel in physics. I thank him for determining me to embrace a career as a physicist.

My thanks go also to the Professors at the Department of Physics, University of Bucharest for inciting my curiosity and making me eager to go further and learn more in the field of Physics. I especially want to thank my former advisor for my Diploma, Dr. Alexandru Jipa and Dr. Ion Silisteanu.

I also enjoyed and benefited from my experience at the Institute of Physics and Nuclear Engineering, Bucharest-Magurele, where I have interacted with many wonderful physicists. I would like to thank Professor Aureliu Sandulescu for his efforts to promoting the work of Romanian physicists,

and especially young students and physicists who choose nuclear physics as their field of study and research. I also want to thank Professors Ion Popescu and Theodor Badica, and Dr. Agata Olariu with whom I worked at the institute.

I am extremely grateful to my parents, Stefana and Marin, who made their top priority my education. They not only respected my decision to become a physicist, but also supported and encouraged me during these years. They often placed my commitment to my study and my goals before their own needs. My words are not enough to express my appreciation, and the least I can hope is that I have been able to live up to their expectations.

Finally and by no means least I would like to thank my friends outside the Nuclear Theory group, for substituting my family that I have missed in the United States. Especially I thank my husband Aurel for being my family and my best friend. I also thank him not only for accepting my decision to pursue my Ph. D. in the United States but also for accompanying me here.

Table of Contents

List of Tables

List of Figures

Abstract

The low-energy spectra and electromagnetic transition strengths in ^{160,162,164}Dy, ^{156,158,160}Gd, and ^{168}Er are described in the framework of the pseudo-SU(3) model. The Hamiltonian includes spherical single-particle energies, the quadrupole-quadrupole interaction, and proton and neutron pairing terms with the strengths of these interaction fixed from systematics. The strengths of an additional four rotor-like terms that are included in the Hamiltonian, which do not mix SU(3) representations and induce only small changes in the spectra, were allowed to vary and a consistent set of these parameters was found. Proton and neutron degrees of freedom are considered explicitly by building the basis states as linear combinations of SU(3) states that are the direct product of SU(3) proton and neutron states with pseudo-spin zero.

The results show that the proton and neutron single particle energies introduce strong mixing of the $SU(3)$ representations, but nevertheless the dominance of the quadrupole-quadrupole two-body interaction ensures that the $SU(3)$ band-structure is maintained. By and large, the excitation energy of the excited 0^+ states is determined by the strength of the single-particle, quadrupole-quadrupole, pairing and C_3 interactions. The interaction strength of the J^2 term in the Hamiltonian is responsible for fine tuning of the effective moments of inertia. The K_J interaction fixes the K-bands relative to the ground-state.

The theoretical normal parity states of the low-energy spectra - states in the ground state, first excited $K^\pi = 2^+$, and $K^\pi = 0^+$ bands - were all found to lie very close to their experimental counterparts. The results analyzed extend beyond quantities used in the fitting procedure, including intra- and inter-band $B(E2)$ strengths, the $M1$ strength distribution of the ground state, and band head energies of the first $K^\pi = 1^+$ and $K^\pi = 4^+$ bands. In all cases the summed strength of the $M1$ distribution is in good agreement with the experimental numbers. The results also show that by adding one- and two-body pairing interactions to the Hamiltonian the experimentally observed fragmentation of the $M1$ strength can be reproduced.

Chapter 1. Introduction

The discovery of the neutron marked the beginning of the modern nuclear physics in 1932 [25]. Shortly thereafter it was suggested by Heisenberg [59, 60, 61] and independently by Ivanenko [63], that the atomic nuclei are built from protons and neutrons. This led to the development of microscopic models that take into account individual nucleon degrees of freedom. The simplest such model is the spherical shell model in which nucleons are bound through an average central potential that produces shell structure and, most notably, major shell closings analogous to noble gases in atomic physics. Away from shell closures the valence nucleons reside in open shells and the residual interaction can scatter the nucleons among the available single-particle states.

The liquid drop model is a complementary theory that focuses on collective degrees of freedom within the nucleus. The most notable early success is its use in describing nuclear fission [99]. It also underpins the so-called collective model that considers the dominate characteristic feature of nuclei, though made up of individual nucleons, to be their deformation [20, 21].

A full microscopic theory is tractable for p and ds shell nuclei, and very successful calculations have been carried out using so-called "realistic" effective interactions. If the valence nucleons reside in the higher major shells, the dimensionality of the model space is enormous and for shell-model calculations to be feasible one must devise a basis truncation scheme.

The $SU(3)$ model is a fully microscopic theory, but it incorporates collective degrees of freedom through nucleon degrees of freedom [42]. The model also provides an elegant truncation scheme for the configuration space using group theoretical methods.

Some nuclei have a spherical shape. From macroscopic observables, however, it was found out that many nuclei prefer deformed shapes. Examples of light deformed nuclei are ^{20}Ne and ^{24}Mg. In general, a deformed nucleus has a valence shell that is $\approx 30\%$ occupied or $\approx 30\%$ unfilled. The nuclei of interest to us are the Lanthanide nuclei ^{156,158,160}Gd, ^{160,162,164}Dy, and ^{168}Er.

Successful applications of the $SU(3)$ shell model [44] to light deformed nuclei have led physicists to explore similar concepts in heavy deformed systems. One of the first challenges encountered when

developing a shell-model theory for heavy nuclei is that the splitting of the single-particle levels generated by the spin-orbit interaction is comparable in magnitude to the major shell separation of the harmonic oscillator and thus renders the usual $SU(3)$ symmetry useless, and with it the logic underlying an $SU(3)$-based truncation scheme that proved to be so valuable in light deformed nuclear systems. An outline of the $SU(3)$ model is given in Chapter 2.

In heavy deformed nuclei another symmetry appears as a result of the large spin-orbit splitting; namely, the so-called pseudo-$SU(3)$ scheme which can be appreciated most easily by considering the near degeneracy of the orbital pairs $[(l-2)_{j=(l-2)+1/2}, l_{j=l-1/2}]$ which together define a pseudo-shell with one quantum less than the original (parent) configuration $\tilde{\eta} = \eta - 1$, where η is the principal quantum number of the parent shell [57, 3, 94]. A second challenge that is encountered in developing a shell-model theory for heavy nuclei is the dimensionality of the model space which increases very sharply as one moves to higher shells. This growth in the dimensionality of the model space can only be managed by truncating the model space to a small, carefully selected subset of the full space. Since in light deformed nuclei the quadrupole-quadrupole interaction is dominant, so the ground state can be represented by a few irreducible representations (irreps) of $SU(3)$ [1, 95, 106, 108], it is natural to assume one can similarly truncate the model space in heavy nuclei to those representations, in this case of pseudo-$SU(3)$, that correspond to the largest (pseudo) intrinsic deformation. Indeed, most calculations carried out to date have truncated the space to a single, or at most 2 or 3 representations with a very simple mechanism for generating the splitting and, in the latter case, mixing of irreps.

The development of a computer code (Bahri and Draayer) that is able to calculate reduced matrix elements for any type of physical operator between different $SU(3)$ irreps within any shell [7, 8] has made it possible to include realistic $SU(3)$ symmetry breaking terms, like the pairing interaction, in $SU(3)$-model Hamiltonians. Indeed, recent results using this code show that the pairing interaction is closely tied to the development of triaxiality in strongly deformed systems [104, 9]. Furthermore, complete model-space calculations in the *pf*-shell [108, 113] show that a very good description of the low-energy spectra can be obtained when the Hilbert space is truncated, following the same logic

as used in the *sd*-shell, namely, a dominance of the quadrupole-quadrupole interaction. These same calculations also showed that the pairing interaction is critical for a correct description of moments of inertia.

As a result of these developments, a very powerful shell-model theory for the description of normal parity states in heavy deformed nuclei has emerged. For example, the low-energy spectra of Gd and Dy isotopes, their $B(E2)$ and $B(M1)$ transition strengths, including both the scissors and twist modes [98] and their fragmentation, have been successfully described using a realistic Hamiltonian [15, 16]. An overview of the pseudo-$SU(3)$ symmetry and pseudo-$SU(3)$ model is presented in the third chapter.

Previous studies have focussed on a Hamiltonian that is built from $SU(3)$-generators (including an operator K_J^2 that produces K-band splitting) plus residual interactions [15, 108, 16]. This Hamiltonian

$$\begin{aligned} H &= H_{SU(3)} + H_{int} \\ &= -(a_2 + a_{sym})C_2 + a_3 C_3 + bK_J^2 + cJ^2 \\ &+ D_\pi \sum_{i_\pi} l_{i_\pi}^2 + D_\nu \sum_{i_\nu} l_{i_\nu}^2 - G_\pi H_P^\pi - G_\nu H_P^\nu \end{aligned} \tag{1.1}$$

was very successful in describing low-energy structure of heavy deformed nuclei. Furthermore, the model was successful in explaining the scissors mode and served to introduced a new oscillation-mode, called twist mode [98]. In order to describe the fragmentation in the $M1$ strength distribution, a residual interaction was included to generate configuration mixing. In the pure $SU(3)$ limit of the theory the model predicts at most four $M1$ transitions from the ground state 0^+ of even-even nuclei, while the experimental situations show that there may be more such transitions. By introducing proton and neutron single-particle energies and pairing interactions as residual terms in the Hamiltonian, and fitting their interaction strengths to reproduce the low-energy spectra, a good

reproduction of the fragmentation in the $M1$ distribution was obtained [15, 16]. Unfortunately, this procedure yielded an apparent lack of consistency in choices for Hamiltonian parameters.

In the present work this lack of consistency in the choice of parameters is removed by reconsidering the structure of the Hamiltonian and by studying the effect of some interactions in the presence of the others.

$$\begin{aligned} H &= H^{\pi}_{sp} + H^{\nu}_{sp} - \frac{1}{2}\chi Q\cdot Q - G_{\pi}H^{\pi}_{P} - G_{\nu}H^{\nu}_{P} \\ &+ aJ^2 + bK^2_J + a_3C_3 + a_{sym}C_2. \end{aligned} \tag{1.2}$$

The main idea in this study is to fix the strength of the proton ($\sigma = \pi$) and neutron ($\sigma = \nu$) single-particle energies (H^{σ}_{sp}), quadrupole-quadrupole ($Q\cdot Q$), and pairing interactions (H^{σ}_{P}) and to consider the other parameters only as fine tuning. This idea is supported by the observation that the correct band structure is already formed by considering only the first five terms mentioned above. This is a wonderful result considering that only $Q\cdot Q$ is part of the $SU(3)$ model and single-particle energies and pairing interactions are associated with destroying the $SU(3)$ symmetry. It was found out that considering single-particle energies with Nilsson parameters [96] in a $Q\cdot Q$ Hamiltonian does not destroy the $SU(3)$ structure. It does introduce a strong mixing but the $SU(3)$ band-structure is maintained.

The strength of the single-particle interaction together with the strength of the C_3 interaction determines the excitation energy of the excited 0^+ states. Hence, the interaction strength of C_3 is varied to fit the energies of the 0^+ states.

For the other four rotor-like terms, which do not mix $SU(3)$ representations and induce only small changes in the spectra, a consistent set of parameters is given. The interaction strength of the J^2 term in the Hamiltonian is responsible for fine tuning of the effective moments of inertia. The K_J interaction fixes the K bands relative to the ground state.

In this study, the theoretical normal parity states of the low-energy spectra were found to be in excellent agreement with experimental data. States in the ground-state, first excited $K = 2$, and first excited $K = 0$ bands were all found to lie very close to their experimental counterparts.

In the ^{156,158,160}Gd nuclei, the first and second excited 0^+ states were fit with the single-particle interaction together with the strength of the C_3 interaction while in the ^{160,162,164}Dy nuclei and ^{168}Er nucleus only the first excited 0^+ state was fit by the strength of the C_3 interaction. In the latter case, a second excited $K^\pi = 0^+$ band was identified at approximately $0.5MeV$ above its experimental counterpart. Two other bands, $K^\pi = 1^+$ and $K^\pi = 4^+$, were also identified for each of these nuclei.

The two sets of parameters obtained in the first case for the ^{156,158,160}Gd nuclei, and in the second case for the ^{160,162,164}Dy nuclei and ^{168}Er nucleus, are consistent with one another and with those used in a description of the odd-mass nuclei [108]. The free parameters a, b, a_{sym}, and a_3 vary smoothly from one nucleus to another. The parameters are discussed in Sections 4.2.1, 4.3.1, and 4.4.1.

The model predicts new states in the $K = 2$ band, in the two excited $K = 0$ bands, as well as in the $K = 1$ and $K = 4$ bands, in the studied Dy isotopes. These states are described in detail in Chapter 4, in the sections 4.3.2 and 4.4.2. Without further fitting the $B(E2)$ transition probabilities are calculated and found in good agreement with the experimental numbers. Furthermore, the calculated $M1$ distribution strengths reproduce reasonably well the experimental ones.

The final chapter summarizes the results and gives new possible extensions of the theory. Basic descriptions of some concepts used in the text are given in the appendix.

Chapter 2. The $SU(3)$ Model

2.1 Introduction

In the late fifties Elliott developed a theory that can be used to describe collective phenomena in nuclei in terms of the underlying many-particle fermionic substructure [42, 43, 45, 47]. The model takes advantage of shell-model principles and makes use of the associated $SU(3)$ symmetry group for a classification of the many-particle states.

In the atomic case a shell structure results from the solution of the Schrödinger equation for a group of non-interacting particles in a central potential. In contrast with the atomic case, there is no obvious center of force in the nucleus. From scattering experiments it is known that the nuclear interaction is comprised of two main parts. At short distances when $r \leq 0.4fm$ there is an infinitely repulsive core. On the other hand, the potential is attractive for distances of $0.4fm < r \leq 1.3fm$.

It is assumed that the attractive nucleon-nucleon interactions can be replaced by an average potential. The actual form of the potential should be determined from self-consistent calculations, but since this is a rather difficult task, one uses phenomenological potentials instead. Various potentials have been used to reproduce the magic numbers. A Hamiltonian which is frequently used in shell-model calculations is comprised of a harmonic oscillator (HO) plus correction terms:

$$H_{shell} = H_{HO} + V_{ll}(r)\mathbf{l}\cdot\mathbf{l} + V_{ls}\mathbf{l}\cdot\mathbf{s}, \tag{2.1}$$

where $\mathbf{l}$ denotes the single-particle orbital angular momentum and $\mathbf{s}$ the corresponding intrinsic spin. The $\mathbf{l}\cdot\mathbf{l}$ term is introduced to make the potential similar to the more realistic square-well potential. The spin-orbit coupling is crucial to reproduce the magic numbers.

Group theoretical methods allow for a mathematically elegant treatment of complex physical systems that have specific symmetry properties. If the system remains unchanged under the full set of transformations that generate the symmetry, the symmetry is called an *exact symmetry*. A well-known example of an exact symmetry is the use of the group SO(3) for rotationally invariant

systems. This symmetry allows for the classification of eigenstates with angular momentum quantum numbers and the use of powerful group theoretical tools like coupling coefficients and the Wigner-Eckart theorem for the evaluation of matrix elements [110].

But even in a more general setting where this strong requirement can not be met, the symmetry concept can still be useful. A second symmetry type is a *dynamical symmetry*. In this case the system is not necessarily left invariant under the symmetry operations, but eigenstates can still be associated with an irreducible representation of the group.

In nuclear physics group theoretical methods have evolved as an important tool because of the complex many-particle nature of the nucleus. An important example is the Interacting Boson model (IBM) which in its earliest version assumes that the nucleus consists of bosonic proton and neutron pairs that are coupled to spin zero and angular momentum zero or two [4, 5]. The group corresponding to this system is U(6).

In the nuclear shell model, where the three-dimensional isotropic harmonic oscillator is used as an approximation for the nuclear mean field, $SU(3)$, which is the symmetry group of the harmonic oscillator, emerges as an important symmetry. $SU(3)$ becomes a *dynamical symmetry* if a quadrupole-quadrupole deformation term is added to the mean field. Due to the dominance of the quadrupole-quadrupole interaction in the mid-shell region, the $SU(3)$ symmetry remains useful as an *approximate symmetry* even if small $SU(3)$ symmetry breaking single-particle or pairing terms are added to the nuclear Hamiltonian.

2.2 $SU(3)$ Model Space

The $SU(3)$ model takes advantage of the fact that the single-particle levels are grouped in shells. The shells are determined by the harmonic oscillator potential. Since the η-th harmonic oscillator shell is $\Omega = (\eta + 1)(\eta + 2)/2$ fold degenerate, it will hold up to 2Ω identical fermions. Once such a major shell is occupied by the maximum possible number of particles, it is considered to be closed. A closed shell is treated as part of the core which is presumed to be spherical and inert so it does not affect the single-particle motion.

In order to determine how the valence particles are distributed among the different orbitals of the valence space one can consider the energy-level scheme as obtained, for example from the Nilsson model [86]. The Nilsson approach, which has been succesful in reproducing a variety of features of deformed nuclei, gives a reasonable accurate picture of the single-particle level ordering as a function of deformation. For a given deformation parameter, the most probable configuration is obtained by filling each energy level, starting at the bottom of the shell and moving upward. It turns out that a rough estimate for the deformation suffices to obtain reasonable particle distributions.

2.2.1 $SU(3)$ Classification

The invariance properties with respect to certain symmetry transformations may be employed to classify basis states for the physical system under investigation. A group that is of special interest in nuclear physics is the symmetry group of the harmonic oscillator. This special symmetry is reflected in the energy spectrum where within a given irreducible representation (irrep) not only do all states with fixed angular momentum have the same energy, which results from the rotational invariance of the Hamiltonian, but all the states within an irrep are degenerate regardless of the L value. The generators of $SU(3)$ are the three components of the angular momentum operator

$$L_\mu = \sum_s l_{s\mu}, \ \mu = -1, 0, 1 \tag{2.2}$$

and the five components of the symmetrized (algebraic) quadrupole operator,

$$Q^a_\mu = \sum_s q^a_{s\mu} = \sqrt{\frac{4\pi}{5}} \sum_s \left(\frac{r_s^2}{b^2} Y_{2\mu}(\hat{r}_s) + b^2 p_s^2 Y_{2\mu}(\hat{p}_s) \right), \ \mu = -2, -1, 0, 1, 2 \tag{2.3}$$

where the s sums run over all particles in the valence shell and $b = \sqrt{\hbar/m\omega}$ is the oscillator length.

Elliott was the first to realize the group theoretical as well as practical implications of introducing the algebraic quadrupole operator in place of the usual "collective" quadruple operator

$$Q^c_\mu = \sum_s q^c_{s\mu} = \sqrt{\frac{4\pi}{5}} \sum_s \frac{r_s^2}{b^2} Y_{2\mu}(\hat{r}_s). \tag{2.4}$$

Within a major oscillator shell the matrix elements of Q^c and Q^a are identical, however Q^c couples states belonging to the η-th shell with those of the η'-th shell with $\eta' = \eta \pm 2$, whereas the matrix elements of Q^a between states belonging to different shells vanish.

The well-known rotational group $SO(3)$, generated by the L_μ, $(\mu = x, y, z)$, is an obvious subgroup of SU(3). The reduction $U(\Omega) \supset SU(3) \supset SO(3)$ yields quantum labels (λ, μ) and L with multiplicities α and κ, respectively. The quantum labels (λ, μ) are related to the number of quanta along the three Cartesian axes. Since the total number of quanta is conserved, the $SU(3)$ irreps [79] only depend on the relative differences in the number of quanta along the three axes. It follows from this that only two quantum numbers are required to label the $SU(3)$ irreps. These two labels can be tied to the so-called highest weight state that is characterized by a maximum number of quanta along the z-axis and the maximum of the remainder along the x-axis as:

$$\lambda = n_z - n_x \tag{2.5}$$

$$\mu = n_x - n_y \tag{2.6}$$

For a single particle in the η-th shell the $SU(3)$ irrep is thus given by $(\lambda, \mu) = (\eta, 0)$. Multiplicity labels α and κ are needed to distinguish between multiple occurrences of (λ, μ) in a given spatial symmtery, $[f]$ symmetry and multiple angular momentum, L values in a given (λ, μ) irrep, as it will be seen in the following subsections.

2.2.2 The $SU(3) \supset SO(3)$ Group Chain

A representation of the $SU(3)$ generators in terms of the three components of the angular momentum and other operators makes it clear that $SO(3)$ is a subgroup of $SU(3)$. A classification scheme for harmonic oscillation states is thus given by the group chain

$$SU(3) \supset SO(3) \supset SO(2)\,, \tag{2.7}$$

where $SO(2)$ is the group of rotations about one axis with projection quantum number m. In order to show this, the $SU(3)$ generators can be written in terms of the $U(3)$ generators

$$A_{ij} = b_i^\dagger b_j \tag{2.8}$$

that shift an oscillator quanta from the j-th direction to the i-th direction. In terms of the A_{ij}, the angular momentum operators L_i and the five components of the algebraic quadrupole operator $Q^a_{2\mu}$ are given by the expressions

$$\begin{aligned}
L_{10} &= i\,(A_{32} - A_{23})\,, && (2.9)\\
L_{1\pm1} &= -\frac{1}{\sqrt{2}}\,(A_{12} - A_{21} \pm i(A_{31} - A_{13}))\,, && (2.10)\\
Q^a_{20} &= 2A_{11} - A_{22} - A_{33}\,, && (2.11)\\
Q^a_{2\pm1} &= \sqrt{\frac{3}{2}}\,(A_{12} + A_{21} \pm i(A_{13} + A_{31}))\,, && (2.12)\\
Q^a_{2\pm2} &= \sqrt{\frac{3}{2}}\,(A_{22} - A_{33} \pm i(A_{23} + A_{32}))\,. && (2.13)
\end{aligned}$$

The commutation relation between these generators of $SU(3)$ are then

$$\begin{aligned}
[L_{1\mu}, L_{1\nu}] &= -\sqrt{2}\langle 1\mu, 1\nu|1, \mu+\nu\rangle\, L_{1\mu+\nu}\,,\\
[L_{1\mu}, Q^a_{2\nu}] &= -\sqrt{6}\langle 1\mu, 2\nu|2, \mu+\nu\rangle\, Q^a_{2\mu+\nu}\,,\\
[Q^a_{2\mu}, Q^a_{2\nu}] &= 3\sqrt{10}\langle 2\mu, 2\nu|1, \mu+\nu\rangle\, L_{1\mu+\nu}\,, && (2.14)
\end{aligned}$$

where $\langle l_1 m_1, l_2 m_2 | l_3 m_3\rangle$ is the usual notation for an $SO(3)$ Clebsch-Gordan coefficient. The allowed angular momenta within the η-th shell are given by:

$$l = \eta, \eta - 2, \ldots 1 \text{ or } 0, \tag{2.15}$$

as is known from the solutions of the harmonic oscillator for the single particle case (see appendix A.6), reflecting the fact that all states within a fixed shell have the same parity $P = (-1)^{\eta}$.

In the many-particle case, where the $SU(3)$ irrep (λ, μ) is not restricted to $(\eta, 0)$, the total angular momentum is given by a generalization of the rule above:

$$l = \lambda + \mu, \lambda + \mu - 2, \ldots, 1 \text{ or } 0 \tag{2.16}$$

for $k = 0$ and

$$l = k, k+1, k+2, \ldots, \lambda + \mu - k \tag{2.17}$$

for $k \neq 0$ where k is given by

$$K = \min(\lambda, \mu), \min(\lambda, \mu) - 2, \ldots, 1 \text{ or } 0\,. \tag{2.18}$$

The quantum number K reflects the fact that in this classification scheme multiple occurrences of a given L within a certain $SU(3)$ irrep (λ, μ) is possible. This label is also associated with the eigenvalue of the third projection of the angular momentum operator along the body-fix axis, as will be seen in the "Quantum Mechanics of the Rotor" section.

A multiplicity label κ can be introduced alternatively to distinguish between multiple occurrences of an angular momentum L. It runs from 0 to κ_{max} with the value of κ_{max} given by:

$$\kappa_{max} = \left[\frac{\lambda + \mu + 2 - L}{2}\right] - \left[\frac{\lambda + 1 - L}{2}\right] - \left[\frac{\mu + 1 - L}{2}\right]. \tag{2.19}$$

Here $[\cdots]$ is the notation for the greatest integer function. Harmonic oscillator eigenstates can thus be labeled by the two $SU(3)$ quantum numbers λ and μ, plus three additional sub-labels L, M_L (which label its $SO(3)$ character) and κ for the multiplicity of L in (λ, μ).

2.2.3 Coupling of Two $SU(3)$ Irreps

In a way that is analogous to the corresponding construction in the angular momentum theory, we couple two $SU(3)$ irreps (λ_1, μ_1) and (λ_2, μ_2) to a good total $SU(3)$ irrep, (λ, μ),

$$(\lambda_1, \mu_1) \otimes (\lambda_2, \mu_2) = \sum_{\rho} (\lambda, \mu)_\rho \tag{2.20}$$

by means of Clebsch-Gordan coupling coefficients for $SU(3)$

$$|\{(\lambda_1, \mu_1)(\lambda_2, \mu_2)\}\, \rho(\lambda, \mu)\alpha\rangle = \sum_{\alpha_1, \alpha_2} \langle (\lambda_1, \mu_1)\alpha_1; (\lambda_2, \mu_2)\alpha_2 | (\lambda, \mu)\alpha\rangle_\rho |(\lambda_1, \mu_1)\alpha_1; (\lambda_2, \mu_2)\alpha_2\rangle \tag{2.21}$$

where the α_i are intra-irrep labels of $SU(3)$ which can be (KLM_L) in the $SU(3) \supset SO(3)$ reduction or $(\epsilon \Lambda M_\Lambda)$ in the $SU(3) \supset SU(2) \otimes U(1)$ case. Note that the occurrence of the outer product multiplicity index ρ is a nontrivial extension for $SU(3)$ of the usual coupling rules for angular momenta. Unlike the $SU(2)$ case where the symmetry properties of the $SU(3)$ Clebsch-Gordan (C-G) are obtained by introducing simple phase factors, in this case we follow the convention by Draayer and Akiyama [35], that is,

1) $1 \leftrightarrow 2$ interchange requires a "geometrical" phase matrix Φ

$$\begin{aligned} \langle (\lambda_1, \mu_1)\alpha_1; (\lambda_2, \mu_2)\alpha_2 | (\lambda, \mu)\alpha\rangle_\rho &= \sum_{\rho'} \Phi_{\rho\rho'}((\lambda_1, \mu_1), (\lambda_2, \mu_2); (\lambda, \mu)) \\ &\times \langle (\lambda_2, \mu_2)\alpha_2; (\lambda_1, \mu_1)\alpha_1 | (\lambda, \mu)\alpha\rangle_{\rho'}. \end{aligned} \tag{2.22}$$

The phase factor matrix Φ does not depend on the subgroup labels. If $\rho_{max} = 1$, this phase matrix reduces to a simple phase factor

$$\Phi_{11}((\lambda_1, \mu_1), (\lambda_2, \mu_2); (\lambda, \mu)) = (-)^\phi, \tag{2.23}$$

where $\phi = (\lambda_1 + \mu_1) + (\lambda_2 + \mu_2) - (\lambda + \mu)$. This equation is a straightforward generalization of the corresponding expression for $SU(2)$. In some cases (like if $\lambda_i = \mu_i$ for all i in eq. (2.22)), the phase matrix turns out to be $\Phi_{\rho\rho'}((\lambda_1,\mu_1),(\lambda_2,\mu_2);(\lambda,\mu)) = (-)^{\phi+\rho_{max}-\rho}\delta_{\rho\rho'}$.

2) $1 \leftrightarrow 3$ interchange preserves the index ρ,

$$\langle(\lambda_1,\mu_1)\alpha_1;(\lambda_2,\mu_2)\alpha_2|(\lambda,\mu)\alpha\rangle_\rho = (-)^{\phi+\chi_2}\sqrt{\frac{dim(\lambda,\mu)}{dim(\lambda_1,\mu_1)}}\langle(\lambda,\mu)\alpha;(\lambda_2,\mu_2)\bar{\alpha_2}|(\lambda_1,\mu_1)\alpha_1\rangle_\rho \quad (2.24)$$

where the bar over the α indicates conjugate quantum numbers, and χ denotes the phase factor that is required to preserve the $SU(3)$ character of the state. Specifically for the $SU(3) \supset SO(3)$ reduction

$$\begin{aligned} \chi &= (\lambda - \mu) + (L - M_L), \\ \bar{\alpha} &= \kappa, L, -M_L. \end{aligned} \quad (2.25)$$

2.2.4 Particle Permutation and Unitary Symmetries

The many-particle shell model scheme starts with a single-particle picture and adds nucleons to orbitals of the valence space subject to the constraint of the Pauli principle. The dimensionality of the single-particle shell-model valence space is $k\Omega$ ($k = 2$ for spin, and 4 for a spin-isospin picture).

A classification of the $m-$particle wavefunction into irreps of the unitary group in N dimensions ($U(N)$, where $N = k\Omega$ is the dimensionality of the single-particle space) simultaneously specifies the irrep of the permutation group on m objects (S_m) to which each of the $m-$particle wavefunctions belongs [31]. This $U(N)$ and S_m complementarity means that it is sufficient to give further consideration to only one of the two, a result that applies to bosonic as well as fermionic schemes. The representations of $U(N)$ are labeled by a symbol $[f] = [f_1, f_2, ..., f_N]$ which has a simple pictorial representation called a Young diagram consisting of placing f_1 boxes directly adjacent to each other in a horizontal row, with $f_2 \leq f_1$ boxes left justified in a second row below and adjacent to the first set, etc. As each box corresponds to one particle, $\sum_i f_i = m$ for an $m-$particle configuration.

Since $N = k\Omega$, an $m-$particle fermionic wavefunction belongs to the antisymmetric irrep of the unitary group in $k\Omega$ dimensions, $U(k\Omega)$. This guarantees that it belongs to the antisymmetric irrep of the permutation group. For m particles this antisymmetric irrep is the one with all the f_i's equal to 1, $[f] = [1, 1, ..., 1] \equiv [1^m]$. However, the full shell model space can be further partitioned into space and spin, or space and spin-isospin parts, with spatial dimensionality Ω. When this is done each part can have any allowed $m-$particle symmetry, so long as its complement has the conjugate symmetry to insure that the product remains totally antisymmetric under particle permutation. The unitary symmetries associated with a factorization of the valence space into a direct product of two are denoted as $U(k\Omega) \supset U(\Omega) \times U(k)$ where $k = (2, 4)$ for the (spin, spin-isospin) cases. Overall antisymmetry in $U(k\Omega)$ requires that the $U(k)$ irrep be conjugate to the irrep of $U(\Omega)$. The $[f]$ irrep of $U(\Omega)$ and the conjugate irrep $[f^c]$ of $U(k)$ are related to one another by row-column interchange.

2.3 Classification of Proton-Neutron Many Particle Wavefunctions

The many-particle proton-neutron wavefunctions can be built using two approaches: (i) one in which the protons and neutrons share the same single-particle levels (light nuclei) where the isospin degree of freedom is introduced to account for the proton-neutron system, and (ii) another one in which the protons and neutrons fill different shells (heavy nuclei). The isospin degree of freedom is introduced with the protons and neutrons interpreted as different states of an isospin 1/2 doublet. With spin and isospin as well as spatial degrees of freedom the total number of states within an oscillator shell is 4Ω with a factor of two coming from the spin part. For a fermion picture, the m-particle wavefunction has to transform like the totally antisymmetric representation $[f^m] = [1]^m$ of $U(4\Omega)$.

For a further classification of the states it is natural to separate the spin and isospin degrees of freedom from the spatial part. The unitary group $U(k)$ - corresponding to the intrinsic part of the wavefunction - can be reduced as $U(2) \supset SU(2)$ for identical particles with the spin S labeling the $SU(2)$ irrep; and $U(4) \supset SU(2) \otimes SU(2)$ in a spin-isospin formalism, which yields quantum numbers

$\beta(ST)$, where S and T denote the spin and isospin, respectively, and β gives the multiplicity of (ST) in the $U(4)$ irrep.

To make use of the $SU(3)$ symmetry of the Hamiltonian, the spatial part of the wavefunction can be classified according to the group chain $U(\Omega) \supset SU(3)$. In this classification scheme, which is motivated by the underlying physics and does not follow the mathematically natural chain of subgroups, a multiplicity label α has to be introduced that distinguishes between multiple occurrences of a $SU(3)$ irrep (λ, μ) in a $U(\Omega)$ irrep $[f]$. For a further classification of the spatial part, the $SU(3) \supset SO(3)$ subchain that was discussed earlier (5) can be used (see Table 2.1). Thus one can construct m-particle states $|\Phi\rangle$ which are labeled as:

$$|\Phi\rangle = |m\,[f]\,\alpha(\lambda\mu)\kappa L, S; JM\rangle \tag{2.26}$$

for an identical-particle system, and

$$|\Phi\rangle = |m\,[f]\,\alpha(\lambda\mu)\kappa L, \beta(ST); JM, M_T\rangle \tag{2.27}$$

in the spin-isospin formalism. Here $[f]$ labels the $U(\Omega)$ irrep, $(\lambda\mu)$ refers to the irrep of $SU(3)$, while L and S are the orbital and spin angular momenta of the system, respectively, and J is the total angular momentum with projection M along the z-axis in the laboratory frame. The quantum numbers that identify the irrep of $U(k)$ are suppressed in eqs. (2.26) and (2.27) since they are fixed by the labels $[f]$ of $U(\Omega)$ and the requirement of overall antisymmetry. Basis states for light nuclei ($A \leq 28$) with neutrons and protons in the same η-th harmonic oscillator shell are of the form in eq. (2.27). As it was mentioned before in this case we have to introduce the isospin quantum number T. For heavy nuclei, where protons and neutrons occupy different major oscillator shells, basis states of each subsystem are of the form given in eq. (2.26); a basis for the combined neutron-proton system

TABLE 2.1. Group chain for m spin 1/2 fermions in the η-th oscillator shell.

$U(2\Omega)$	$\supset$	$U(\Omega)\otimes U(2)$	$\supset$	$SU(3)\otimes SU(2)$	$\supset$	$SO(3)\otimes SU(2)$
$[1^m]$		$[f]$, $[f^*]$	α	$(\lambda\mu)$, S	κ	L, S

is obtained via coupling of the neutron and proton states in the $SO(3)$ (angular momentum) coupled ($SU(3)$ uncoupled) scheme or in the $SU(3)$ coupled scheme.

For heavy nuclei ($A \geq 150$) where protons and neutrons occupy different shells, the totally antisymmetric wavefunctions for protons, $|\pi\rangle$, and neutrons, $|\nu\rangle$, are coupled to a total wavefunction $|\pi,\nu\rangle = |\pi\rangle \otimes |\nu\rangle$. The coupling of these two systems is possible on different levels. For example the basis states have the expression

$$\begin{aligned}[& |N_\pi[f_\pi]\alpha_\pi(\lambda_\pi,\mu_\pi)\kappa_\pi L_\pi[f_\pi^c]\, S_\pi; J_\pi\rangle \otimes \\ & |N_\nu[f_\nu]\alpha_\nu(\lambda_\nu,\mu_\nu)\kappa_\nu L_\nu[f_\nu^c]\, S_\nu; J_\nu\rangle \quad]^{J\,M}\end{aligned} \tag{2.28}$$

in a $SU(3)$ uncoupled (J_π-J_ν coupled) scheme or

$$\begin{aligned}[& |N_\pi[f_\pi]\alpha_\pi(\lambda_\pi,\mu_\pi))\otimes \\ & |N_\nu[f_\nu]\alpha_\nu(\lambda_\nu,\mu_\nu))\rangle \quad]^{[\rho(\lambda,\mu)\kappa L,(S_\pi\, S_\nu)S]J\,M}\end{aligned} \tag{2.29}$$

in a $SU(3)$ coupled scheme. In the latter, the proton and neutron $SU(3)$ irreps are coupled to a total $SU(3)$ irrep (λ,μ) with multiplicity ρ as described in the previous section, and the proton spin S_π is coupled with the neutron spin S_ν to the total spin S. Finally, the angular momentum L is coupled with the spin S to the total angular momentum J.

One can relate the basis states obtained in the strong coupling scheme to the states in the uncoupled scheme by a unitary transformation. The transformation from one to the other [37]

$$
\begin{aligned}
&|[(\lambda_\pi,\mu_\pi)\kappa_\pi L_\pi S_\pi J_\pi T_\pi;(\lambda_\nu,\mu_\nu)\kappa_\nu L_\nu S_\nu J_\nu T_\nu]J\rangle \\
&= \sum_{LS} \left\{ \begin{array}{ccc} L_\pi & S_\pi & J_\pi \\ L_\nu & S_\nu & J_\nu \\ L & S & J \end{array} \right\} \sum_{\rho(\lambda\mu)\kappa} \langle(\lambda_\pi,\mu_\pi)\kappa_\pi L_\pi;(\lambda_\nu,\mu_\nu)\kappa_\nu L_\nu||(\lambda,\mu)\kappa L)_\rho \\
&\qquad \times|[(\lambda_\pi,\mu_\pi)S_\pi T_\pi(\lambda_\nu,\mu_\nu)S_\nu T_\nu]\rho(\lambda\mu)\kappa LSJ\rangle
\end{aligned}
\tag{2.30}
$$

can be used to determine the matrix elements of the operators that are not diagonal in one basis but are diagonal in the other one. In this formula the numbers of particle N_π, N_ν and the symmetry labels brackets is a *unitary* $R(3)9-j$ symbol and $[f]$ are suppressed to keep the formula simple. The symbol in brackets is a *unitary* $R(3)$ $9-j$ symbol and the $SU(3)$ Wigner coefficient takes care of the the $SU(3)$ coupling $(\lambda_\pi,\mu_\pi)\times(\lambda_\nu,\mu_\nu)to(\lambda,\mu)$. The index ρ is introduced to distinguish multiple occurrences of (λ,μ) in the direct product.

2.4 The $SU(3)$ Hamiltonian

2.4.1 Introduction

Many nuclei from the rare earth region have rotational behavior. Their level spectrum can be fit by an asymmetric rotor Hamiltonian,

$$H_{ASM} = \sum A_\alpha\, I_\alpha^2, \tag{2.31}$$

where A_α are the inertia parameters with the convention $A_1 \leq A_2 \leq A_3$ with I_α the projection of the angular momentum operator I along the α-axis in a body-fixed frame of reference. This rotor Hamiltonian, when rewritten in a frame-independent form using the collective quadrupole operator Q^c, can be mapped onto an $SU(3)$-equivalent Hamiltonian [69, 70]:

$$H_{ASM} = \sum A_\alpha\, I_\alpha^2 \rightarrow a\, L^2 + b\, X_3^a + c\, X_4^a = H_{SU(3)}, \tag{2.32}$$

where $X_3^a = (LQ^aL)^0$ and $X_4^a = (LQ^aQ^aL)^0$ are algebraic analogs of the collective operators $X_3^c = (LQ^cL)^0$ and $X_4^c = (LQ^cQ^cL)^0$. The $Q^c \rightarrow Q^a$ mapping implies a restriction of the action of the quadrupole operator to a single major oscillator shell.

Since $H_{SU(3)}$ is written entirely in terms of $SU(3)$ generators, it does not mix different $SU(3)$ irreps. In this $SU(3)$ model for one irrep (λ, μ) the rules that give the values for the orbital angular momentum are determined by the $SU(3) \supset SO(3)$ chain, eq. (2.16) for $K = 0$, and eq. (2.17) for $K \neq 0$, where K, that is also called sometimes the Elliott quantum number [62], has been shown by Elliott [42] to have a maximum value of $\min(\lambda, \mu)$, eq. (2.18).

Hence, an angular momentum L can occur several times in a $SU(3)$ irrep. The $K-$label serves to resolve this multiplicity. As it will be shown in the "Rotor Model" section, a $K-$band appears naturally within the framework of the rotor model where the operator $K^2 = I_3^2$ (I_3 is the projection of the total angular momentum on the third body-fixed axis) generates $K-$bands that are shifted in energy relative to the ground-state band. For example, for an even-even nucleus the ground state has spin and parity 0^+ and the corresponding $SU(3)$ irrep is even-even. If we take as an example $(\lambda, \mu) = (10, 4)$ then the allowed values for K are $K = 0, 2, 4$. In this case an angular momentum $I = 2$ will occur twice, once for $K = 0$ and once for $K = 2$. A term in the Hamiltonian proportional to I_3^2 will shift the allowed K bands relative to one another.

Following these rules (2.16, 2.17, and 2.18), a state of angular momentum $L = 0^+$ can only occur in an even-even (λ, μ) irrep, but only once. However, experimental data show many states with angular momentum zero even in the low-energy part of the spectrum. These states can be described in the $SU(3)$ model by considering more than one even-even irrep.

On the other hand, it can be shown quite generally that the dominant part of the long range nucleon-nucleon interaction is given by the quadrupole-quadrupole force [46]. This interaction can be given in terms of $SU(3)$ generators,

$$H_{Q\cdot Q}^a = -Q^a \cdot Q^a = 3L^2 - 4C_2, \tag{2.33}$$

where C_2 is the second order Casimir operator of the $SU(3)$ with eigenvalue

$$\langle C_2 \rangle = (\lambda + \mu)(\lambda + \mu + 3) - \lambda\mu. \tag{2.34}$$

If $H^a_{Q\cdot Q}$ is evaluated within an irrep (λ, μ), it has the eigenvalues

$$E_{Q\cdot Q} = 3L(L+1) - 4\langle C_2 \rangle. \tag{2.35}$$

The assumption of a $Q^a \cdot Q^a$ interaction leads to a rotational spectrum. The (λ, μ) dependence is contained in C_2 which determines the energy where that particular rotational spectrum begins. Since a state of angular momentum $L = 0$ occurs in each even-even (λ, μ) irrep, the number of $L = 0$ states is equal to the number of even-even irreps. A non-degenerate $K = 0$ energy spectra can be obtained by combining the two Hamiltonians, H_{ASM} and $H_{Q\cdot Q}$, and rewriting the $SU(3)$ Hamiltonian as

$$H_{SU(3)} = \chi Q \cdot Q + aL^2 + bK_J^2 \tag{2.36}$$

where K_J^2 is a linear combination of X_3^a and X_4^a. In this case, states with angular momentum $L = 0$ have eigenvalues

$$E(L = 0) = -4\chi\langle C_2 \rangle. \tag{2.37}$$

We have shown so far that by using a $SU(3)$ Hamiltonian we can describe a deformed nucleus with many $K^\pi = 0^+$ states. By inspecting the rules that give the possible values of angular momentum L in a given (λ, μ), and by knowing that in many cases the leading irrep that describes the ground state has $\mu \neq 0$, we can show that there exist other bands with $K \neq 0$. Indeed most of the heavy deformed nuclei have a gamma ($K^\pi = 2^+$) band, and some of them have a $K = 4$ band.

Due to the underlying many-particle nature of the theory, single-particle and many-particle terms that do not have a collective counterpart can be included in the theory. A more realistic Hamiltonian

can be obtained by including pairing and spin-orbit interactions [10, 11, 49]. The matrix elements of these operators in the framework of the $SU(3)$ model are given later in this chapter.

2.4.2 Quantum Mechanics of the Rotor

The Hamiltonian of a general rotor is given by [41]:

$$H_{ASR} = \sum_{\alpha} A_{\alpha} I_{\alpha}^2 \tag{2.38}$$

where $A_\alpha = 1/2\mathcal{I}_\alpha$ are the inertia parameters with the convention $A_1 \leq A_2 \leq A_3$, $\mathcal{I}_\alpha$ are the moments of inertia, and I_α are the projections of the angular momentum operators I along the body-fixed α-axis. The commutation rules for the I_α differ from those for the appropriate laboratory frame operators by a minus sign:

$$[I_\alpha, I_\beta] = -i\epsilon_{\alpha\beta\gamma} I_\gamma \tag{2.39}$$

and

$$[L_\alpha, L_\beta] = +i\epsilon_{\alpha\beta\gamma} L_\gamma \tag{2.40}$$

If the shape is given by a quadrupole surface the inertia parameters can be related to the shape variables:

$$\mathcal{I}_\alpha \approx \beta^2 \sin^2(\gamma - \frac{2}{3}\pi\alpha) \tag{2.41}$$

Using the commutation rules for the I_α (2.39), the rotor Hamiltonian can be rewritten in terms of the total angular momentum, its third projection on the intrinsic frame of reference and the ladder operators $I_\pm$,

$$\begin{aligned} I_+ &= I_1 + iI_2 \\ I_- &= I_1 - iI_2, \end{aligned} \tag{2.42}$$

$$H_{ASR} = \frac{A_1 + A_2}{2} I^2 + (A_3 - \frac{A_1 + A_2}{2}) I_z^2 + (\frac{A_1 - A_2}{4})(I_+^2 + I_-^2) \tag{2.43}$$

TABLE 2.2. Irreducible representations of Vierergruppe D_2.

Symmetry	Transformation				Index		Dimension	
Type	1	T_1	T_2	T_3	λ	μ	I(even)	I(odd)
A	1	1	1	1	e	e	$(I+2)/2$	$(I-1)/2$
B_1	1	1	−1	−1	e	o	$I/2$	$(I+1)/2$
B_2	1	−1	1	−1	o	o	$I/2$	$(I+1)/2$
B_3	1	−1	−1	1	o	e	$I/2$	$(I+1)/2$

The first two terms are diagonal while the third one has diagonal elements only for $I = 1$. An asymmetry parameter κ is defined as

$$\kappa = \frac{2A_2 - A_1 - A_3}{A_3 - A_1} \tag{2.44}$$

The limiting values $\kappa = -1(+1)$ describe a prolate (oblate) symmetric top while $\kappa = 0$ is called the most asymmetric case. It should be emphasized that κ refers to the inertia ellipsoid and not directly to the shape of an object. In these limiting cases of a prolate ($\kappa = -1; A_1 = A_2$) and an oblate ($\kappa = +1; A_2 = A_3$) top, the Hamiltonian is diagonal with eigenvalues:

$$E_{SYM} = A_1 I(I+1) + (A_3 - A_1)K_p^2 \quad for\ (\kappa = -1) \tag{2.45}$$

$$E_{SYM} = A_2 I(I+1) - (A_1 - A_2)K_o^2 \quad for\ (\kappa = +1) \tag{2.46}$$

where $K_{p,o}$ is the eigenvalue of the projection of the angular momentum I onto the intrinsic symmetry axis. The subscripts refer to prolate and oblate, respectively. For each $K-$value there exists an infinite series of levels with an $I(I+1)$ spacing, which is commonly referred to as a rotational sequence. States with the same K value are members of a rotational band. K is a good quantum number only in the limiting cases of a prolate or an oblate top. In general the eigenvalues of the H_{ASR} are determined numerically.

H_{ASR} is invariant under π rotations about the principal axes. This means that the Hamiltonian commutes with the rotation operators $T_\alpha = exp(i\pi I_\alpha)$, with $\alpha = 1, 2, 3$. The set of operators

$\{E, T_1, T_2, T_3\}$ forms the Vierergruppe (D_2), where E denotes the identity operator. The fact that the Hamiltonian has D_2 symmetry leads to some important consequences. The Vierergruppe has four symmetry classes as shown in the group table (Table 2.2). As a result of this symmetry the Hamiltonian matrix becomes block diagonal with four blocks. The matrix elements of H_{ASR} can be calculated in the basis of the symmetric rotor,

$$\psi^{KI}_{SYM\ \ M} = \left\{\frac{2I+1}{16\pi^2(1+\delta_{K0})}\right\}^{1/2} (D^I_{MK} + (-1)^{\lambda+\mu+I} D^I_{M,-K}) \tag{2.47}$$

$$\psi^{(\lambda\mu)\nu I}_{ASR\ \ M} = \sum_{K\geq 0}{}' C^{(\lambda\mu)KI}_{SYM\ \ M}. \tag{2.48}$$

Here $D^I_{MK}(\Omega)$ denotes a D function where the Euler angles specify the orientation of the lab frame with respect to the body-fixed frame of the rotor. The prime indicates that the summation is over even or odd K values only. The values of the coefficients C are determined numerically. Also, λ can be even or odd while μ is even for even K, and odd for odd K. In the traditional work on the rotor the labels λ and μ are replaced by the single quantity $\gamma = \lambda + \mu + I$. (The $\lambda + \mu + I$ convention follows from the $SU(3)$ interpretation of the rotor picture.) The parity of the ψ_{SYM} and ψ_{ASR} is given by $\pi = \lambda + \mu$. The label ν is a running index to distinguish states with the same values of (λ, μ) and I.

In conclusion, in both cases of the symmetric and the asymmetric rotor, the eigenstates can be labeled by the angular momentum, K-its third projection along the body-fix axis, and M-its third projection on the laboratory-fix axis. These states can be grouped in bands of a certain K-value, hence we have the ground-state band corresponding to $K = 0$, and the other K-bands of odd or even values according to the γ-value.

The rotor model can be very useful in a description of low-energy spectra of deformed nuclei. Using this model as a starting point many other models have been developed to describe various experimental phenomena. Some of these are the two-particle model, the symmetric core model as

well as the asymmetric core model [99], the rotation-vibration model [56], and more complex models like the generalized collective model [56].

2.4.3 The $SU(3)$-Rotor Correspondence

The collective aspects of the nuclear interaction can be described naturally within the framework of $SU(3)$ model. The close relation between the rotor and the $SU(3)$ algebras translates into the ability of a $SU(3)$ symmetry preserving Hamiltonian to describe the rotational spectrum of well-deformed nuclei and also allows one to map $SU(3)$ eigenstates $|(\lambda,\mu)\rangle$ onto shapes parameterized by the deformation parameters β and γ of the quantum rotor [69, 28, 29].

The rotor algebra $T_5 \wedge SO(3)$ is generated by the five moments of the *collective* quadrupole operator (see eq. (2.3)) which coincide with the moments of the corresponding inertia tensor and three components of the angular momentum. The commutation relation between these generators of the semi-direct product of T_5 and $SO(3)$ are

$$\begin{aligned}
[L_\mu, L_\nu] &= -\sqrt{2}\langle 1\mu, 1\nu|1\mu+\nu\rangle\, L_{\mu+\nu}, \\
[L_\mu, Q^c_\nu] &= -\sqrt{6}\langle 1\mu, 2\nu|2\mu+\nu\rangle\, Q^c_{\mu+\nu}, \qquad (2.49)\\
[Q^c_\mu, Q^c_\nu] &= 0\,, \qquad (2.50)
\end{aligned}$$

reflecting the structure of the semi-direct product group with two sets of generators, each separately closed under commutation ($[T_5, T_5] \rightarrow T_5, [SO(3), SO(3)] \rightarrow SO(3)$) but with the commutator of an element of one group with an element of the other yielding an element of only one of the sets ($[T_5, SO(3)] \rightarrow T_5$). These commutation relations are similar to the ones between the *algebraic* quadrupole operator, Q^a_μ and the angular momentum, L, that are generators of $SU(3)$, namely,

$$\begin{aligned}
[L_\mu, L_\nu] &= -\sqrt{2}\langle 1\mu, 1\nu|1\mu+\nu\rangle\, L_{\mu+\nu}, \\
[L_\mu, Q^a_\nu] &= -\sqrt{6}\langle 1\mu, 2\nu|2\mu+\nu\rangle\, Q^a_{\mu+\nu}, \qquad (2.51)\\
[Q^a_\mu, Q^a_\nu] &= 3\sqrt{10}\langle 2\mu, 2\nu|1\mu+\nu\rangle L_{\mu+\nu},
\end{aligned}$$

where only the last commutation relation for the quadrupole operators are different, giving zero in the rotor case and non-zero in the $SU(3)$ case.

The $SU(3)$ algebra contracts to the $T_5 \wedge SO(3)$ algebra, when L is small compared to $\sqrt{C_2}$, which can be seen by rescaling Q^a as $Q^a/\sqrt{C_2}$. The rescaling leaves the first two commutation relations unchanged but implies $[Q^a_\mu, Q^a_\nu] \approx 0$ for $C_2 \gg L$ in the $SU(3)$ case. This is equivalent to the statement that the $SU(3)$ model describes rotational states very well as long as

$$L \ll \max[(2\lambda+\mu),(\lambda+2\mu)] \,. \tag{2.52}$$

This is related to the fact that $SU(3)$ is a compact algebra with a maximum value for the angular momentum, L, whereas the rotor algebra is non-compact with unbound L.

Since both the rotor and $SU(3)$ theory are describing the same physical phenomena – that is, a rotational spectrum – and their algebras are closely related it is natural to require a correspondence between the invariants of both groups. The two invariants C_2 and C_3 of the rank two group $SU(3)$ can be expressed by the $SU(3)$ labels (λ,μ) as:

$$\begin{aligned} C_2 &= (\lambda+\mu)(\lambda+\mu+3)-\lambda\mu \quad \text{and} \\ C_3 &= \frac{1}{9}(\lambda-\mu)(\lambda+2\mu+3)(2\lambda+\mu+3) \,. \end{aligned} \tag{2.53}$$

The symmetry group of the rotor, $T_5 \wedge SO(3)$, also has two invariants, the traces of the square and cube of the collective quadrupole matrix:

$$\begin{aligned} Tr[(Q^c)^2] &= \lambda_1^2+\lambda_2^2+\lambda_3^2 \quad \text{and} \\ Tr[(Q^c)^3] &= \lambda_1\lambda_2\lambda_3 \,. \end{aligned} \tag{2.54}$$

Here the λ_α are the expectation values of the quadrupole matrix in its body-fixed principal axis frame ($Q^c_{\alpha\beta} = \lambda_\alpha \delta_{\alpha\beta}$) that can be parameterized by the shape variables (β, γ) as:

$$\lambda_\alpha = \sqrt{\frac{5}{\pi}} \frac{Ar_0^2}{3} \cos(\gamma - 2\pi\alpha/3) \quad \alpha = 1, 2, 3 \tag{2.55}$$

where A denotes the number of nucleons and r_0 the root-mean-square radius.

Requiring a correspondence between the invariants of the two groups, i. e. $C_2 \sim Tr[(Q^c)^2]$ and $C_3 \sim Tr[(Q^c)^3]$, leads to the following relation between the $SU(3)$ labels (λ, μ) and the λ_i's [29]:

$$\begin{aligned} \lambda_1 &= -\frac{1}{3}(\lambda - \mu) \\ \lambda_2 &= -\frac{1}{3}(\lambda + 2\mu + 3) \\ \lambda_3 &= \frac{1}{3}(2\lambda + \mu + 3) \end{aligned} \tag{2.56}$$

This set of equations translates into the following relation between the shape variables (β, γ) and the $SU(3)$ irreps (λ, μ):

$$\beta^2 = \frac{4\pi}{5} \frac{1}{(Ar_0^2)^2} \left(\lambda^2 + \lambda\mu + \mu^2 + 3(\lambda + \mu + 1)\right) \tag{2.57}$$

$$\tan\gamma = \frac{\sqrt{3}(\mu + 1)}{2\lambda + \mu + 3}. \tag{2.58}$$

This relation can be interpreted also as a mapping between the labels (λ, μ) and spherical coordinates $(k\beta, \gamma) \leftrightarrow (r, \gamma)$, where the abbreviation $k = \sqrt{4/9\pi} A r_0$ has been used.

$$k\beta\cos(\gamma) = k\beta_x = (2\lambda + \mu + 3)/3 \tag{2.59}$$

$$k\beta\sin(\gamma) = k\beta_y = (\mu + 1)/\sqrt{3} \tag{2.60}$$

Following these equations, each irrep (λ, μ) corresponds to an unique shape parameterized by (β, γ). For example, eq. (2.58) implies that for $\mu = 0$ the deformation parameter γ is close to zero. A

$SU(3)$ irrep with $\mu = 0$ thus corresponds to a prolate – cigar-like – shape. For the case $\lambda = \mu$ the $SU(3)$ irrep describes a particle distribution with maximum triaxiality, $\gamma = 30°$. A $SU(3)$ irrep with $\lambda = 0$ corresponds to an oblate – pancake-like – shape with $\gamma = 60°$.

The fermionic nature of the nucleons, a feature that is not included in the collective models, is reflected in the $SU(3)$ model through the values the quantum numbers λ and μ can assume. Each (λ, μ) corresponds to an unique shape parameterized by (β, γ), but the vice versa is not always true. Were β and parameterized by (β, γ), but the opposite is not always true. While β and γ can vary continuously, the group structure $U(\Omega) \supset SU(3)$ dictates a limited set of allowed (λ, μ) values depending upon the number of nucleons in a shell. The $SU(3)$-Rotor correspondence[69] has left a strong imprint on the development of the $SU(3)$-shell model as it is being used in this context.

2.4.4 Shell-model Operator for K_J-band Splitting

An important step in the development of the $SU(3)$-shell mode was the realization of of a shell-model expression for an operator $\mathcal{K}^2$ that produces $K-$band splitting. Since K^2 is the eigenvalue of the a special rotor Hamiltonian, namely I_3^2, where I_3^2 is the projection of the total angular momentum on the body-fixed symmetry axis, this result led Naqvi and co-workers to a $\mathcal{K}$-operator, and provided analytic results for its matrix elements in the Elliott $SU(3) \supset SO(3)$ basis [82, 83]. The eigenvalue of the $\mathcal{K}^2$ operator is exactly K^2 in the limit $L << \min(\lambda, \mu)$, where K is the Elliott K quantum number defined through projection on an intrinsic state of maximum deformation.

To derive the $SU(3)$ model equivalent of the K^2 operator which is necessary for a realistic description of the rotational structure, the relation between the $SU(3)$ algebra and the rotor algebra is used. Ideally, in addition to being a rotational invariant such a $SU(3)$ model equivalent of K^2 should conserve the $SU(3)$ symmetry of the system. In the case of $S = 0$, by employing a special minimal set of $SO(3)$ scalars the so-called $SU(3) \rightarrow SO(3)$ integrity basis, which has been shown [64] to contain five operators that give rise to real symmetric matrix forms, the Hamiltonian can be rewritten in a frame-independent expression. The operators can be chosen to be the Casimir invariants L^2, C_2 and C_3, and two non-$SU(3)$ invariant rotational scalars, labeled X_3^a and X_4^a, which are of degree three

and four, respectively, in the $SU(3)$ generators:

$$\begin{aligned} X_3^a &= \sum_{i,j} L_i Q_{ij}^a L_j \\ X_4^a &= \sum_{i,j,k} L_i Q_{ij}^a Q_{jk}^a L_k \ . \end{aligned} \tag{2.61}$$

Since only the operators X_3^a and X_4^a are able to couple and mix multiple occurrences of a given $SO(3)$ irrep in $SU(3)$, they have to be part of a $SU(3)$ Hamiltonian that is able to reproduce a more complex rotational spectrum. In the most general case, this Hamiltonian has the form

$$H_{SU(3)} = a_1 C_2 + a_2 C_3 + a_3 L^2 + a_4 X_3^a + a_5 X_4^a \ . \tag{2.62}$$

In order to extract the shell-model equivalent of the K^2 operator from this Hamiltonian, the collective version of the three terms in $H_{SU(3)}$ with an angular momentum dependence has been rewritten, replacing the algebraic quadrupole operator with its collective counterpart that is diagonal in the body-fixed principle axis frame ($Q_{\alpha\beta}^c = \lambda_\alpha \, \delta_{\alpha\beta}$):

$$\begin{aligned} L^2 &= \sum_i L_i L_i = \sum_i I_i^2 \\ X_3^c &= \sum_{i,j} L_i Q_{ij}^c L_j = \sum_i \lambda_i I_i^2 \\ X_4^c &= \sum_{i,j,k} L_i Q_{ij}^c Q_{jk}^c L_k = \sum_i \lambda_i^2 I_i^2 . \end{aligned} \tag{2.63}$$

As before, the notation I and L is used for the angular momentum in the body-fixed and lab-frame respectively. This set of equations (2.63) can be inverted [82] to yield the following expression for the I_i^2 in terms of L^2 and X^c's:

$$I_i^2 = [(\lambda_1\lambda_2\lambda_2)L^2 + (\lambda_i^2)X_3^c + (\lambda_i)X_4^c]/D_i \ , \quad D_i \equiv 2\lambda_i^3 + \lambda_1\lambda_2\lambda_3 \ . \tag{2.64}$$

Substituting these expressions into the Hamiltonian for an asymmetric Rotor,

$$H_{rot} = A_x I_x^2 + A_y I_y^2 + A_z I_z^2 \,, \tag{2.65}$$

gives a frame-independent expression for H_{rot}, namely,

$$H_{rot} = aL^2 + bX_3^c + cX_4^c \tag{2.66}$$

where the parameters a, b and c are given as

$$\begin{aligned} a &= \sum_i \lambda_1\lambda_2\lambda_3 A_i/D_i \\ b &= \sum_i \lambda_i^2 A_i/D_i \\ c &= \sum_i \lambda_i A_i/D_i \,. \end{aligned} \tag{2.67}$$

To derive a $SU(3)$ shell model image of $K^2 = I_3^2$ from this Hamiltonian, the operators X_3^c and X_4^c that couple shells differing by two quanta have to be changed back to their algebraic counterparts that were introduced in eq. (2.61). As was shown by Leschber [70], this substitution does indeed yield a shell model Hamiltonian that is able to reproduce the rotor results and observed rotational phenomena in nuclei. The algebraic equivalent of H_{ROT} in eq. (2.66) for the special case $A_1 = A_2 = 0$ and $A_3 = 1$ is thus a natural definition for a shell model operator K^2

$$K^2 = (\lambda_1\lambda_2 L^2 + \lambda_3 X_3^a + X_4^a)/(2\lambda_3^2 + \lambda_1\lambda_2) \;. \tag{2.68}$$

From of the correspondence between the invariants of the rotor group $T_5 \wedge SO(3)$ and $SU(3)$, the parameters λ_i are given as a function of the $SU(3)$ labels λ and μ by

$$\lambda_1 = -\frac{1}{3}(\lambda - \mu) \quad \lambda_2 = -\frac{1}{3}(\lambda + 2\mu + 3) \quad \lambda_3 = \frac{1}{3}(2\lambda + \mu + 3) \,. \tag{2.69}$$

Since the $SU(3)$ irreps are related to the shape of nuclear distribution, this can be seen as a generalization of the rotor Hamiltonian given in eq. (2.65) where the coefficients are determined by the moments of inertia.

As in the case of rotational spectra generated by the quadrupole-quadrupole operator, the correspondence between the $\mathcal{K}$ operator in the $SU(3)$ and rotor pictures is best for small values of L. This reflects the fact that $SU(3)$ is a compact group with finite-dimensional irreps, while the symmetry group of the rotor is non-compact reproduce the K-band with infinite-dimensional representations. Naqvi was able to reproduce the K-band splitting in the ^{24}Mg and ^{168}Er by applying this theory to only the leading representations of these nuclei [82]. So far the $\mathcal{K}^2$ operator is actually $\mathcal{K}_L^2$, since the total spin considered was $S = 0$, and therefore $J = L$.

Following the development of a shell-model operator to describe the the K-band splitting in even-even nuclei, Naqvi and Draayer introduced a shell-model operator that generate K_J-band splitting in odd-A nuclei [83]. $K_J = K_L + K_S$ is the projection of the total angular momentum, $J = L + S$, on the principal symmetry axis of the system. The appropriate form for S $\neq 0$ states, has to reduce to the algebraic equivalent of $\mathcal{K}_L^2$ for S = 0 in even-A nuclei. The presence of this operator in the $SU(3)$-shell model picture is very important.

In this case the Hamiltonian of a generalized triaxial rotor is given by

$$H_{rot} = \sum_{i=1}^{3} A_i I_i^2 \,, \tag{2.70}$$

where I, $(I^2 = I_1^2 + I_2^2 + I_3^2)$ is now the total angular momentum that can be either half-integral or integral.

$$\begin{aligned} J^2 &= \sum_i J_i J_i = \sum_i I_i^2 \\ X_3^c &= \sum_{i,j} J_i Q_{ij}^c J_j = \sum_i \lambda_i I_i^2 \\ X_4^c &= \sum_{i,j,k} J_i Q_{ij}^c Q_{jk}^c J_k = \sum_i \lambda_i^2 I_i^2 \,. \end{aligned} \tag{2.71}$$

eqs. (2.71) can be solved for the I_i's to obtain a frame-independent rotor Hamiltonian that in turn gives a frame-independent expression for K_J^2 with the inertia parameters $A_1 = A_2 = 0$ and $A_3 = 1$:

$$K_J^2 = (\lambda_1\lambda_2 J^2 + \lambda_3 X_3^c + X_4^c)/(2\lambda_3^2 + \lambda_1\lambda_2) \,. \tag{2.72}$$

Replacing X_3^c and X_4^c with their algebraic counterparts – for which the algebraic quadrupole operator $Q_{\alpha\beta}^a$ is used instead of its collective version – is then a natural definition for a $SU(3)$ shell model image of K_J^2.

For the evaluation of the matrix elements of the X_3^a and X_4^a operators and therefore of $(\lambda,\mu)K^2$ in the spin-coupled basis of the $SU(3)$ scheme [27],

$$|\gamma(\lambda,\mu)\kappa LSJM_J\rangle \quad \text{with } \gamma = N[f]\alpha[\bar{f}]\beta \,, \tag{2.73}$$

it is useful to express these operators in a tensor notation,

$$X_3^a = \sum_{\alpha\beta} J_\alpha Q_{\alpha\beta} J_\beta = \frac{1}{6}\sqrt{30}\,[[J \otimes Q]^1 \otimes J]^0 \tag{2.74}$$

and

$$X_4^a = \sum_{\alpha\beta\gamma} J_\alpha Q_{\alpha\beta} Q_{\beta\gamma} J_\gamma = -\frac{5}{18}\sqrt{3}\,[[J \otimes Q]^1 \otimes [J \otimes Q]^1]^0 \,. \tag{2.75}$$

The reduced matrix elements for X_3^a and X_4^a can be evaluated using the reduced matrix elements of the $SU(3)$ generator Q^a, and are given by

$$\begin{aligned} &\langle\gamma(\lambda,\mu)\kappa LSJ||X_3^a||\gamma(\lambda,\mu)\kappa' L'SJ\rangle \\ &= \sqrt{\frac{5}{6}}J(J+1)\sqrt{(2J+1)}W(J1J1;J2) \\ &\quad \times <(\lambda,\mu)\kappa LSJ\,||Q^a||\,(\lambda,\mu)\kappa' L'SJ> \end{aligned} \tag{2.76}$$

and

$$\begin{aligned}
&\langle\gamma(\lambda,\mu)\kappa LSJ||X_4^a||\gamma(\lambda,\mu)\kappa' L'SJ\rangle \\
&= \frac{5}{6}J(J+1)\sqrt{(2J+1)}\sum_{\kappa'' L'' J''}(-1)^{J-J''}W(J1J1;J2)^2 \\
&\quad \times <(\lambda,\mu)\kappa LSJ\,||Q^a||\,(\lambda,\mu)\kappa'' L''SJ> \\
&\quad <(\lambda,\mu)\kappa'' L''SJ\,||Q^a||\,(\lambda,\mu)\kappa' L'SJ> \qquad (2.77)
\end{aligned}$$

where the reduced matrix element for Q^a, which has $SU(3)$ tensor character $(\lambda_0,\mu_0)\kappa_0 L_0 = (1,1)12$, is given by

$$\begin{aligned}
&<(\lambda,\mu)\kappa LSJ\,||Q^a||\,(\lambda,\mu)\kappa' L'SJ'> \\
&= (-1)^{\phi}2\sqrt{C_2(\lambda,\mu)(2J'+1)(2J+1)}W(SJ'L2;L'J) \\
&\quad \times <(\lambda,\mu)\kappa' L';(1,1)12||(\lambda,\mu)\kappa L>_{\rho=1}\ . \qquad (2.78)
\end{aligned}$$

Here the Ws are $SU(2)$ Racah coefficients and the $<(\lambda,\mu)\kappa' L';(1,1)12||(\lambda,\mu)\kappa L>_{\rho=1}$ denote $SU(3)\supset SO(3)$ coupling coefficients. The phase factor, $(-1)^{\phi}=-1$ if $\mu\neq 0$ and $+1$ if $\mu=0$, is required for consistency with the definition of $SU(3)$ coupling coefficients [2, 35].

The matrix elements for K_J^2 do reduce to those of the simpler K_L^2 operator in the $S=0$ configurations. Naqvi and Draayer have calculated the eigenvalues of the $\mathcal{K}_{\mathcal{J}}$ operator, determined in the leading normal-SU(3) irrep for ^{25}Mg $[(\lambda,\mu)=(9,3);S=\frac{1}{2}]$ and for two heavy nuclei ^{159}Dy and ^{165}Er [83]. The results show that for low-J values in each band the calculated eigenvalues are almost equal to the collective model values: $(\frac{1}{2})^2$, $(\frac{3}{2})^2$, $(\frac{5}{2})^2$, etc.

2.4.5 One and Two-body Interactions

A more realistic Hamiltonian can be obtained by including single-particle energies and pairing interaction terms that are, respectively, one- and two-body interactions. This is possible since the $SU(3)$ model is a many-particle theory, even though these terms do not appear naturally in the

$SU(3)$ formalism. Draayer and collaborators proposed in the 80's and 90's a shell-model theory for deformed nuclei [26, 27, 82, 83]. In this section the matrix elements for single-particle energies and the pairing interactions will be given in the framework of the $SU(3)$ model.

The observation that the last unpaired nucleon determines the spin of the nucleon reflects on the importance of the pairing interaction which lowers the energy of nucleon pairs coupled to total angular momentum zero. Indeed, the pairing-plus-quadrupole model [12] has been used to simulate both few-particle non-collective and many-particle collective features of nuclei [13]. The addition of this two-body interaction is thus an important step towards a more realistic Hamiltonian. Pairing correlations are normally attributed to the short-range part of the nucleon-nucleon interaction. Since the spatial overlap of two-nucleon densities is at its maximum if the nucleons have the same l and $|m|$ value, this configuration is energetically favored by a short-range attractive interaction.

The effect of the pairing interaction can be seen in the energy gap of about 1 MeV in the spectrum of even-even nuclei that are just a few nucleons away from a closed shell. The "pairing gap" occurs between the $J^\pi = 0^+$ and a set of nearly degenerate states ($J^+ = 2^+, 4^+, 6^+ \ldots$) and corresponds to the energy necessary to break up a nucleon pair. This gives an estimate for the strength of the pairing interaction.

A general one-body operator that acts symmetrically on a system of identical particles is given by the expression

$$\mathcal{F} = \sum_s f(\mathbf{r}_s, \sigma_s), \tag{2.79}$$

where $\mathbf{r}_s$ and σ_s represent the position and the spin coordinates, of the s-th particle. The one body-operator takes the following form in the second quantization formalism:

$$\mathcal{F} = \sum_{\rho,\rho'} \langle \rho' | f(\mathbf{r}_s, \sigma_s) | \rho \rangle a^\dagger_{\rho'} a_\rho \tag{2.80}$$

The set of anti-commutation relations for the fermion creation and annihilation operators ($a^\dagger_\rho$ and a_ρ) requires that a many-particle fermionic wavefunction to be totally antisymmetric,

$$\begin{aligned} \{a^\dagger_\gamma,\, a_{\gamma'}\} = a^\dagger_\gamma a_{\gamma'} + a_{\gamma'} a^\dagger_\gamma &= \delta_{\gamma,\gamma'} \\ \{a^\dagger_\gamma,\, a^\dagger_{\gamma'}\} = \{a_\gamma,\, a_{\gamma'}\} &= 0\,. \end{aligned} \tag{2.81}$$

For a proton or neutron in the $\eta-$th shell, for example, the abbreviation $|\gamma\rangle$ corresponds to the state $|(\eta,0)l, m_l, \frac{1}{2}m_s\rangle$ if the $SU(3) \supset SO(3)$ group chain is used and angular momentum and spin are not coupled. Here the single-particle $SU(3)$ irrep label $(\lambda,\mu) = (\eta,0)$ is used in place of the principal quantum number. This is done to stress the fact that the single-particle creation operator is an $(\eta,0)$ irreducible tensor of $SU(3)$. The corresponding annihilation operator transforms according to the conjugate representation $(0,\eta)$; see eq. (2.81). The annihilation operator introduced above is not a $SU(3)$ tensor, but an operator $\tilde{a}_\gamma$ that does have good $SU(3)$ transformation behavior under $SU(3)$ only differs from a_γ by a phase factor [27]:

$$\tilde{a}_\gamma = \tilde{a}_{(0,\eta)\, l, m_l, \frac{1}{2}m_s} \equiv (-1)^{\eta+l+m+\frac{1}{2}+m_s} a_{(\eta,0)\, l, -m_l, \frac{1}{2}-m_s} \tag{2.82}$$

The following notation will be used throughout the text

$$\begin{aligned} &\left[a^\dagger_{(\eta',0)\frac{1}{2}} \otimes \tilde{a}_{(0,\eta)\frac{1}{2}}\right]^{(\lambda\mu)\kappa L M_l S M_s} \\ &= \sum_{ll'} \langle((\eta,0)l',(0,\eta)l||(\lambda,\mu)\kappa L\rangle \sum_{m_s m_s'} \langle\tfrac{1}{2}m_s',\tfrac{1}{2}m_s|SM_S\rangle \qquad (2.83) \\ &\quad\times \sum_{m'm} \langle l'm', lm|LM_L\rangle\, a^\dagger_{(\eta' 0) l' m' \frac{1}{2} m'_s} \tilde{a}_{(0\eta) l m \frac{1}{2} m_s}, \qquad (2.84) \end{aligned}$$

and

$$\left[a^\dagger_{(\eta',0)\frac{1}{2}} \otimes \tilde{a}_{0,\eta)\frac{1}{2}}\right]^{(\lambda\mu)\kappa LS}_{JM} = \sum_{M_L M_S} \langle LM_L, SM_S|JM\rangle \left[a^\dagger_{(\eta' 0) l' m' \frac{1}{2}} \otimes \tilde{a}_{(0\eta) l m \frac{1}{2}}\right]^{(\lambda\mu)\kappa L M_l S M_s}. \tag{2.85}$$

where the coupling coefficients that enter are $SO(3)$ Clebsch-Gordan coefficients, $\langle\cdots|\cdot\rangle$, and their $SU(3)$ equivalent, reduced with respect to $SU(3)$, for which a notation with double bars, $\langle\cdots||\cdot\rangle$, has been introduced (see Appendix A.5). With these definitions, it is possible to construct a general one-body operator in terms of single-particle creation and annihilation operators.

$$\mathcal{F}^{(\lambda,\mu)S}_{\kappa LM_L M_S} = \sum_{\{-\}} \langle (\eta',0) l' m' \tfrac{1}{2} m'_s | f^{(\lambda,\mu)S}_{\kappa LM_L M_S} | (\eta,0) l m \tfrac{1}{2} m_s \rangle a^{\dagger}_{(\eta',0)l'm',\frac{1}{2}m'_s} a_{(\eta,0)lm,\frac{1}{2}m_s}, \tag{2.86}$$

with the abbreviation $\{-\} = \{\eta, l, m, m_s, \eta', l', m', m'_s\}$. The possible (λ,μ) values are given by the coupling rule $((\eta',0)\otimes(0,\eta) = \oplus_{k=0}^{\min(\eta',\eta)}(\eta'-k,\eta-k))$ [88].

In this formalism the orbital angular momentum and spin have the following expressions

$$L_{1\mu} \equiv \mathcal{F}^{(1,1)\,0}_{11\mu\,0}, \quad S_{1\mu} \equiv \mathcal{F}^{(0,0)\,1}_{100\,\mu} \tag{2.87}$$

A frequently occurring $SU(3)$ tensor is the one-body unit tensor, which according with the general formula for coupling $SU(3)$ tensor operators (2.86) is simple a tensor product of $SU(3)$ creation and annihilation operators,

$${}^{(1,1)}\mathcal{F}^{(\lambda\mu)\kappa LM_L SM_S}_{(\eta',0)(0,\eta)\frac{1}{2}\frac{1}{2}} = \left[a^{\dagger}_{(\eta',0)\frac{1}{2}} \otimes \tilde{a}_{(0,\eta)\frac{1}{2}}\right]^{(\lambda\mu)\kappa LM_L SM_s}. \tag{2.88}$$

For the single-shell calculations, using the one-body unit tensor operator defined by the eq. (2.88), a general $SU(3)$ tensor given by the eq. (2.86) will be written in terms of the reduced single-particle matrix elements [27]

$$\begin{aligned}
\mathcal{F}^{(\lambda,\mu)S}_{\kappa LM_L M_S} &= \langle (\eta 0)\tfrac{1}{2} || f^{(\lambda,\mu)S} || (\eta 0)\tfrac{1}{2}\rangle \\
&\times \left(\frac{2\dim(\eta,0)}{(2S+1)(\dim(\lambda,\mu))}\right)^{1/2} \{\sum_{ll'}\sum_{mm'}\sum_{m_s m'_s} (-1)^{\eta+l-m+1/2-m_s} \\
&\times \langle \tfrac{1}{2} m'_s, \tfrac{1}{2} - m_s | S M_S\rangle
\end{aligned}$$

$$\times \quad \langle((\eta,0)l';(0,\eta)l||(\lambda,\mu)\kappa L)\langle l'm',l-m|LM\rangle$$

$$\times \quad a^{\dagger}_{(\eta 0)l'm'\frac{1}{2}m'_s} a_{(0\eta)lm\frac{1}{2}m_s}\} \tag{2.89}$$

An $SU(3)$ reduced (triple-barred) matrix element $\langle \ldots ||| - ||| \ldots \rangle$ (see Appendix A.5) has been used in this result. As the functional form of the operator is the same for protons and neutrons, the label σ can be suppressed. The $SU(3)$ and $SU(2)$ tensor forms for the corresponding single-particle operators are given [27]

$$l_\mu = f^{(1,1);0}_{11\mu\ 0}, \tag{2.90}$$

$$s_\mu = f^{(0,0);1}_{100\ \mu}, \tag{2.91}$$

$$q_\mu = \sqrt{1/3} f^{(1,1);0}_{12m\ 0}. \tag{2.92}$$

$$\tag{2.93}$$

The triple-bar matrix elements for the orbital angular momentum, spin, and quadrupole operators are listed [27] below:

$$\langle(\eta,0);\frac{1}{2}|||\mathbf{l}|||(\eta,0);\frac{1}{2}\rangle = \left[\frac{4}{3}C_2(\eta,0)\right]^{1/2}, \tag{2.94}$$

$$\langle(\eta,0);\frac{1}{2}|||\mathbf{s}|||(\eta,0);\frac{1}{2}\rangle = \left[\frac{3}{4}\right]^{1/2}, \tag{2.95}$$

$$\langle(\eta,0);\frac{1}{2}|||\mathbf{q}|||(\eta,0);\frac{1}{2}\rangle = [4C_2(\eta,0)]^{1/2}, \tag{2.96}$$

where $C_2(\lambda,\mu)$ indicates the eigenvalue of the second order Casimir invariant of $SU(3)$ in the (λ,μ) irrep. Substituting the last three formulas into the general formula for an $SU(2)$ operator, and following the labeling convention from eq. (2.85), yields

$$\mathcal{L}_\mu = [1/3\dim(\eta,0)C_2(\eta,0)]^{1/2}\left[a^{\dagger}_{(\eta,0)\frac{1}{2}} \otimes \tilde{a}_{(0,\eta)\frac{1}{2}}\right]^{(1,1);110}_{1\quad\ \mu} \tag{2.97}$$

$$\mathcal{S}_\mu = [1/2\dim(\eta,0)]^{1/2}\left[a^{\dagger}_{(\eta,0)\frac{1}{2}} \otimes \tilde{a}_{(0,\eta)\frac{1}{2}}\right]^{(0,0);101}_{1\quad\ \mu} \tag{2.98}$$

$$Q_M = [\dim(\eta,0)C_2(\eta,0)]^{1/2}\left[a^\dagger_{(\eta,0)\frac{1}{2}} \otimes \tilde{a}_{(0,\eta)\frac{1}{2}}\right]^{(1,1);120}_{2\quad M} \tag{2.99}$$

Examples that will be used later are the tensor expansions for the single particle spin-orbit and orbit-orbit interactions [94]:

$$\begin{aligned}\sum_i l_i \cdot s_i &= \sum_{(\lambda,\lambda)l} [a^\dagger_{(\eta,0)l\frac{1}{2}} \tilde{a}_{(0,\eta)l\frac{1}{2}}]^{(\lambda,\lambda)0,0,0}_0 \langle((\eta,0)l,(0,\eta)l\|(\lambda,\lambda)0\rangle \\ &\quad \times(-)^\eta [\frac{1}{2}l(l+1)(2l+1)]^{\frac{1}{2}}\end{aligned} \tag{2.100}$$

and

$$\begin{aligned}\sum_i l_i^2 &= \sum_{(\lambda,\lambda)l} [a^\dagger_{(\eta,0)l\frac{1}{2}} \tilde{a}_{(0,\eta)l\frac{1}{2}}]^{(\lambda,\lambda)1,1,0}_0 \langle((\eta,0)l,(0,\eta)l\|(\lambda,\lambda)1\rangle \\ &\quad \times(-)^\eta [l(l+1)][2(2l+1)]^{\frac{1}{2}}.\end{aligned} \tag{2.101}$$

It is possible to define a two-body $SU(3)$ unit tensor, ${}^{(2,2)}\mathcal{F}$, as a product of a unit tensor ${}^{(2,0)}\mathcal{F}$ that creates a pair of particles and one ${}^{(0,2)}\mathcal{F}$ that annihilates a particle pair,

$$\begin{aligned}&{}^{(2,2)}\mathcal{F}^{\rho(\lambda,\mu)\kappa LM_L SM_S}_{(\lambda_1,\mu_1)(\lambda_2,\mu_2)S_1S_2} \equiv \\ &\quad \left[{}^{(2,0)}\mathcal{F}^{(\lambda_1,\mu_1)S_1}_{(\eta_1',0)(\eta_1,0)\frac{1}{2}\frac{1}{2}} \times {}^{0,2}\mathcal{F}^{(\lambda_2,\mu_2)S_2}_{(0,\eta_2')(0,\eta_2)\frac{1}{2}\frac{1}{2}}\right]^{\rho(\lambda,\mu)\kappa LM_L SM_S},\end{aligned} \tag{2.102}$$

where the pair creation and annihilation unit tensors are defined as:

$$\begin{aligned}{}^{(2,0)}\mathcal{F}^{(\lambda,\mu)\kappa LM_L SM_S}_{(\eta',0)(\eta,0)\frac{1}{2}\frac{1}{2}} &\equiv \left[a^\dagger_{(\eta',0)\frac{1}{2}} \otimes a^\dagger_{(\eta,0)\frac{1}{2}}\right]^{(\lambda,\mu)\kappa LM_L SM_S} \\ {}^{(0,2)}\mathcal{F}^{(\mu,\lambda)\kappa LM_L SM_S}_{(0,\eta')(0,\eta)\frac{1}{2}\frac{1}{2}} &\equiv \left[\tilde{a}_{(0,\eta')\frac{1}{2}} \otimes \tilde{a}_{(0,\eta)\frac{1}{2}}\right]^{(\mu,\lambda)\kappa LM_L SM_S}.\end{aligned} \tag{2.103}$$

A general two-body operator,

$$G = \sum_{i<j=1}^{N} g(x_i\,\sigma_i, x_j\,\sigma_j)\,, \tag{2.104}$$

can be expressed in second quantization as

$$G = \frac{1}{4} \sum_{\beta,\gamma,\delta,\epsilon} \langle \beta\gamma | f | \delta\epsilon \rangle a^{\dagger}_{\beta} a^{\dagger}_{\gamma} a_{\delta} a_{\epsilon} \ , \tag{2.105}$$

where $\langle \beta\gamma|$ and $|\delta\epsilon\rangle$ are normalized antisymmetric two-particle states.

As an example, consider the pairing interaction which can be written in second quantization as

$$V_P = -\frac{1}{4} G \sum_{\gamma,\gamma'} a^{\dagger}_{\gamma} a^{\dagger}_{\tilde{\gamma}} a_{\gamma'} a_{\tilde{\gamma}'} \ , \tag{2.106}$$

where $\tilde{\gamma}$ and $\tilde{\gamma}'$ denote the time reversed partners of single-particle states γ and γ' respectively, and G is the strength of the pairing interaction. In terms of second quantization [9],

$$V_P = \frac{G}{2} \sum_{(\lambda_1,\mu_1)(\lambda_2,\mu_2)} \sum_{\eta\eta'} P_{\eta\eta'}((\lambda_1,\mu_1)(\lambda_2,\mu_2)\rho_0(\lambda_0\mu_0)) \tag{2.107}$$

$$\left[[a^{\dagger}_{\eta} \otimes a^{\dagger}_{\eta}]^{\lambda_1\mu_1} \otimes [\tilde{a}_{\eta'} \otimes \tilde{a}_{\eta'}]^{\lambda_2\mu_2}\right]^{\rho_0\lambda_0\mu_0\kappa_0=1l_0=s_0=0} \ , \tag{2.108}$$

where the coefficient $P_{\eta\eta'}(\ldots)$ involves a sum over the product of three $SU(3)$ reduced coupling coefficients

$$\begin{aligned} & P_{\eta\eta'}((\lambda_1,\mu_1)(\lambda_2,\mu_2)\rho_0(\lambda_0\mu_0)) \\ &= (-1)^{l-l'}\sqrt{(2l+1)(2l'+1)} < (\eta 0)l;(\eta 0)l||(\lambda_1\mu_1)10 > \\ &\quad \times < (\eta' 0)l;(\eta' 0)l||(\lambda_2\mu_2)10 >< (\lambda_1\mu_1)l;(\lambda_2\mu_2)l||(\lambda_0\mu_0)10 >_{\rho_0} \ . \end{aligned} \tag{2.109}$$

In the pairing-plus-quadrupole model realized in the framework of the $SU(3)$ scheme [9], the pairing force is shown to break the $SU(3)$ symmetry and remove almost all degeneracies which occur in the pure symmetry limits of the theory.

Adding the one-body spin-orbit and orbit-orbit interactions, and the two-body pairing interaction to a $SU(3)$ Hamiltonian breaks the $SU(3)$ symmetry. If a dominating quadrupole-quadrupole

interaction is assumed, however, $SU(3)$ still remains extremely useful as an approximate symmetry. Specifically, this allows one to restrict the configuration space to $SU(3)$ irreps with a large C_2 value and to use group theoretical tools for the evaluation of all required matrix elements.

A realistic Hamiltonian that accounts for single-particle effects as well as collective properties is given by the expression

$$\mathbf{H}_{SU(3)} = \frac{\chi}{2}\mathbf{Q}\cdot\mathbf{Q} + G_\pi \mathbf{H}_P^\pi + G_\nu \mathbf{H}_P^\nu + \sum_{i,\ \sigma=\pi,\nu} (D_\sigma \mathbf{l}_{i\sigma}^2 + C_\sigma \mathbf{l}_{i\sigma}\cdot\mathbf{s}_{i\sigma}) + a\mathbf{K}_J + b\mathbf{J}^2 \qquad (2.110)$$

where i runs over all particles in the shell. The spin-orbit force tends to keeps a system from realizing its maximum deformation, that is, it drives the system towards smaller $k\beta$ values. For a strong spin-orbit interaction, mixing becomes so strong that the shape is no longer defined [9].

Although symmetry breaking effects of the single-particle spin-orbit interaction are strong in all nuclei, they do not preclude the use of the $SU(3)$ scheme for light nuclei with $A \leq 28$ nor in heavy deformed systems with $A \geq 150$ because in the latter case the pseudo-spin concept can be applied which then leads to a pseudo-realization of $SU(3)$. In this representation the spin-orbit interaction is weak enough to yield good pseudo-$SU(3)$ quantum numbers.

Chapter 3. Pseudo-$SU(3)$ Model

3.1 Introduction

Recent improvements in nuclear spectroscopy have made possible the measurements of lifetimes of highly excited, low-spin states that were previously inaccessible. On-going experiments are searching for new energy levels. For example, in the last few years new levels have been identified in well-deformed rotational nuclei of the lanthanide region: ^{168}Er [22, 32, 87], ^{154}Gd [114], ^{164}Dy [33], ^{166}Er [50], ^{158}Gd [23], ^{162}Dy [111].

Successful applications of the $SU(3)$ shell model [42, 43] to light deformed nuclei have led physicists to explore similar concepts in heavy deformed systems. One of the first challenges encountered when developing a shell-model theory for heavy nuclei is that the splitting of the single-particle levels generated by the spin-orbit interaction is comparable in magnitude to the major shell separation of the harmonic oscillator and thus renders the usual $SU(3)$ symmetry useless, and with it the logic underlying an $SU(3)$-based truncation scheme that proved to be so valuable in light deformed nuclear systems.

Fortunately, another symmetry appears as a result of the large spin-orbit splitting; namely, the so-called pseudo-$SU(3)$ scheme which can be appreciated most easily by considering the near degeneracy of the orbital pairs $[(l-2)_{j=(l-2)+1/2}, l_{j=l-1/2}]$ which together define a pseudo-shell with one quantum less than the original (parent) configuration, $\tilde{\eta} = \eta - 1$ where η is the principal quantum number of the parent shell [58, 1, 94]. The pseudo-spin doublets with quantum numbers $\tilde{j} = j$ and $\tilde{l} = l - 1$ define the sub-shell structure of the pseudo-shell, which is just the original shell less its highest $j = \eta + 1/2$ level. The physical underpinnings of the pseudo-spin symmetry, and by extension the pseudo-$SU(3)$ model, have been explored recently in terms of a relativistic (Dirac) formulation of mean-field results for heavy nuclei [18, 52, 78].

A second challenge that is encountered in developing a shell-model theory for heavy nuclei is the dimensionality of the model space which increases very sharply as one moves to higher shells. This growth in the dimensionality of the model space can only be managed by truncating the model space

to a small, carefully selected subset of the full space. Since in light deformed nuclei the quadrupole-quadrupole interaction is dominant so the ground state can be represented by a few irreducible representations (irreps) of $SU(3)$ [1, 95, 106, 108], it is natural to assume that one can similarly truncate the model space in heavy nuclei to those representations, in this case of pseudo-$SU(3)$, that correspond to the largest (pseudo) intrinsic deformation. Indeed, most calculations carried out to date have truncated the space to a single, or at most 2 or 3 irreps with a very simple mechanism for generating the splitting and, in the latter case, mixing of pseudo-$SU(3)$ representations.

The development of a computer code that is able to calculate reduced matrix elements for any type of physical operator between different $SU(3)$ irreps [7] has made it possible to include realistic $SU(3)$ symmetry breaking terms, like the pairing interaction, in $SU(3)$-model Hamiltonians. Indeed, recent results using this code show that the pairing interaction is closely tied to the development of triaxiality in strongly deformed systems [104, 9]. Furthermore, complete model-space calculations in the pf-shell [108, 113] show that a very good description of the low-energy spectra can be obtained when the Hilbert space is truncated, albeit not so severely, following the same logic as used in the sd-shell, namely, a dominance of the quadrupole-quadrupole interaction. These same calculations also showed that the pairing interaction is critical for a correct description of moments of inertia.

As a result of these developments, a very powerful shell-model theory for the description of normal parity states in heavy deformed nuclei has emerged. For example, the low-energy spectra of Gd and Dy isotopes, their $B(E2)$ and $B(M1)$ transitions strengths, including both the scissors and twist modes [98] and their fragmentation, have been successfully described using a realistic Hamiltonian [15].

In this chapter, the pseudo-spin symmetry and the shell model truncation and basis states are described. The $SU(3)$ Hamiltonian undergoes a unitary transformation into the pseudo-$SU(3)$ Hamiltonian. The interaction terms affected by this transformation are described in the following sections. In this chapter, the matrix elements of the transition operators in the $SU(3)$ formalism are also given.

3.2 Pseudo-$SU(3)$ Symmetry

A short review of the pseudo-spin symmetry will be given in this section. The pseudo-spin concept that was introduced first by Hecht and Adler in late sixties [58], follows naturally from the single-particle shell-model scheme. The single-particle Hamiltonian consists of the three-dimensional harmonic oscillator, H_0, and the usual one-body orbit-orbit, $\mathbf{l}^2$, and spin-orbit terms, $\mathbf{l}\cdot\mathbf{s}$,

$$H = H_0 + C\mathbf{l}\cdot\mathbf{s} + D\mathbf{l}^2. \tag{3.1}$$

The $\mathbf{l}^2$ term with $D < 0$ pushes high angular momentum states down relative to those with lower l values. The phenomenological $\mathbf{l}\cdot\mathbf{s}$ term with $C < 0$, which couples space and spin degree of freedom, is required to achieve shell closure at the magic numbers 2, 8, 20, 50, 82, and 184.

For heavy deformed nuclei, the required value of C to obtain the shell closure is so large that the spin-orbit interaction actually destroys the underlying $SU(3)$ symmetry of the oscillator. The pseudo symmetry is motivated by the observation that the $j = \eta + 1/2$ orbital of the η-th oscillator shell, which includes levels with $j = l \pm 1/2$, where $l = \eta,\ \eta - 2,\ ...,\ 1$ or 0, is pushed down among the orbitals of the next lower shell. This yields new shells with normal parity $j = 1/2,\ 3/2,\ ...,\ \eta - 1/2$ orbitals plus a $j = \eta + 1/2$ unique parity intruder in the shell above [86]. The orbitals l_j and $(l+2)_{j+2}$ form sub-shell doublets (for example, $s_{1/2} - d_{3/2}$ and $d_{5/2} - g_{7/2}$ for $\eta = 4$, or $p_{3/2} - f_{5/2}$ and $p_{7/2} - f_{9/2}$ for $\eta = 5$) which can be treated as almost degenerate levels with the same pseudo angular momentum, $\tilde{l} = l_j + 1 = (l+2)_{j+1} - 1$, and almost decoupled pseudo-spin, $\tilde{s}$.

The condition $C \approx 4D$ (or the Nilsson parameter $\mu = 2D/C \approx 0.5$) insures that the pseudo-spin is a good symmetry because the level splitting generated by the $\mathbf{l}\cdot\mathbf{s}$ and $\mathbf{l}^2$ interactions can be duplicated by the pseudo oscillator Hamiltonian plus a pseudo $\mathbf{l}^2$ interaction and a very small pseudo $\mathbf{l}\cdot\mathbf{s}$ term [3, 58]. In Figure 3.1 the eigenvalues of the single-particle Hamiltonian (3.1) are plotted as a function of the Nilsson parameter $\mu = 2D/C$ that measures the relative strengths of the $\mathbf{l}^2$ and $\mathbf{l}\cdot\mathbf{s}$ terms. The orbital pairs with $j = l + 1/2$ and $j = (l+2) - 1/2$ are found to be degenerate for all l values for $\mu = 0.5$. Bahri *et.al.* have defined a special "normal $\leftrightarrow$ pseudo" unitary transformation,

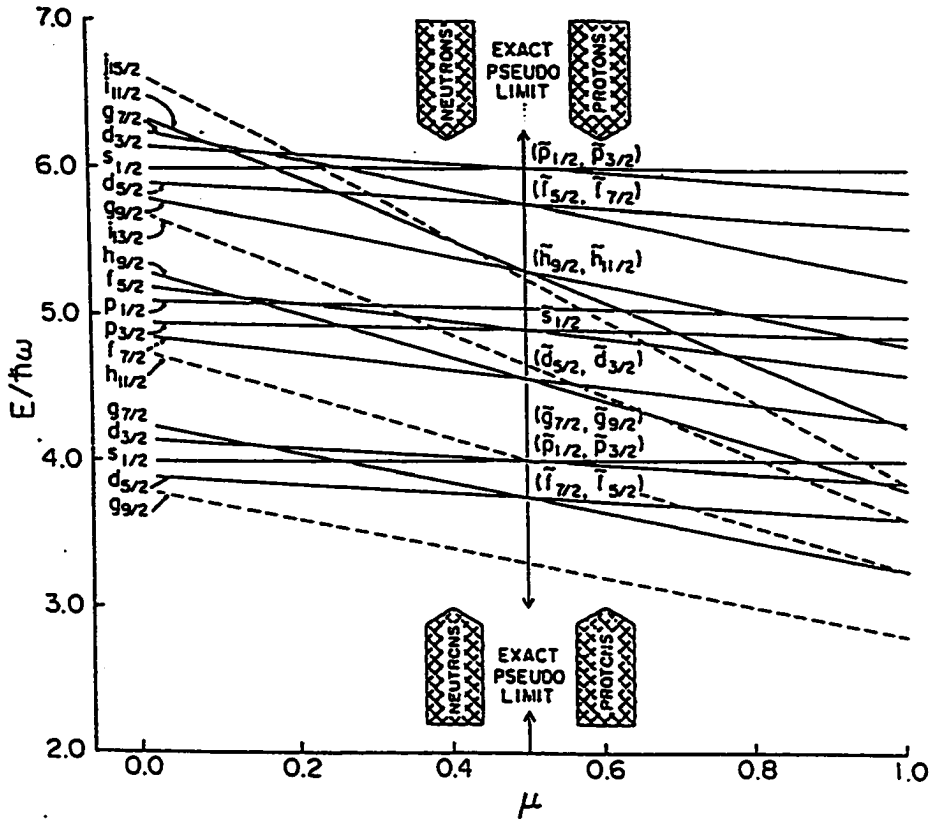

FIGURE 3.1. Eigenvalues of the reduced single-particle Hamiltonian given by $H/(\hbar\omega) = n - \kappa(2l \cdot s + \mu l^2)$, where $\mu = 2D/C$ and $\kappa = -C/(2\hbar\omega)$, for the value $\kappa = 0.05$ and $0.0 \leq \mu \leq 1.0$. (From Bahri, Draayer and Moszkowski, Ref. [6].)

that takes the quantum numbers η, l, s, j and m into the pseudo partners, $\tilde{j} = \tilde{l} + \tilde{s}$, where $\tilde{j} = j$, $\tilde{l} = l + 1$, $\tilde{\eta} = \eta - 1$, and $\tilde{s} = 1/2$,

$$|\tilde{\eta}(\tilde{l}, \tilde{s})\tilde{j}\tilde{m}\rangle = U_{\eta jm,\tilde{\eta}\tilde{j}\tilde{m}}(l, \tilde{l})|\eta(l, s)j, m\rangle, \tag{3.2}$$

$$U_{\eta jm,\tilde{\eta}\tilde{j}\tilde{m}}(l, \tilde{l}) = \delta_{\eta-1,\tilde{\eta}}\delta_{j,\tilde{j}}\delta_{m,\tilde{m}}\delta_{l\pm 1/2,\tilde{l}\mp 1/2}. \tag{3.3}$$

The $U_{\eta jm,\tilde{\eta}\tilde{j}\tilde{m}}(l, \tilde{l})$ is simply a relabeling of the basis states that associates all levels of the η-th shell, except the defector with $j = \eta + 1/2$, with levels of the $\tilde{\eta}$-th shell of a "pseudo" oscillator, $\tilde{\eta} = \eta - 1$. This unitary transformation can be written in the following label-independent operator form:

$$U_{\eta jm,\tilde{\eta}\tilde{j}\tilde{m}}(l, \tilde{l}) = 2(\eta \cdot \xi - 2l \cdot s + 3)^{-1/2}(\xi \cdot s), \tag{3.4}$$

where η creates while ξ annihilates oscillator quanta, and l and s are the single-particle orbital angular momentum and spin operators respectively. The structure of the unitary pseudo-spin transformation has been investigated extensively in the last few years [30, 17, 19].

The single-particle Hamiltonian transforms under this mapping as follows:

$$H_0 + C\mathbf{l}\cdot\mathbf{s} + D\mathbf{l}^2 \xrightarrow[-pseudo\rightarrow]{\leftarrow normal-} \tilde{H}_0 + (4D - C)\tilde{\mathbf{l}}\cdot\tilde{\mathbf{s}} + D\tilde{\mathbf{l}}^2 + (\hbar\omega + 2D - C). \tag{3.5}$$

when $\hbar\tilde{\omega} = \hbar\omega$, $\tilde{C} = (4D - C)$, and $\tilde{D} = D$, the pseudo form of the Hamiltonian $\tilde{H}$ has the same excitation spectrum as the normal one, H, since the $(\hbar\omega + 2D - C)$ term is an additive constant. For systems with $A \geq 100$, $C \approx 4D$, therefore $\tilde{C} \approx 0$. The average μ value is almost 0.5 for medium and heavy mass nuclei where $\mu_\nu \approx 0.4$ and $\mu_\pi \approx 0.6$ (ν for neutrons and π for protons).

3.3 Shell Model Truncation and Basis States

A shell-model theory for heavy nuclei requires a severe truncation of the spherical shell-model basis. The goal of truncation is to reproduce the essential physics found in low-lying states of a large space in a smaller one. This can only be achieved if the basis selection is made relative to those parts of the interaction that dominate the low-energy structure. Here the truncation is realized by utilizing physical arguments and special group symmetries. The model we employ is a many-particle Nilsson scheme with the dominance of the quadrupole-quadrupole interaction between pairs of nucleons providing justification for a further truncation. The scheme is, in essence, an adaptation for heavy nuclei of the highly successful Elliott model for light nuclei. However, since the neutrons and protons are filling different shells and the single-particle spaces are much richer, the extensions are major. The basic ingredients of the theory [36, 37, 27] are reviewed in this section.

The experimental evidence in nuclear physics supports the view that the nuclear effective interaction appropriate to low-energy excitations must have a strong correlation with the pairing and quadrupole-quadrupole ($Q \cdot Q$) interactions. In a restrictive space, pairing dominates and favors pairwise $J = 0$ couplings of nucleons. In larger, richer dimensional spaces the collective quadrupole

mode dominates and induces deformation. The dominance of the $(Q \cdot Q)$ interaction for deformed nuclei lies at the heart of the truncation scheme.

It is known that $SU(3)$ is a useful coupling scheme for deformed nuclei when the asymptotic Nilsson quantum numbers $[Nn_z\Lambda]\Omega$ for single-particle states are approximately good and when members of the Nilsson spin-orbit doublet with $\Omega = \Lambda \pm \frac{1}{2}$ are nearly degenerate [3, 58]. Since the nuclear shell structure is not much different from that of the HO for lower ds-shell nuclei, $SU(3)$ was proposed by Elliot [42, 45] as a reasonable ds-shell symmetry, one that could be used to truncate the full model space ($\sim 10^{3-5}$) down to tractable size ($\sim 10^{1-2}$). Since $Q \cdot Q$ is dominant and $Q \cdot Q = 4C_2 - 3L \cdot L$, where C_2 is the second order Casimir invariant of $SU(3)$, irreducible representations (irreps) of $SU(3)$ which have the largest values for C_2 should dominate the structure of low-lying states. Basis states belonging to this "leading" irrep of $SU(3)$ are those which have the largest intrinsic quadrupole deformation, $\langle Q_0 \rangle \propto \langle Q \cdot Q \rangle^{1/2}$. A severe truncation scheme would restrict basis states to the leading irrep. Full space ds-shell calculations have confirmed that the leading irreps do indeed comprise $(60 - 80)\%$ of yrast (lowest state of a given spin) eigenstates. Thus, for example, the (8, 4) irrep of $SU(3)$ dominates the ground state band of ^{24}Mg. The single-particle levels are then filled in the order $n_z = \eta, \eta - 1, \ldots$ and this leads to an intrinsic many-particle state which is the so-called leading irrep of $SU(3)$, that is, the configuration with the maximum eigenvalue of the second order Casimir invariant of $SU(3)$, C_2. For nuclei of the lower ds-shell these conditions are approximately satisfied and in each case the leading irrep of $SU(3)$ forms $(60 - 80)\%$ of the yrast eigenstates.

For the higher major shells the spin-orbit and centrifugal stretching perturbations completely destroy the HO shell structure. The magnitude of the spin-orbit splitting is so large that the Nilsson $\Omega = \Lambda \pm \frac{1}{2}$ levels are widely separated and $SU(3)$ is not a good symmetry. And in addition, the spin-orbit interaction pushes the state of maximum j down into the next lower shell. But the normal parity levels that remain have the same total angular momenta as the levels of an oscillator shell of one less quantum. The pseudo-$SU(3)$ scheme exploits this relationship. In all cases, however, there are new major shells. These new major shells are comprised of all of the j sub-shells of the

corresponding HO major shell except for the largest j sub-shell which is pushed into the next lower major shell. The remaining j sub-shells are grouped together and called the normal (N) parity orbitals of the new shell. In addition to these, there is the highest j sub-shell from the next higher HO shell. This "intruder" level has parity opposite to the other levels in the major shell and is called the abnormal (A) parity level. As an example consider the $\eta = 4$ harmonic oscillator shell (see Figure A.5). The $g_{9/2}$ orbital is pushed down by the spin-orbit interaction into the $\eta = 3$ shell. This accounts for the fact that 50 rather than 40 defines a shell closure. The remaining normal parity levels are relabeled by the mapping

$$(g_{7/2}, d_{5/2}, d_{3/2}, s_{1/2}) \rightarrow (\tilde{f}_{7/2}, \tilde{f}_{5/2}, \tilde{p}_{3/2}, \tilde{p}_{1/2}), \tag{3.6}$$

where $\mathbf{l} + \mathbf{s} = \mathbf{j} = \tilde{\mathbf{l}} + \tilde{\mathbf{s}}$. This mapping defines the pseudo ($\tilde{f}\tilde{p}, \tilde{\eta} = 3$) shell. (A tilde over a variable is used to denote a pseudo quantity). Hence j denotes the total angular momentum while $\tilde{f}$ is an $\tilde{l} = 3$ orbital with $\tilde{s} = \frac{1}{2}$). The $h_{11/2}$ intruder orbit of the next ($\eta = 5$) harmonic oscillator shell that is pushed down into this region by the spin-orbit term is called the abnormal parity level. A Nilsson diagram, relabeled with pseudo oscillator quantum numbers $[\tilde{\eta}\tilde{n}_z\tilde{\Lambda}]\tilde{\Omega}$, shows a clustering of the levels into pseudo spin-orbit doublets ($\tilde{\Omega} = \tilde{\Lambda} \pm \frac{1}{2}$) with small splitting which is the criterion for a successful implementation of the $SU(3)$ scheme. Here, $\tilde{\Omega}$ is the projection of the total angular momentum, $\tilde{\eta}$ is spherical principal oscillator quantum number, $\tilde{n}_z$ is the number of quanta in the z-direction, and $\tilde{\Lambda}$ is the projection of the angular momentum. As an example, see the levels $(\tilde{\Omega} = 1 - \frac{1}{2} = \frac{1}{2})[321]$ and $(\tilde{\Omega} = 1 + \frac{1}{2} = \frac{3}{2})[321]$ in Figure 3.2.

The relabeled levels form a major shell for a pseudo oscillator potential. The symmetry of this oscillator is, of course, $\widetilde{SU(3)}$. (The tilde denotes the pseudo shell realization but the abstract algebra is just $SU(3)$.) This "real" to "pseudo" shell mapping is a unitary transformation and does not change anything as far as exact full space results are concerned. A tensor decomposition of the real $Q \cdot Q$ interaction into its pseudo-$SU(3)$ components shows that it is predominantly $\tilde{Q} \cdot \tilde{Q}$, i.e., the quadrupole-quadrupole interaction of the pseudo shell. Also, although it is the spin-orbit

interaction that destroys the HO shell structure, for deformations appropriate to well-deformed nuclei ($\epsilon \sim 0.3$) one sees that the levels are grouped into pseudo spin-orbit doublets ($\tilde{\Omega} = \tilde{\Lambda} \pm 1/2$) (see Figures. 3.2-3.5). This implies that the pseudo spin-orbit splitting is small. Similarly, the equivalent of the centrifugal stretching interaction which spreads as $\tilde{l}$ values is less strong here than in the HO picture. The adding of nucleons to the closed shell tends to create an intrinsic state with the largest possible total $\tilde{n}_z$ (for fixed ϵ, $\tilde{n}_z$ decreases as energy increases) and hence the largest quadrupole moment, $\langle \tilde{Q}_0 \rangle \propto 2\tilde{n}_z - \tilde{n}_x - \tilde{n}_y = 3\tilde{n}_z - \tilde{\eta}$. These criteria are precisely what is required for a successful implementation of an $SU(3)$ scheme.

In heavy nuclei the valence protons (π) and valence neutrons (ν) fill different major shells, and hence for a given nucleus there are two open shells, one for protons and one for neutrons. Each proton or neutron shell is composed of a set of normal parity levels and the associated abnormal parity level. The normal parity space is partitioned into irreps of pseudo-$SU(3)$ and the abnormal parity space is spanned by configurations of identical particles in a single j shell. The seniority coupling scheme is appropriate for a description of the abnormal parity configurations, since in a restricted space like a single j shell the pairing part of the residual interaction tends to dominate.

In this case, the low-energy structure of the normal parity part of the space will be dominated by a few irreps of pseudo-$SU(3)$. Arrangements with high seniority are not favored because the pairing gap is large as compared to the spacing of low-lying rotational levels. Hence, we expect the configurations with low seniority to be the most important ones in the abnormal parity parts of the neutron and proton shells.

The many-particle states of N nucleons in a shell of dimension Ω are characterized by the totally antisymmetric irrep of a unitary group of dimension Ω, that is [81],

$$\begin{aligned} U(\Omega) &\leftarrow \text{group symbol} \\ [1^N] &\leftarrow \text{irrep label.} \end{aligned} \tag{3.7}$$

This group can be reduced to a direct sum of two unitary groups associated with the normal and abnormal parity spaces [81],

$$\begin{array}{ccccc} U(\Omega) & \rightarrow & U(\Omega_N) & + & U(\Omega_A) \\ [1^N] & & [1^{n_N}] & & [1^{n_A}]. \end{array} \tag{3.8}$$

The quantum numbers n_N and n_A denote the number of nucleons in the normal and abnormal parity spaces, respectively. These satisfy the inequalities

$$0 \leq n_N \leq N, \quad 0 \leq n_A \leq N \quad \text{with} \quad N = n_N + n_A. \tag{3.9}$$

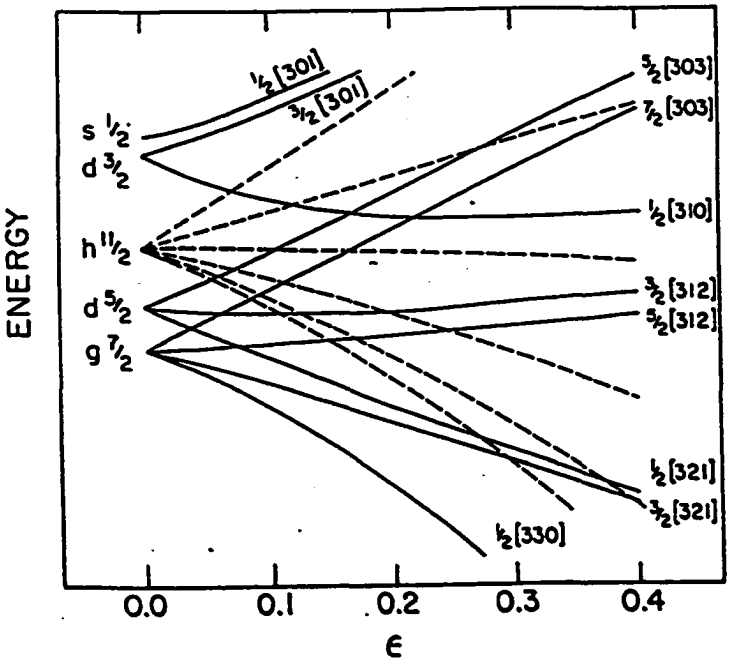

FIGURE 3.2. Nilsson level scheme for the $\tilde{\eta} = 3$ proton shell. At deformation $\epsilon = 0$ the levels are labeled with spherical shell-model quantum numbers while at $\epsilon \neq 0$ with the asymptotic pseudo quantum labels $\tilde{\Omega}[\tilde{\eta}\tilde{n}_z\tilde{\Lambda}]$ [Taken from [37]].

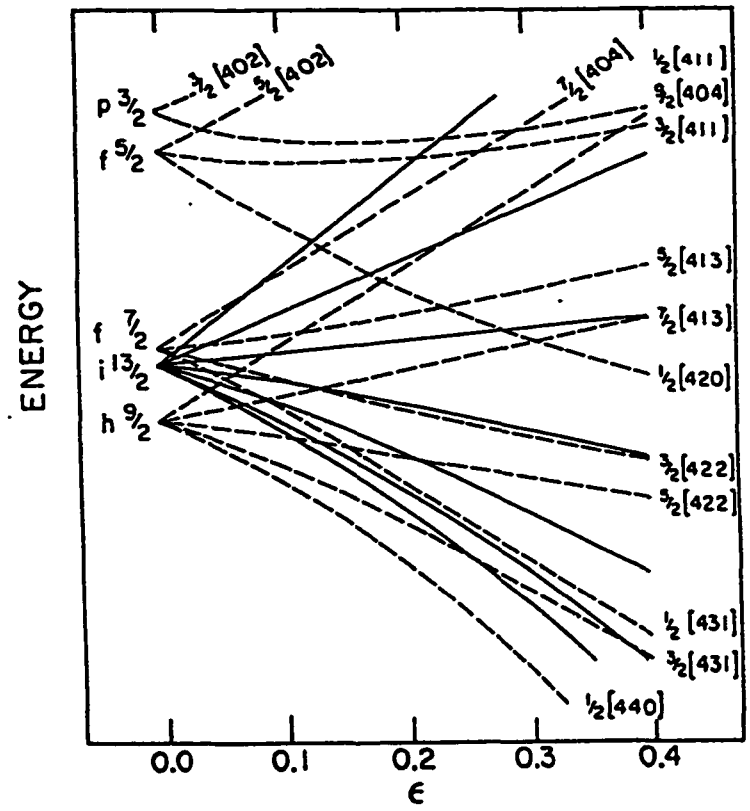

FIGURE 3.3. Nilsson level scheme for the $\tilde{\eta} = 4$ proton shell. At deformation $\epsilon = 0$ the levels are labeled with spherical shell-model quantum numbers while at $\epsilon \neq 0$ with the asymptotic pseudo quantum labels $\tilde{\Omega}[\tilde{\eta}\tilde{n}_z\tilde{\Lambda}]$ [Taken from [37]].

The strong-coupled normal parity states, $|J_N M_N\rangle$, are coupled in $O(3)$ to the abnormal parity basis states, $|J_A M_A\rangle$, to yield states of good total angular momentum,

$$|JM\rangle \equiv \{|J_N\rangle \times |J_A\rangle\}_{JM}.$$

Usually, only the normal and abnormal parity spaces associated with the most probable values of n_N and n_A are considered. These numbers are determined from the appropriate Nilsson diagrams (See Figs. 1-4). Each level is filled with a pair of protons (neutrons) in order of increasing energy. A deformation of $\epsilon \sim 0.25$ is considered appropriate for well-deformed nuclei.

The normal parity spaces are build by single-particle orbits of the pseudo harmonic oscillator shells, which for the nuclei in the rare earth region are $\tilde{\eta} = 3$ (protons) and $\tilde{\eta} = 4$ (neutrons). The

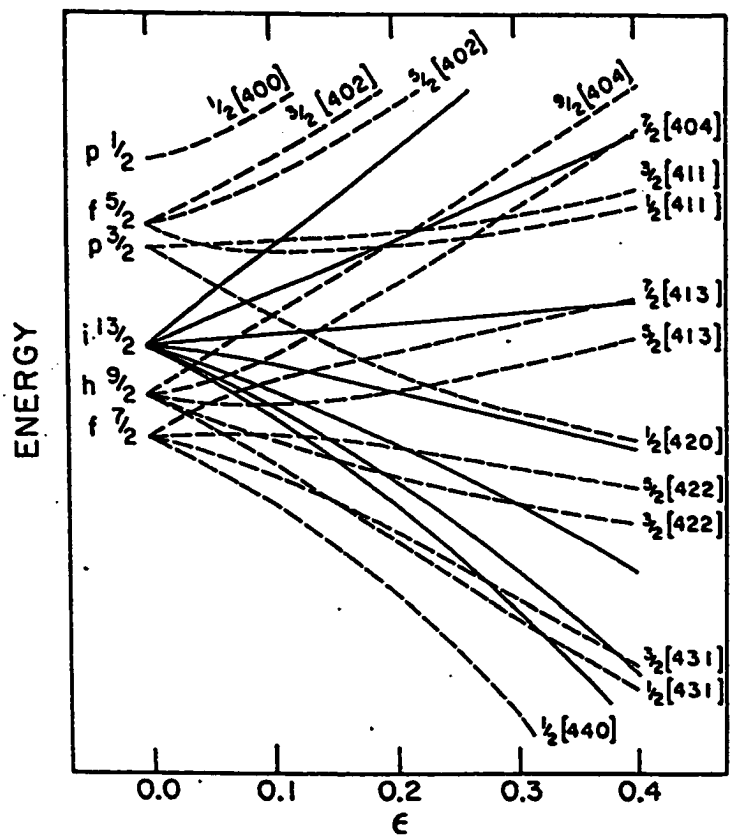

FIGURE 3.4. Nilsson level scheme for the $\tilde{\eta} = 4$ neutron shell. At deformation $\epsilon = 0$ the levels are labeled with spherical shell-model quantum numbers while at $\epsilon \neq 0$ with the asymptotic pseudo quantum labels $\tilde{\Omega}[\tilde{\eta}\tilde{n}_z\tilde{\Lambda}]$ [Taken from [37]].

corresponding intruder levels are $h_{11/2}$ and the $i_{13/2}$, respectively. The dimensions of these spaces are given by:

$$\Omega_\pi = 32, \Omega_N^\pi = 20, \Omega_A^\pi = 12$$

$$\Omega_\nu = 44, \Omega_N^\nu = 30, \Omega_A^\nu = 14.$$

These numbers are in the pseudo-shell notations, the tilde on symbols will be omitted since its presence can be inferred from context.

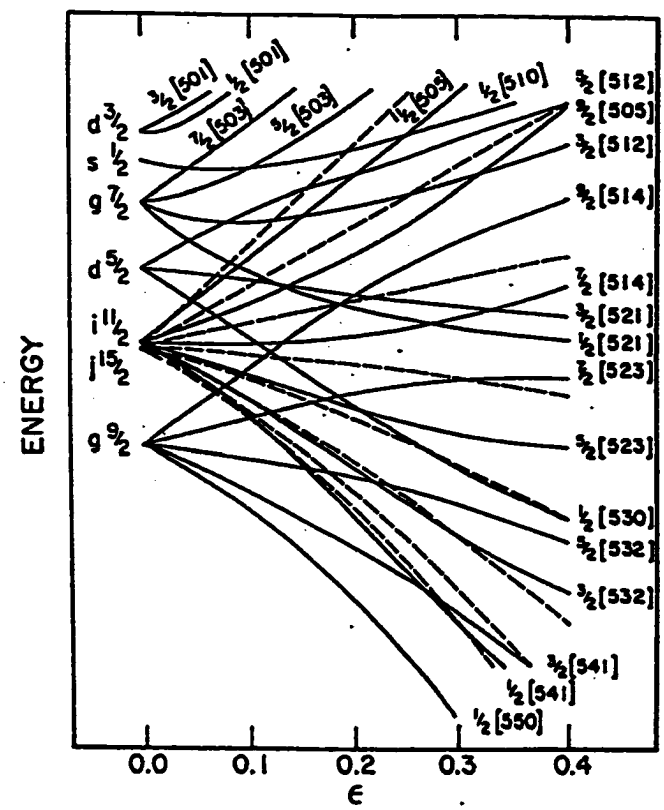

FIGURE 3.5. Nilsson level scheme for the $\tilde{\eta} = 5$ neutron shell. At deformation $\epsilon = 0$ the levels are labeled with spherical shell-model quantum numbers while at $\epsilon \neq 0$ with the asymptotic pseudo quantum labels $\tilde{\Omega}[\tilde{\eta}\tilde{n}_z\tilde{\Lambda}]$ [Taken from [37]].

The most probable occupancy of the normal and abnormal parity spaces is

$$N_\sigma = n_A^\sigma + n_N^\sigma,$$

where σ is π for protons or ν for neutrons. In terms of the group chains, the basis states are:

$$U(\Omega_N^\sigma) \rightarrow U(\Omega_N^\sigma/2) \times U(2) \rightarrow SU(3) \times SU(2) \rightarrow O(3) \times SU(2) \rightarrow SU(2), \qquad (3.10)$$

$$[1^{n_N^\sigma}] \qquad \{f_\sigma\} \qquad \{\tilde{f}_\sigma\} \quad \alpha_\sigma(\lambda_\sigma\mu_\sigma) \quad S_\sigma \quad \kappa_\sigma L_\sigma \qquad J_N^\sigma \qquad (3.11)$$

$$U(\Omega_A^\sigma) \rightarrow Sp(\Omega_A^\sigma) \rightarrow O(3), \qquad (3.12)$$

$$[1^{n_A^\sigma}] \qquad [1^{v_\sigma}] \qquad \beta_\sigma J_A^\sigma. \qquad (3.13)$$

Underneath each group the quantum numbers that characterize its irreps are given. The decomposition of $U(\Omega_N)$ into $U(\Omega_N/2) \times U(2)$ is a factorization of the normal parity space into orbital and spin degree of freedom. This is an $LS-$coupling scheme. The indices α, k, and β are multiplicity labels of the indicated reductions. Since the abnormal parity space is a single j shell, a $jj-$coupled geometry is appropriate. However, the present calculations are made under the assumption that in the abnormal parity space only the lowest total angular momentum configuration needs to be taken into account. This implies that $\beta_\pi = \beta_\nu = 1$ and $J^\pi_\lambda = J^\nu_\lambda = 0$.

Two other assumptions are made. One is that the most important normal parity configurations are those with highest spatial symmetry, $\{f\} = \{2^{n_N/2}\}$. This implies that only pseudo spin zero configurations are taken into account ($S_\pi = S_\nu = 0$). The second assumption is that the leading pseudo $SU(3)$ irreps in the proton and neutron spaces will dominate. For these representations $\alpha_\pi = \alpha_\nu = 1$.

Following these considerations, the basis states are given by

$$
\begin{aligned}
&|\{f_\pi\}(\lambda_\pi\mu_\pi), \{f_\nu\}(\lambda_\nu\mu_\nu); \rho(\lambda\mu)\kappa JM\rangle = \\
&\sum_{\substack{\kappa_\pi\kappa_\nu \\ L_\pi L_\nu}} \langle(\lambda_\pi\mu_\pi)\kappa_\pi L_\pi; (\lambda_\nu\mu_\nu)\kappa_\nu L_\nu || (\lambda\mu)\kappa J\rangle_\rho \\
&[|\{f_\pi\}(\lambda_\pi\mu_\pi)\kappa_\pi L_\pi\rangle \times |\{f_\nu\}(\lambda_\nu\mu_\nu)\kappa_\nu L_\nu\rangle]^J_M. \qquad (3.14)
\end{aligned}
$$

In this equation, $\langle -; - || - \rangle_\rho$ is a reduced $SU(3) \rightarrow O(3)$ coupling coefficient and $[\ldots]^J_M$ denotes angular momentum coupling.

3.4 Tensorial Expansions of the Electromagnetic Transitions Operators

The electric (E) and magnetic (M) transition operators as well as their matrix elements in the pseudo-$SU(3)$ model are given in this section. These operators in the long-wavelength approximation

are given by [24]:

$$T^L_M(E) = b_0^L \sum_\sigma \sum_i e_\sigma r^L_\sigma(i) Y_{LM}(r_\sigma(i)), \tag{3.15}$$

$$T^L_M(M) = b_0^{(L-1)} \mu_N \sum_\sigma \sum_i \left\{ \left[g^s_\sigma \mathbf{s}^\sigma(i) + \frac{2g^o_\sigma}{L+1} \mathbf{l}^\sigma(i) \right] \cdot [\nabla_\sigma(i) r^L_\sigma(i) Y_{LM}(r_\sigma(i))] \right\} \tag{3.16}$$

where $\sigma = \pi$ or ν, $b_0 = A^{1/6} fm$ is the harmonic oscillator size parameter, g^s and g^o are spin and orbital g factors, e is the charge, and μ_N denotes the nuclear magneton. Since other theories use effective g-factors, it has to be noted that in this work the "bare" orbital and spin g factors for protons and neutrons are used, that is,

$$g^o_\pi = 1, \;\; g^o_\nu = 0 \quad \text{and} \quad g^s_\pi = 5.5857, \;\; g^s_\nu = -3.8263 \,. \tag{3.17}$$

Using the following operators:

$$L^\sigma_\mu = \sum_i l^\sigma_\mu(i) = \frac{1}{i\sqrt{2}} \sum_i [\mathbf{r}_\sigma(i) \times \mathbf{p}_\sigma(i)]_{1\mu} \tag{3.18}$$

$$S^\sigma_\mu = \sum_i \mathbf{s}^\sigma_\mu(i), \tag{3.19}$$

$$Q^\sigma_M = \sum_i q^\sigma_M(i) = \sum_i \sqrt{16\pi/5} r^2_\sigma(i) Y_{2M}(r_\sigma(i)), \tag{3.20}$$

the M1 and E2 transition operators are rewritten as:

$$T^1_\mu(M) = \sqrt{3/4\pi} \mu_N \sum_\sigma \left\{ g^o_\sigma L^\sigma_\mu + g^s_\sigma S^\sigma_\mu \right\}, \tag{3.21}$$

$$T^2_M(E) = \sqrt{5/16\pi} b_0^2 \sum_\sigma e_\sigma Q^\sigma_M. \tag{3.22}$$

Employing the $SU(3)$-tensorial expressions for the orbital and spin angular momentum operators and that of the quadrupole operator, the transition operators will be written in a general expression:

$$\begin{aligned} T^{J_0}_{M_0} &= \sum_{\sigma=\pi,\nu} T^{J_0}_{M_0}(\sigma) \\ &= \sum_{\sigma} A_{J_0} C^{J_0}_t(\tilde{\eta}_\sigma; \tilde{\lambda}_0, \tilde{\mu}_0, \tilde{\kappa}_0, \tilde{L}_0, \tilde{S}_0) \\ &\times \left\{ a^\dagger_{(\tilde{\eta}_\sigma,0);1/2)} \times a^\dagger_{(0,\tilde{\eta}_\sigma);1/2} \right\}^{(\tilde{\lambda}_0,\tilde{\mu}_0);\tilde{S}_0, J_0,}_{\tilde{\kappa}_0 \tilde{L}_0 \quad M_0}, \end{aligned} \tag{3.23}$$

where,

$$A_1 \equiv \sqrt{3/4\pi}\mu_N, \tag{3.24}$$

$$A_2 \equiv \sqrt{5/16\pi} b_0^2, \tag{3.25}$$

$$A_3 \equiv \sqrt{105/16\pi}\mu_N b_0^2, \tag{3.26}$$

and the tensor expansion coefficients $C^{J_0}_t$ can be evaluated employing angular momentum and $SU(3)$ coupling coefficients.

From eq. (3.21) we see immediately that the tensorial coefficients for the magnetic dipole transition operator can be written as

$$C^1_t(\tilde{\eta}_\sigma; \tilde{\lambda}_0, \tilde{\mu}_0, \tilde{\kappa}_0, \tilde{L}_0, \tilde{S}_0) = g^o_\sigma C^1_l(\tilde{\eta}_\sigma; \tilde{\lambda}_0, \tilde{\mu}_0, \tilde{\kappa}_0, \tilde{L}_0, \tilde{S}_0) + g^s_\sigma C^1_s(\tilde{\eta}_\sigma; \tilde{\lambda}_0, \tilde{\mu}_0, \tilde{\kappa}_0, \tilde{L}_0, \tilde{S}_0) \tag{3.27}$$

where C^1_l and C^1_s are the coefficients of the orbital and spin angular momenta, respectively. To calculate these two coefficients, we need to calculate first the reduced matrix elements of **l** and **s** with respect to the single-particle states and then substitute the results in the following equation:

$$C^J_g(\tilde{\eta}; (\tilde{\lambda}_0, \tilde{\mu}_0), \tilde{\kappa}_0, \tilde{L}_0, \tilde{S}_0) =$$

$$
\begin{aligned}
&= \sum_{ll'}\sum_{jj'}\langle(\eta,0)l;\tfrac{1}{2},j||g^J||(\eta,0)l';\tfrac{1}{2},j'\rangle \\
&\quad\times\{(-1)^{\eta}\sqrt{(2j+1)(2J+1)}\begin{Bmatrix} \tilde{l} & \frac{1}{2} & j \\ \tilde{l}' & \frac{1}{2} & j' \\ \tilde{L}_0 & \tilde{S}_0 & 1 \end{Bmatrix} \\
&\quad\times\langle(\tilde{\eta},0)\tilde{l};(0,\tilde{\eta})\tilde{l}'||(\tilde{\lambda}_0,\tilde{\mu}_0)\tilde{\kappa}_0\tilde{L}_0\rangle\} \\
&= \sum_{ll'}\sum_{jj'}\langle(\eta,0)l;\tfrac{1}{2},j||g^J||(\eta,0)l';\tfrac{1}{2},j'\rangle \\
&\quad\times B^J(j,j',\tilde{l},\tilde{l}';\tilde{\eta};\tilde{\lambda}_0,\tilde{\mu}_0,\tilde{\kappa}_0,\tilde{L}_0,\tilde{S}_0) \qquad (3.28)
\end{aligned}
$$

The expresion $B^J(\ldots)$ depends only on the tensorial rank, J, of the one-body operator. The symbol $\{\ldots\}$ is used to denote a unitary 9-J symbol and the B^J coefficient is defined by eq. (3.28). There are computer codes [2] available for calculating both $SU(3) \rightarrow O(3)$ coupling and recoupling coefficients and hence for all the factors that enter in eq. (3.23). After the substitution, the coefficients are given by the following expresions:

$$
\begin{aligned}
&C^1_l(\tilde{\eta};(\tilde{\lambda}_0,\tilde{\mu}_0),\tilde{\kappa}_0,\tilde{L}_0,\tilde{S}_0) = \\
&\quad= \sum_{l}\sum_{jj'}[2(2l+1)l(l+1)/(2j+1)]^{1/2}\begin{Bmatrix} l & \frac{1}{2} & j \\ l & \frac{1}{2} & j' \\ 1 & 0 & 1 \end{Bmatrix} \\
&\qquad\times B^1(j,j',\tilde{l},\tilde{l};\tilde{\eta}_\sigma;\tilde{\lambda}_0,\tilde{\mu}_0,\tilde{\kappa}_0,\tilde{L}_0,\tilde{S}_0) \qquad (3.29)
\end{aligned}
$$

$$
\begin{aligned}
&C^1_s(\tilde{\eta};(\tilde{\lambda}_0,\tilde{\mu}_0),\tilde{\kappa}_0,\tilde{L}_0,\tilde{S}_0) = \\
&\quad= \sum_{l}\sum_{jj'}[(3/2)(2l+1)/(2j+1)]^{1/2}\begin{Bmatrix} l & \frac{1}{2} & j \\ l & \frac{1}{2} & j' \\ 0 & 1 & 1 \end{Bmatrix} \\
&\qquad\times B^1(j,j',\tilde{l},\tilde{l};\tilde{\eta}_\sigma;\tilde{\lambda}_0,\tilde{\mu}_0,\tilde{\kappa}_0,\tilde{L}_0,\tilde{S}_0)\,, \qquad (3.30)
\end{aligned}
$$

The tensorial coefficients for the electric quadrupole transition operator are given by

$$C_t^2(\tilde{\eta}_\sigma;\tilde{\lambda}_0,\tilde{\mu}_0,\tilde{\kappa}_0,\tilde{L}_0,\tilde{S}_0) = e_\sigma C_q^2(\tilde{\eta}_\sigma;\tilde{\lambda}_0,\tilde{\mu}_0,\tilde{\kappa}_0,\tilde{L}_0,\tilde{S}_0) \tag{3.31}$$

The expression for the C_q^2 coefficient is:

$$\begin{aligned} & C_q^2(\tilde{\eta_\sigma};(\tilde{\lambda}_0,\tilde{\mu}_0),\tilde{\kappa}_0,\tilde{L}_0,\tilde{S}_0) \\ &= \sum_{ll'}\sum_{jj'}[8(2l+1)C_2(\eta_\sigma,0)/(2j+1)]^{1/2}\,\langle(\eta_\sigma,0)l';(1,1)12||(\eta_\sigma,0)l\rangle \\ &\quad \times\chi \begin{Bmatrix} l & \frac{1}{2} & j \\ l' & \frac{1}{2} & j' \\ 2 & 0 & 2 \end{Bmatrix} B^2(j,j',\tilde{l},\tilde{l}';\tilde{\eta}_\sigma;\tilde{\lambda}_0,\tilde{\mu}_0,\tilde{\kappa}_0,\tilde{L}_0,\tilde{S}_0) \end{aligned} \tag{3.32}$$

In the present calculations the pseudo quadrupole operator $\tilde{Q}$ instead of the real operator Q is used. Castaños *et.al.* have shown in [27] that the results for $E2$ strengths using the real quadrupole operator Q differ by less than 5% from these of calculations that use the operator $\tilde{Q}$ which is a generator of the pseudo-$SU(3)$ symmetry. The $(\tilde{\lambda}_0,\tilde{\mu}_0) = (1,1)$ tensor dominates in all the shells. This means that the real quadrupole moment operator is effectively proportional to the corresponding operator of the pseudo space; that is,

$$Q_m = \chi\,\tilde{Q}_m, \tag{3.33}$$

where χ is given by the ratio of the expectation value of r^2 in the $\eta_\sigma = \tilde{\eta}_\sigma + 1$ and $\tilde{\eta}_\sigma$ shells ($\chi = \frac{\langle C_2\rangle_{\max}}{\langle \tilde{C}_2\rangle_{\max}} = \frac{\eta+1}{\eta}$). The label $\sigma = \pi$, or ν is used to denote protons or neutrons and we have to keep in mind that they belong to different shells.

3.4.1 Matrix Elements of Transition Operators

The reduced matrix elements of the transition operator, Eq. (3.23), between $SU(3)$ strong-coupled wavefunctions, Eq. (2.29), are given by:

$$\begin{aligned}
&\langle\{f_\pi\}(\lambda'_\pi,\mu'_\pi),\{f_\nu\}(\lambda'_\nu,\mu'_\nu);\rho'(\lambda',\mu')\kappa'J'||T^{J_0}||\{f_\pi\}(\lambda_\pi,\mu_\pi),\{f_\nu\}(\lambda_\nu,\mu_\nu);\rho(\lambda,\mu)\kappa J\rangle \\
&= \sum_\sigma \sum_{\lambda_0\mu_0\kappa_0} A_{J_0} C_t^{J_0}(\eta_\sigma;\lambda_0,\mu_0,\kappa_0,J_0,0) \\
&\times \langle\{f_\pi\}(\lambda'_\pi,\mu'_\pi),\{f_\nu\}(\lambda'_\nu,\mu'_\nu);\rho'(\lambda',\mu')\kappa'J'||\Lambda^{\sigma;(\lambda_0,\mu_0)}_{\kappa_0 J_0}|| \\
&\times \{f_\pi\}(\lambda_\pi,\mu_\pi),\{f_\nu\}(\lambda_\nu,\mu_\nu);\rho(\lambda,\mu)\kappa J\rangle, \qquad (3.34)
\end{aligned}$$

where:

$$\Lambda^{\sigma;(\lambda_0,\mu_0)}_{\kappa_0 J_0 M_0} \equiv \left\{ a^+_{(\eta_\sigma,0);1/2} \times \tilde{a}_{(0,\eta_\sigma);1/2} \right\}^{(\lambda_0,\mu_0);0}_{\kappa_0 J_0 M_0;0}. \qquad (3.35)$$

The $\{f_\sigma\}$ with σ equal to π or ν are chosen to be the most symmetric partitions that characterize the irreps of $U(\Omega^\sigma_N)$. This means that total spin of the states is zero and as a consequence the matrix elements of tensors with $S_0 \neq 0$ vanish. To simplify the notation, the spin labels are therefore suppressed in labeling the basis states, and the tilde over the quantum numbers is also suppressed whenever its presence can be easily inferred from context. The matrix element can be rewritten by introducing a 9-$(\lambda,\ \mu)$ coefficient, hence in this way no sums over outer multiplicity labels are involved [57].

$$\begin{aligned}
&\langle\{f_\pi\}(\lambda'_\pi,\mu'_\pi),\{f_\nu\}(\lambda'_\nu,\mu'_\nu);\rho'(\lambda',\mu')\kappa'J'||T^{J_0}||\{f_\pi\}(\lambda_\pi,\mu_\pi),\{f_\nu\}(\lambda_\nu,\mu_\nu);\rho(\lambda,\mu)\kappa J\rangle \\
&= \sum_\sigma \sum_{\lambda_0\mu_0\kappa_0} A_{J_0} C_t^{J_0}(\eta_\sigma;\lambda_0,\mu_0,\kappa_0,J_0,0) \\
&\times \sum_{\rho_f} ((\lambda,\mu)\kappa J;(\lambda_0,\mu_0)\kappa_0 J_0||(\lambda',\mu')\kappa' J')_{\rho_f}
\end{aligned}$$

$$\times \sum_{\rho_\pi \rho_\nu} \chi \left\{ \begin{array}{cccc} (\lambda_\pi, \mu_\pi) & (\lambda_\tau, \mu_\tau) & (\lambda'_\pi, \mu'_\pi) & \rho_\pi \\ (\lambda_\nu, \mu_\nu) & (\lambda_s, \mu_s) & (\lambda'_\nu, \mu'_\nu) & \rho_\nu \\ (\lambda, \mu) & (\lambda_0, \mu_0) & (\lambda', \mu') & \rho_f \\ \rho & 1 & \rho' & \end{array} \right\}$$
$$\times \langle \{f_\sigma\}(\lambda'_\sigma, \mu'_\sigma) \; ||| \Lambda^{\sigma;(\lambda_0,\mu_0)} ||| \; \{f_\sigma\}(\lambda_\sigma, \mu_\sigma) \rangle, \tag{3.36}$$

where $(\lambda_\tau, \mu_\tau) = (\lambda_0, \mu_0)$ $[(0, 0)]$ and $(\lambda_s, \mu_s) = (0, 0)$ $[(\lambda_0, \mu_0)]$ if $\sigma = \pi$ $[\nu]$. One can find computer codes for calculating the required reduced $SU(3)$ coupling coefficients and the 9-(λ, μ) in references [2, 80].

Since the operators $\Lambda^{\sigma;(0,0)}$ and $\Lambda^{\sigma;(1,1)}$ are related to the fermionic realization of the generators of $U(3)$, their triple-barred reduced matrix elements have the following closed analytic expressions:

$$\begin{aligned} & \langle \{f\}(\lambda_\sigma, \mu_\sigma) \; ||| \Lambda^{\sigma;(0,0)} ||| \; \{f\}(\lambda_\sigma, \mu_\sigma) \rangle_1 \\ = \; & [2 \dim(\eta_\sigma, 0)]^{-1/2} n_N^\sigma, \end{aligned} \tag{3.37}$$

$$\begin{aligned} & \langle \{f\}(\lambda_\sigma, \mu_\sigma) \; ||| \Lambda^{\sigma;(1,1)} ||| \; \{f\}(\lambda_\sigma, \mu_\sigma) \rangle_1 \\ = \; & (-1)^\phi \left[\frac{4 C_2(\lambda_\sigma, \mu_\sigma)}{\dim(\eta_\sigma, 0) \; C_2(\eta_\sigma, 0)} \right]^{1/2}, \end{aligned} \tag{3.38}$$

where the phase factor ϕ is 1 if $\mu_\sigma \neq 0$ and 0 if $\mu_\sigma = 0$.

Chapter 4. Shell Model Description of Normal Parity Bands in Lanthanide Isotopes

In this chapter, we report on a study of the ^{156,158,160}Gd, ^{160,162,164}Dy, and ^{168}Er nuclei that was carried out within the framework of the pseudo-$SU(3)$ model. We give a consistent set of parameters for terms in a realistic pseudo-$SU(3)$ model Hamiltonian. The quadrupole-quadrupole and monopole pairing interaction strengths are taken from systematics. Four low-lying bands of positive parity are identified with angular momentum $J \leq 8$, for which good agreement with experimental data is achieved. The theory also gives correct values for the sumrule for $M1$ transitions from the ground-state of these nuclei, the correct positions of the 1^+ energies, and a reasonable reproduction of the fragmentation of the $M1$ strength. A comparison of theoretical and experimental $B(E2)$ transition strengths is also given. A few additional levels are predicted in the $K^\pi = 2^+$ as well as in the first and second $K^\pi = 0^+$ bands. To support the predictions, the $B(E2)$ transition rates between these levels and their co-band members are given, as well as the $SU(3)$ content of the corresponding eigenvectors.

4.1 Basis States

In this section, a short review of the way basis states are built is given. An example is given to illustrate the procedure. As it was mentioned in the description of the model, in building the basis states only the valence particles are taken into account. The numbers of protons and neutrons in the valence shells are given in the second and third columns of Table 4.1. In the lanthanide nuclei, the valence shells are $\eta = 4$ for protons and $\eta = 5$ for neutrons, which correspond, respectively, to pseudo-shells $\tilde{\eta}_\pi = 3$ and $\tilde{\eta}_\nu = 4$. The corresponding intruder levels in these two shells are, respectively, the $h_{11/2}$ and $i_{13/2}$. The dimensions of the normal parity and abnormal (intruder levels from the above shell) parity spaces are given by:

$$\Omega_\pi = 32, \quad \Omega_N^\pi = 20, \quad \Omega_A^\pi = 12$$

$$\Omega_\nu = 44, \quad \Omega_N^\nu = 30, \quad \Omega_A^\nu = 14. \tag{4.1}$$

TABLE 4.1. The number of protons and neutrons in the valence shells as well as the partitions into normal and abnormal parity states. The leading pseudo-$SU(3)$ irreps calculated from the nucleons in the normal parity states are also given.

nucleus	N_π	N_ν	N_N^π	N_A^π	N_N^ν	N_A^ν	(λ_π,μ_π)	(λ_ν,μ_ν)	(λ,μ)
^{156}Gd	14	10	8	6	8	4	(10,4)	(18,0)	(28,4)
^{158}Gd	14	12	8	6	8	6	(10,4)	(18,4)	(28,8)
^{160}Gd	14	14	8	6	8	6	(10,4)	(18,4)	(28,8)
^{160}Dy	16	12	10	6	8	4	(10,4)	(18,4)	(28,8)
^{162}Dy	16	14	10	6	8	6	(10,4)	(18,4)	(28,8)
^{164}Dy	16	16	10	6	10	6	(10,4)	(20,4)	(30,8)
^{168}Er	18	18	10	8	10	8	(10,4)	(20,4)	(30,8)

The number of nucleons in normal (N) and abnormal (A) parity orbitals were determined by filling the Nilsson levels in order of increasing energy with pairs of particles for deformation $\beta \sim 0.3$. This yields the numbers of protons and neutrons in normal and abnormal parity states given in fourth, fifth, sixth and seventh columns of Table 4.1, which in turn uniquely determines the highest symmetries in the $\alpha = \nu$ and $\alpha = \pi$ chains, $U(\Omega_\alpha^N) \supset U(\Omega_\alpha^N/2) \times U(2)$. The leading pseudo-$SU(3)$ irreps, determined from the numbers of protons and neutrons in the normal parity orbitals, are given in the last three columns of Table 4.1 for the seven Lanthanide nuclei.

TABLE 4.2. Proton and neutron pseudo-$SU(3)$ irreps with largest C_2 values used in the description of ^{158}Gd.

(λ_π,μ_π)	C_2^π	(λ_ν,μ_ν)	C_2^ν
(10,4)	198	(18,4)	478
(12,0)	180	(20,0)	460
(8,5)	168	(16,5)	424
(5,8)	168	(17,3)	409
(9,3)	153	(13,8)	400

If we consider all possible proton-neutron couplings, there are a few hundred allowed pseudo-$SU(3)$ configurations. Out of all possible $SU(3)$ irreps, we take into account only about twenty, the ones with the largest values of the second order Casimir operator, $C_2 = (1/4)(Q \cdot Q + 3L^2)$. It was found that for describing low-lying levels, only a few even-even $SU(3)$ irreps suffice, but for describing the $M1$ transitions we need to consider some B-type symmetry irreps, since only they can give states of

angular momentum $J^{\pi} = 1^{+}$. In Table 4.2, the five proton and five neutron $SU(3)$ irreps with the largest C_2 values, used in the description of ^{158}Gd, are given. By taking the direct product of these proton and neutron irreps we obtain the strong coupled $SU(3)$ irreps. As an example, the eighteen pseudo-$SU(3)$ irreps with the largest values for the second order Casimir operator that were used in this calculations, for ^{158}Gd, are listed in Table 4.3.

The many-particle states of n_α active nucleons in a given normal parity shell η_α, $\alpha = \nu$ (neutrons) or π (protons), can be classified by the following group chain:

$$\begin{array}{cccccccc} \{1^{n_\alpha^N}\} & & \{\tilde{f}_\alpha\} & & \{f_\alpha\}\ \gamma_\alpha\ (\lambda_\alpha,\mu_\alpha) & \tilde{S}_\alpha & K_\alpha \tilde{L}_\alpha & J_\alpha^N \end{array}$$

$$U(\Omega_\alpha^N) \supset U(\Omega_\alpha^N/2) \times U(2) \supset SU(3) \times SU(2) \supset SO(3) \times SU(2) \supset SU_J(2), \tag{4.2}$$

where above each group the quantum numbers which characterize its irreps are given. The quantum numbers, γ_α and K_α, are multiplicity labels of the indicated reductions.

The many-particle state $|J_i M\rangle$, where J is the total angular momentum and M its projection with i an integer index which enumerates the states with the same J and M starting from the one with the lowest energy, is built as a linear combination

$$|J_i M\rangle = \sum_\alpha C_\alpha^{JMi} |\alpha JM\rangle \tag{4.3}$$

of the strong coupled proton-neutron states,

$$\begin{aligned} |\alpha JM\rangle \equiv & \left|\left\{\tilde{f}_\pi\right\}(\lambda_\pi,\mu_\pi)S_\pi, \left\{\tilde{f}_\nu\right\}(\lambda_\nu,\mu_\nu)S_\nu; \rho(\lambda,\mu)kL, S\ JM\right\rangle \\ = & \sum_{M_L M_S} (LM_L, SM_S|JM) \sum_{M_{S_\pi} M_{S_\nu}} (S_\pi M_{S_\pi}, S_\nu M_{S_\nu}|SM_S) \\ & \sum_{k_\pi k_\nu L_\pi L_\nu M_\pi M_\nu} \langle (\lambda_\pi,\mu_\pi) k_\pi L_\pi M_\pi; (\lambda_\nu,\mu_\nu) k_\nu L_\nu M_\nu | (\lambda,\mu) kLM\rangle_\rho \\ & \left|\left\{\tilde{f}_\pi\right\}(\lambda_\pi,\mu_\pi) k_\pi L_\pi M_\pi, S_\pi M_{S_\pi}\right| \left\{\tilde{f}_\nu\right\}(\lambda_\nu,\mu_\nu) k_\nu L_\nu M_\nu, S_\nu M_{S_\nu}\rangle. \end{aligned} \tag{4.4}$$

TABLE 4.3. The eighteen pseudo-$SU(3)$ irreps used in the description of ^{158}Gd.

(λ_π, μ_π)	(λ_ν, μ_ν)	coupled (λ, μ)						
(10,4)	(18,4)	(28,8)	(29,6)	(30,4)	(31,2)	(32,0)	(26,9)	(27,7)
(10,4)	(20,0)	(30,4)						
(10,4)	(18,4)	(32,0)						
(10,4)	(16,5)	(26,9)	(27,7)					
(10,4)	(17,3)	(27,7)						
(10,4)	(13,8)	(23,12)						
(12,0)	(18,4)	(30,4)						
(12,0)	(20,0)	(32,0)						
(8,5)	(18,4)	(26,9)	(27,7)					
(9,3)	(18,4)	(27,7)						
(5,8)	(18,4)	(23,12)						

As throughout the text, the expressions $\langle -; -|-\rangle$ and $(-, -|-)$ denote the $SU(3)$ and $SU(2)$ Clebsch-Gordan coefficients, respectively. The most important configurations are those with highest spatial symmetry [36, 108]. This implies that only configurations with pseudo-spin equal to zero need to be taken into account when considering an even-even number of nucleons. In eq. (4.4) the spin quantum numbers can be dropped for even-even nuclei since both proton and neutron spin quantum numbers and total spin are zero.

4.2 Hamiltonian

The Hamiltonian includes spherical single-particle terms for both protons and neutrons $H_{sp}^{\pi[\nu]}$, an isoscalar quadrupole-quadrupole interaction $Q \cdot Q$, neutron and proton pairing terms $H_p^{\pi[\nu]}$, and four smaller "rotor-like" terms that preserve the pseudo-$SU(3)$ symmetry:

$$\begin{aligned} H &= H_{sp}^{\pi} + H_{sp}^{\nu} - \frac{1}{2}\chi\, Q\cdot Q - G_\pi\, H_p^{\pi} - G_\nu\, H_p^{\nu} \\ &\quad + a\, J^2 + b\, K_J^2 + a_3\, C_3 + a_{sym}\, C_2. \end{aligned} \tag{4.5}$$

(Note that tildes, commonly used to denote pseudo quantities, are suppressed throughout the section to simplify the notation). The term proportional to J^2 represents a small correction to the moment of inertia, the K_J^2 breaks the degeneracy of the different K bands within a pseudo-$SU(3)$ irrep [36, 37, 27], the third term, which is the cubic Casimir invariant of pseudo-$SU(3)$, serves to fix the position of

the $J^{\pi} = 0^{+}$ energies relative to one another, and the last one, which distinguishes between A-type and B_{α}-type ($\alpha = 1, 2, 3$) internal symmetries of the rotor, pushes the 1^{+} energies up as they are all band-heads of B_{α}-type structures. The spherical single-particle Hamiltonian has the form

$$H^{\sigma}_{sp} = \sum_{i_{\sigma}} (C_{\sigma}\, l_{i_{\sigma}} \cdot s_{i_{\sigma}} \; + \; D_{\sigma}\, l^{2}_{i_{\sigma}}), \tag{4.6}$$

where σ stands for protons (π) or neutrons (ν). Since only pseudo-spin zero states are considered for the even-even nuclei in the present application of the theory, matrix elements of the spin-orbit part of this interaction vanish identically.

The quadrupole-quadrupole interaction has diagonal matrix elements given by a relation involving the second order Casimir of $SU(3)$ and the square of the angular momentum, $Q \cdot Q = 4C_2 - 3L^2$. As described in the last section, the quadrupole operator used in this Hamiltonian is the algebraic pseudo quadrupole operator. Within a major shell the matrix elements of both collective and algebraic quadrupole operators are identical. When transformed to the pseudo-$SU(3)$ basis it maps to a linear combinations of $SU(3)$ tensors that is dominated by the pseudo quadrupole operator $\tilde{Q}$, which is the generator of the pseudo algebra [27]. In first order, the relationship between both quadrupole operators can be written as

$$Q^{a}_{\mu} = \frac{\tilde{\eta} + 1}{\tilde{\eta}} \tilde{Q}_{\mu} = \frac{\eta}{\eta - 1} \tilde{Q}_{\mu}. \tag{4.7}$$

The third order Casimir operator of $SU(3)$, C_3 is also diagonal in our basis and has matrix elements given by the pseudo-$SU(3)$ coupled irreps:

$$\langle C_3 \rangle = \frac{1}{9}(\lambda - \mu)[2\lambda^2 + 5\lambda\mu + 2\mu^2 + 9(\lambda + \mu + 1)]. \tag{4.8}$$

The pairing interaction is

$$V^{\sigma}_{P}(\sigma = \pi, \nu) = -\frac{1}{4} G_{\sigma} \sum_{jj'} a^{\dagger}_{j} a^{\dagger}_{\bar{j}} a_{j'} a_{\bar{j}'}, \tag{4.9}$$

where $\bar{j}$ denotes the time reversed partner of the single-particle state j and G is the strength of the pairing force with $\sigma = \pi$ for protons and $\sigma = \nu$ for neutrons.

4.2.1 Parameters

In the following calculations, the interaction strength of the realistic terms in the Hamiltonian (4.5) are fixed and the others are allowed to vary to gain a best fit to the energies of the states in the first four low-lying bands. Therefore, the pairing and quadrupole-quadrupole interaction strengths were taken from systematics [96, 38]. We choose for the pairing interaction strengths the following parameterization, $G_\pi = 21/A$ and $G_\nu = 17/A$. On the other hand, it is necessary to rescale the expression for the quadrupole-quadrupole interaction strength ($\chi = 23\ A^{-5/3}$) to reflect the effect of the pseudo-spin transformation on the quadrupole operator. To determine this scale factor, consider for a moment that a tilde is used to denote pseudo quantities. Then the necessary factor can be determined by requiring the equality $\tilde{\chi}\tilde{Q}\cdot\tilde{Q} = \chi Q\cdot Q$. A numerical value can be determined by applying this result to the leading ground-state configuration: $\tilde{\chi} = (\langle C_2\rangle_{\max}/\langle\tilde{C}_2\rangle_{\max})\ \chi$. For the nuclei under consideration, $\langle C_2\rangle_{\max}/\langle\tilde{C}_2\rangle_{\max} \approx 1.5$ so the strength factor multiplying $Q\cdot Q$ in eq. (4.5) needs to be $35\ A^{-5/3} \simeq 1.5 \times\ 23\ A^{-5/3}$. The strength of the single-particle orbit-orbit (l^2) interaction given by systematics [96] is

$$D_\sigma(\sigma = \pi, \nu) = \hbar\omega\kappa_\sigma\mu_\sigma, \tag{4.10}$$

where $\hbar\omega = 41/A^{1/3}$ with κ_σ and μ_σ assigned their usual harmonic oscillator values [96]:

$$\begin{aligned} \kappa_\pi &= 0.0637, \quad \mu_\pi = 0.60 \\ \kappa_\nu &= 0.0637, \quad \mu_\nu = 0.42. \end{aligned} \tag{4.11}$$

The single-particle strengths that were used for Gadolinium nuclei are lower than the standard values [96] by a factor of 4. This means the $D_{\pi[\nu]}$ parameters are negative for both protons and neutrons and of about the same magnitude as those used in previous calculations [15, 16]. This

reduction in the strength of the single-particle orbit-orbit interaction can be shown to be tied to the truncation of the model space. In particular, increasing the single-particle orbit-orbit interaction strength enhances the mixing of $SU(3)$ irreps in the ground-state, and with this a sizeable fraction of the $M1$ strength is shifted to 1^+ states that fall outside the model space. The a, b, a_2, and a_{sym} parameters, which have an overall small effect on the spectra, were optimized to yield best fits to experiment.

For the Dysprosium and Erbium nuclei, calculations were carried out in two cases. In the first case, the single-particle orbit-orbit (l^2) interaction strengths were fixed by systematics [96], $D_\sigma(\sigma = \pi,\nu) = \hbar\omega\kappa_\sigma\mu_\sigma$, where $\hbar\omega = 41/A^{1/3}$ with κ_σ and μ_σ assigned their usual harmonic oscillator values (eq. 4.11), and in the other case we scaled these values back by an overall factor to achieve a better fit to the first and second excited $K^\pi = 0^+$ states.

4.2.2 Analysis

In our Hamiltonian, (4.5), we start by fixing the single-particle energies, the quadrupole-quadrupole, and pairing interaction strengths with values from systematics (see Sect. 4.2.1). This leaves four free parameters. Each of these parameters was varied for different fixed combinations of the other three parameters in order to find out how each affects the energy spectra and the electromagnetic transitions. For example, to see how the C_3 interaction changes the energy and $M1$ spectra, we give results for two sets of calculations: one in which a_3 is varied such that both excited $K^\pi = 0^+$ band-heads fit the experimental energies (left side of Fig. 4.1), and another one in which a_3 is set to zero (right side of Fig. 4.1). The other parameters are not changed from the values given in Table 4.19. These calculations were carried for all nuclei, but only the ones for ^{164}Dy are reported.

For these two sets of parameters, the experimental (left-hand-side) and calculated (right-hand-side) levels for the four lowest bands are plotted in the upper part of the Fig. 4.1. Also, the $M1$ transition spectra with experimental and calculated transition probabilities are shown in the lower part of the figure. This figure shows that the C_3 interaction moves three bands down in energy, namely, the $K = 2^+$ and the first two excited $K = 0^+$ bands. It also compresses these three bands

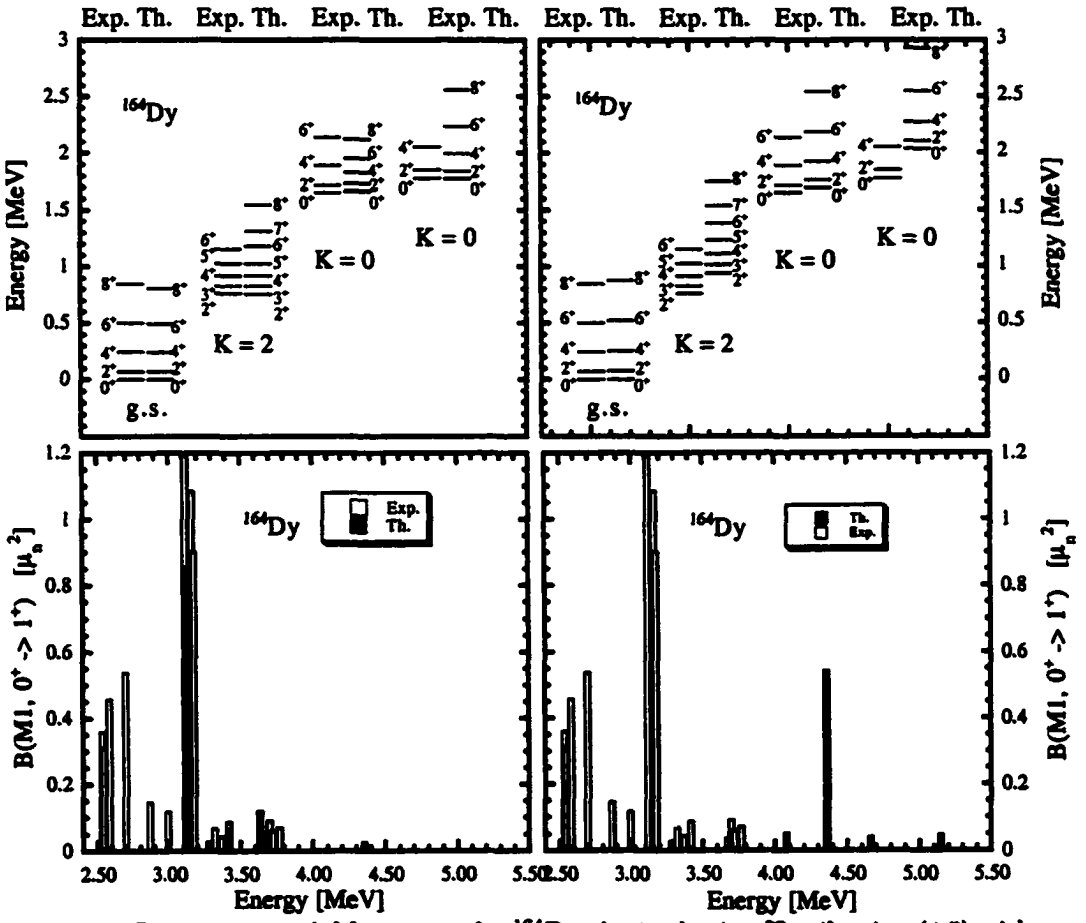

FIGURE 4.1. Low-energy and $M1$ spectra for ^{164}Dy obtained using Hamiltonian (4.5) with parameters from Table 4.19 for the plots on the left, and with the same parameters except for $a_3 = 0$ for the plots on the right. 'Exp.' represents the experimental results and 'Th.' the calculated ones. The lower plots give the theoretical and experimental $M1$ transition strengths from the $J^\pi = 0^+$ ground-state to the various $J^\pi = 1^+$ levels for the two situations considered here.

and the ground-state band, with a small effect on the last one. The $J^{\pi} = 1^{+}$ states moves down in energy too, with the 1^{+} state corresponding to the centroid of the $M1$ distribution moving down by about 1.5 MeV. Similar behavior was found in the other Lanthanide nuclei.

The K_J^2 interaction is given by a particular combination of 2-, 3-, and 4-body terms, which corresponds to the square of the third component of the angular momentum in the intrinsic frame [82] (Section 2.4.4). Since this interaction is related to the third component of the angular momentum in the intrinsic frame, it can be used to adjust the band-head energy of the $K \neq 0^{+}$ bands, in particular in this study the band-head of the $K = 2^{+}$ band. Changes in energies of the states in the ground-state and $K = 2^{+}$ bands as a function of the b parameter are shown in the lower part of Fig. 4.2. The energies of the first and second excited $J = 0^{+}$ states and the first 1^{+} state are also plotted versus b. The spectra were calculated using the Hamiltonian (4.5) with the single-particle energies, the quadrupole-quadrupole, and pairing interaction strengths fixed by systematics (see Sect. 4.2.1). Out of the other three parameters, two were fixed at the following values: $a = -0.001$ MeV and $a_3 = 0$ MeV. The third parameter, a_{sym}, was fixed at two values: $a_{sym} = 0.00$ MeV (left side of the Fig. 4.3) and $a_{sym} = 0.0008$ MeV (right side of the Fig. 4.3).

As it is expected, the energies of the states in the ground-state band do not change as b changes, and the energies of the states in the $K = 2^{+}$ band go up. This is seen in both calculations with $a_{sym} = 0$ and $a_{sym} = 0.0008$ MeV. Also, in both cases the energies of the first and second excited 0^{+} states, as well as the first 1^{+} state, do not change with b. In the upper part of the Fig. 4.2 there are two plots which show how the energies of the third and fourth states of angular momentum 2, 4, 6, and 8 vary with b. The two excited 0^{+} states are given again for an easy comparison in the lower plots. Note the change in slope of these levels and the crossing of the bands. The energies of the states in the first excited $K = 0^{+}$ band do not vary with b, but the energies of the states in the second excited $K = 0^{+}$ band increase as b increases. All four plots have the same energy scale.

Another feature of the states in the $K = 2^{+}$ band that can be observed here is that as b increases the energies of the states corresponding to odd angular momentum, 3^{+}, 5^{+}, 7^{+}, move slightly lower

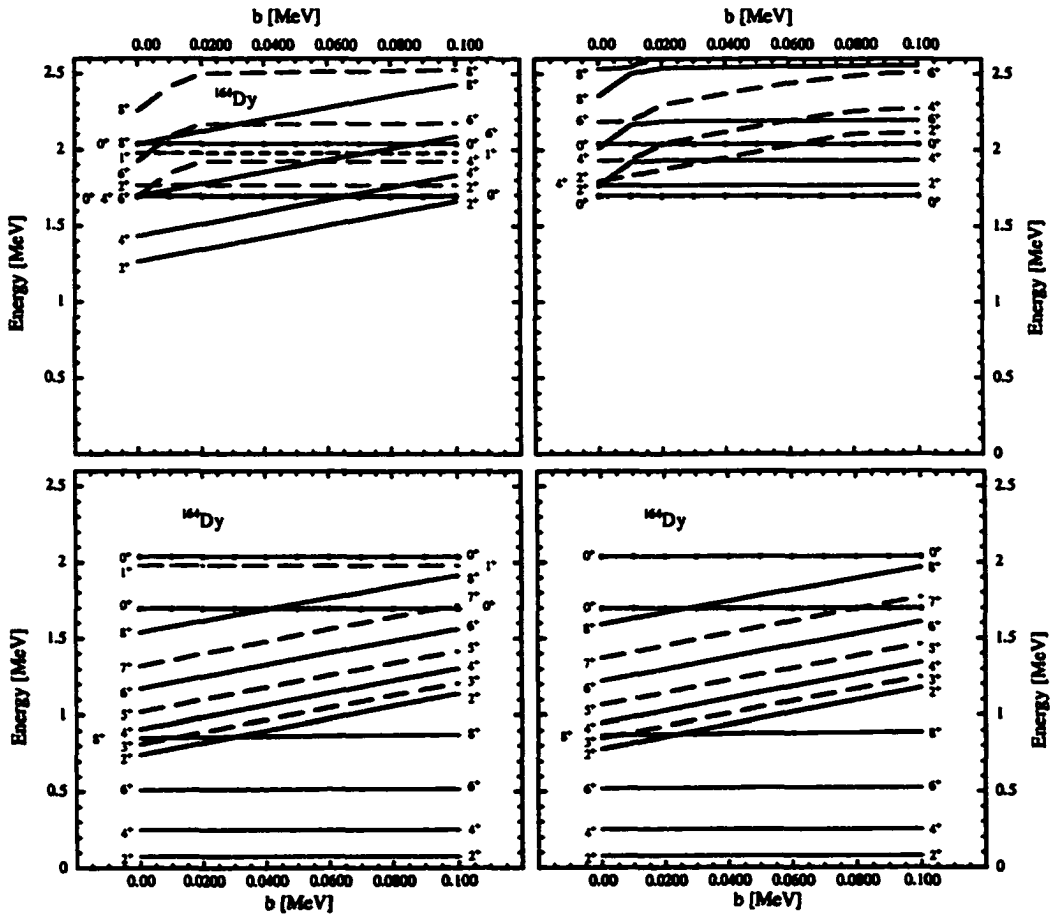

FIGURE 4.2. Low-energy spectra as a function of the K_J^2 interaction strength in ^{164}Dy. The energies of the states are calculated using Hamiltonian (4.5) with parameters from Table 4.19, except for $a_3 = 0$ MeV. The parameter a_{sym} is 0 MeV for the plots on the left, and 0.0008 MeV for the plots on the right. The states corresponding to even angular momentum are given as full lines, and the one corresponding to odd angular momentum with broken lines in the lower plots. The first and second excited 0^+ states are indicated as lines with points. The states corresponding to the ground-state and $K = 2^+$ bands are given in the lower plots, and the third and fourth 2^+, 4^+, 6^+, and 8^+ states are given in the upper plots. In the upper plots the third set of states is given with full lines, and the fourth set with broken lines. The same convention as the one used in the lower plots is followed for the excited 0^+ states.

towards the corresponding states of even angular momentum with one unit less. For example the 3^+ state moves toward the 2^+ state as b increases. This effect was found for all nuclei studied. For $b \geq 0.03\ MeV$ the relative distance between the energies in the first and second excited $K = 0^+$ bands is almost constant. Again this effect was observed in all cases.

The asymmetry parameter that was introduced to move the 1^+ states (which belong to B_3-type symmetry) up in energy enhances the contributions of the $SU(3)$ states that have both λ and μ even. The experimental 1_1^+ state is above the second excited 0^+ state for most of these nuclei, and without using this parameter it is below. Moreover, this in turn has an important effect on the states with higher angular momentum and the states above a certain energy. The states in the ground-state and $K = 2^+$ bands are unaffected by changing a_{sym} from 0 to 0.0008 MeV (see the two lower plots in Fig. 4.2), but the states in the higher bands are affected by changing a_{sym}. Hence, the sequence of states with angular momentum 2^+, 4^+, 6^+, and 8^+ with the energy of the 2^+ state below the first excited $K = 0^+$ state in the upper left plot, moves above the first excited $K = 0^+$ state in the upper right plot, where a_{sym} is increased to 0.0008 MeV. Since this parameter directly affects the energy of the 1^+ states, it also moves the $M1$ distribution up in energy.

The low-energy spectra calculated with the Hamiltonian (4.5) versus the a_{sym} parameter in ^{164}Dy is given in the Fig. 4.3 for two values of the a_3 parameter. The plot in the left-hand-side of the Fig. 4.3 corresponds to $a_3 = 0.00\ MeV$, and the one in the right-hand-side to $a_3 = 0.000065\ MeV$. The values for the other parameters are from Table 4.19 in both calculations except for $b = 0\ MeV$. The first set of states, 2^+, 3^+, 4^+, 5^+, 6^+, 7^+, and 8^+, corresponds to the $K = 2^+$ band. In this figure we see that these states move slightly (less than 5%) higher in energy as a_{sym} increases from 0 to 0.001 MeV. An interesting feature can be observed from these two plots in Fig. 4.3, namely, above a certain value of a_{sym} the low-lying states have nearly constant eigenvalues and only the 1^+ states go up in energy. This particular value for a_{sym} depends upon the values of the other parameters. In the plot on the left $a_{sym} \approx 0.0008\ MeV$ while for the plot on the right $a_{sym} \approx 0.0004\ MeV$.

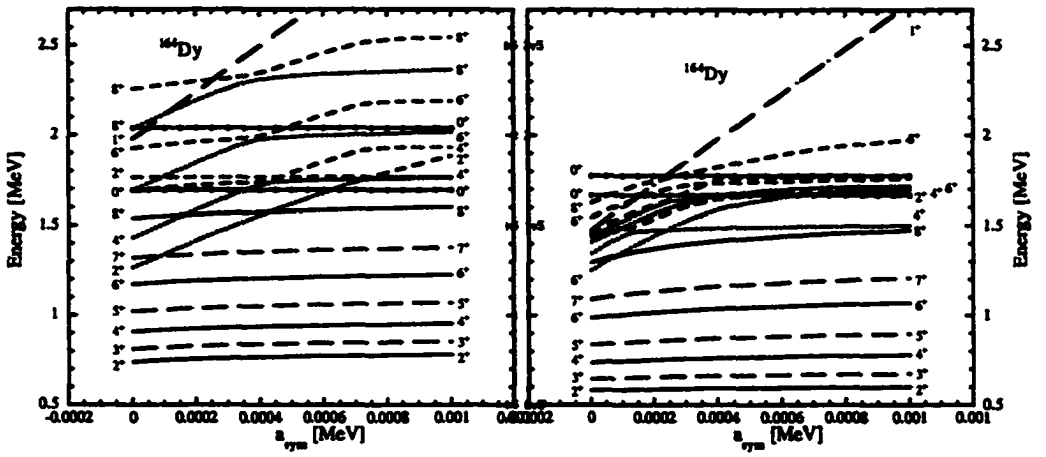

FIGURE 4.3. Low-energy spectra versus the a_{sym} parameter in ^{164}Dy, calculated with the Hamiltonian (4.5). The second set of states with even angular momentum, 2^+, 4^+, 6^+, and 8^+ are plotted as continuous lines, the third set of states as dotted lines, and the fourth set as short broken lines. The states corresponding to odd angular momentum are plotted as long broken lines, and the ones for the first and second excited 0^+ states as lines with points. Parameters from Table 4.19 were used in both calculations except for $b = 0$ MeV. The parameter a_3 has the values 0.00 MeV for the plot on the left, and 0.000065 MeV for the plot on the right.

The J^2 term in the Hamiltonian serves to correct the moments of inertia of the bands. A very small value for a suffices to accomplish this; for all nuclei studied, $|a| < 0.005$ MeV. Figure 4.4 shows excited states of the first, second and third, 2^+, 4^+, 6^+, and 8^+ levels plus the first 1^+, 3^+, 5^+, and 7^+ levels. The levels in the ground-state band, 2^+, 4^+, 6^+, and 8^+, are plotted with short broken lines, the second set of states with even angular momentum with continuous lines, and the third set with dotted lines. The states corresponding to odd angular momentum are plotted with long broken lines, and the first and second excited 0^+ states as lines with points. Parameters from Table 4.19 were used in both calculations except for $b = 0$ MeV in the plot on the left-hand-side. The bands are well reproduced even without the J^2 term, which serves to expand or contract the bands. All the levels vary smoothly as a changes. The behavior of all the bands is similar in both plots. As in Fig. 4.2, the energies of the $K = 2^+$ band are higher in the plot on the right where $b > 0.00$ MeV.

Since the behavior of the low-energy spectrum with different parameters has been established, the "free" parameters were varied to obtain an energy spectrum as close as possible to the experimental one for each nucleus considered. Each parameter takes values over an interval such that the eigenval-

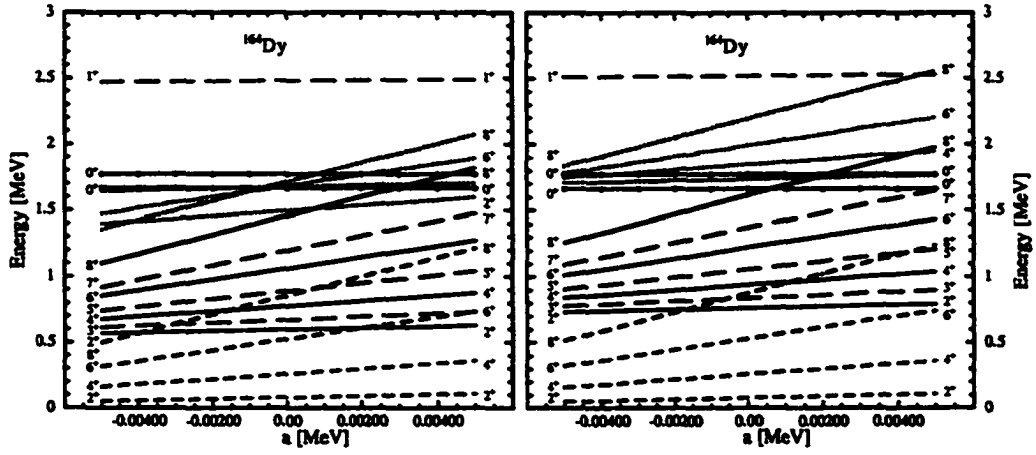

FIGURE 4.4. Low-energy spectra versus the a parameter in ^{164}Dy, calculated with Hamiltonian (4.5). The states in the ground-state band, corresponding to 2^+, 4^+, 6^+, and 8^+ angular momentum, are plotted with short broken lines, the second set of states with even angular momentum are plotted with continuous lines, and the third set with dotted lines. The states corresponding to odd angular momentum are plotted with long broken lines, and the ones for first and second excited 0^+ states as lines with points. Parameters from Table 4.19 were used in both calculations except for $b = 0$ MeV in the plot on the left-hand-side.

ues of the Hamiltonian, corresponding to the low-lying states, do not exhibit abrupt changes. The sets of parameters found in this way for the ^{156,158,160}Gd, ^{160,162,164}Dy, and ^{168}Er are given in the following sections.

4.3 Results for Gadolinium Isotopes

4.3.1 Parameters

A set of parameters which describe the best the energy and the electromagnetic transitions for ^{156}Gd, ^{158}Gd, and ^{160}Gd is given in Table 4.4. The parameters have very small variations from one nucleus to another. From the Table 4.4 we observe that a remains almost constant for the three isotopes, ^{156}Gd, ^{158}Gd, and ^{160}Gd. This parameter is responsible for fine tuning of the effective moments of inertia, and is in agreement with the value used in the neighboring odd-mass study. The b parameter changes slightly from case to case. This is understandable since it fixes the $K = 2^+$ band relative to the ground-state and the placement of these band-heads is different in the three cases. In this regard, it is important to note that the second experimental 2^+ states are not always the band-head of a $K = 2^+$ band. For ^{158}Gd and ^{160}Gd the second 2^+ energy is the $K = 2^+$ band-head, but for

^{156}Gd it is a member of the first excited $K^\pi = 0^+$ band. This detail is well reproduced by the model.

TABLE 4.4. Parameters used in the pseudo-$SU(3)$ Hamiltonian (4.5) for ^{156,158,160}Gd.

parameter	^{156}Gd	^{158}Gd	^{160}Gd
χ	0.0077	0.0076	0.0074
D_π	-0.075	-0.075	-0.075
D_ν	-0.054	-0.052	-0.052
G_π	0.135	0.133	0.131
G_ν	0.109	0.108	0.106
a $\times 10^{-3}$	-2.0	-3.0	-3.0
b	0.14	0.23	0.19
$a_{sym} \times 10^{-3}$	1.50	1.50	1.62
$a_3 \times 10^{-4}$	5.05	7.50	10.00

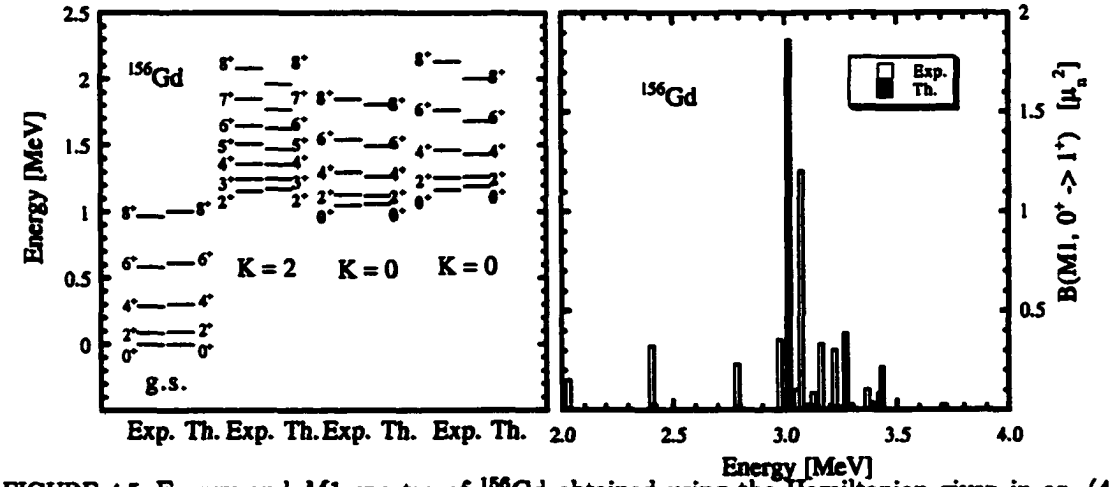

FIGURE 4.5. Energy and $M1$ spectra of ^{156}Gd obtained using the Hamiltonian given in eq. (4.5) with parameters from Table 4.4. 'Exp.' represents the experimental results and 'Th.' the calculated ones. The plot from the right side gives the theoretical and experimental $M1$ transition strengths from the $J^\pi = 0^+$ ground-state to the various $J^\pi = 1^+$ levels.

The a_{sym} parameter, which shifts B_α-type ($\alpha = 1, 2, 3$) intrinsic $SU(3)$ configurations [15] relative to the A-type, has an almost constant value for these nuclei. This parameter is used to position the 1^+ states, which are band-heads of B_α-type internal configurations, relative to the ground-state 0^+, which has an A-type internal symmetry. The a_3 parameter, which multiplies the third-order Casimir invariant C_3 of $SU(3)$ and which has an eigenvalue that is proportional to the irrep's intrinsic

asymmetry $(\lambda - \mu)$ (eq. (4.8)), increases slightly in going from ^{156}Gd to ^{160}Gd. This is consistent with the fact that the second 0^+ state moves up in energy in going from ^{156}Gd to ^{160}Gd. Note that since χ, the coefficient multiplying $Q \cdot Q$ and hence C_2 is fixed, the C_3 term in the Hamiltonian is the only one that directly affects the relative position of the 0^+ energies. This term, which is small relative to the others in the Hamiltonian, was necessary to obtain the detailed reproduction of the energy spectra shown in Figs. 1-3, as was found in a previous study [16].

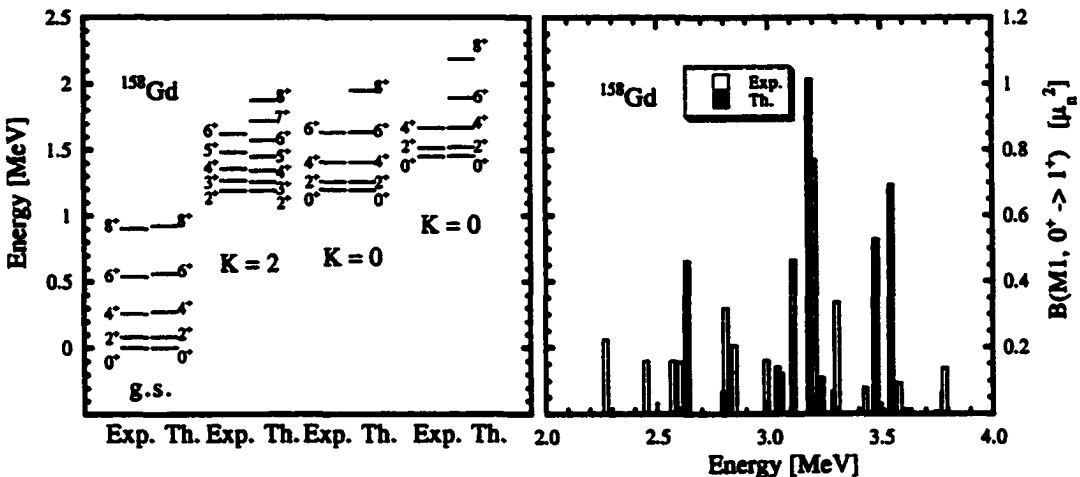

FIGURE 4.6. Energy and $M1$ spectra of ^{158}Gd obtained using the Hamiltonian given by eq. (4.5) with parameters from Table 4.4. 'Exp.' represents the experimental results and 'Th.' the calculated ones. The plot from the right gives the theoretical and experimental $M1$ transition strengths from the $J^\pi = 0^+$ ground-state to the various $J^\pi = 1^+$ levels.

4.3.2 Energy Spectra

The left part of Figs. 4.5, 4.6, and 4.7, shows the calculated and experimental [85] ground-state, $K^\pi = 2^+$, and two excited $K^\pi = 0^+$ energy bands in $^{(156,158,160)}$Gd. Experimental energies are plotted in the left hand side, while those obtained using the Hamiltonian space and Hamiltonian parameters discussed in the previous sections are in the right hand side. The theoretical energy levels are in excellent agreement with the experimental data. The model predicts more energy levels in the $K^\pi = 2^+$ and in the two excited $K^\pi = 0^+$ bands.

TABLE 4.5. $SU(3)$ content of calculated wavefunctions in ^{158}Gd. in the ground-state and $K^\pi = 2^+$ bands.

band	J [$\hbar$]	c^2 [%]	(λ, μ)	(λ_π, μ_π)	(λ_ν, μ_ν)
g.s.	0_1	78.1	(10, 4)	(18, 4)	(28, 8)
		4.3	(10, 4)	(18, 4)	(30, 4)
		5.6	(10, 4)	(20, 0)	(30, 4)
		8.5	(12, 0)	(18, 4)	(30, 4)
		2.5	(10, 4)	(18, 4)	(32, 0)
	2_1	78.8	(10, 4)	(18, 4)	(28, 8)
		4.0	(10, 4)	(18, 4)	(30, 4)
		5.4	(10, 4)	(20, 0)	(30, 4)
		8.3	(12, 0)	(18, 4)	(30, 4)
		2.4	(10, 4)	(18, 4)	(32, 0)
	4_1	80.5	(10, 4)	(18, 4)	(28, 8)
		3.4	(10, 4)	(18, 4)	(30, 4)
		5.0	(10, 4)	(20, 0)	(30, 4)
		7.8	(12, 0)	(18, 4)	(30, 4)
		2.2	(10, 4)	(18, 4)	(32, 0)
	6_1	83.0	(10, 4)	(18, 4)	(28, 8)
		2.4	(10, 4)	(18, 4)	(30, 4)
		4.3	(10, 4)	(20, 0)	(30, 4)
		7.1	(12, 0)	(18, 4)	(30, 4)
	8_1	85.8	(10, 4)	(18, 4)	(28, 8)
		3.4	(10, 4)	(20, 0)	(30, 4)
		6.2	(12, 0)	(18, 4)	(30, 4)
$K^\pi = 2^+$	2_γ	93.7	(10, 4)	(18, 4)	(28, 8)
		2.3	(10, 4)	(20, 0)	(30, 4)
		3.6	(12, 0)	(18, 4)	(30, 4)
	3_γ	93.8	(10, 4)	(18, 4)	(28, 8)
		2.2	(10, 4)	(20, 0)	(30, 4)
		3.6	(12, 0)	(18, 4)	(30, 4)
	4_γ	92.8	(10, 4)	(18, 4)	(28, 8)
		3.5	(12, 0)	(18, 4)	(30, 4)
	5_γ	93.7	(10, 4)	(18, 4)	(28, 8)
		3.5	(12, 0)	(18, 4)	(30, 4)
	6γ	88.1	(10, 4)	(18, 4)	(28, 8)
		3.3	(12, 0)	(18, 4)	(30, 4)
	7_γ	93.5	(10, 4)	(18, 4)	(28, 8)
		3.4	(12, 0)	(18, 4)	(30, 4)
	8_γ	2.3	(10, 4)	(18, 4)	(28, 8)
		79.0	(10, 4)	(18, 4)	(28, 8)
		6.2	(10, 4)	(18, 4)	(30, 4)
		3.8	(10, 4)	(20, 0)	(30, 4)
		2.9	(12, 0)	(18, 4)	(30, 4)

TABLE 4.6. $SU(3)$ content of calculated wavefunctions for states of the $K^\pi = 0_2^+$ band in ^{158}Gd.

J [$\hbar$]	c^2 [%]	(λ,μ)	(λ_π,μ_π)	(λ_ν,μ_ν)
0_a	19.2	(10, 4)	(18, 4)	(28, 8)
	18.6	(10, 4)	(18, 4)	(30, 4)
	23.7	(10, 4)	(20, 0)	(30, 4)
	23.4	(12, 0)	(18, 4)	(30, 4)
	15.1	(12, 0)	(20, 0)	(32, 0)
2_a	18.3	(10, 4)	(18, 4)	(28, 8)
	20.1	(10, 4)	(18, 4)	(30, 4)
	24.7	(10, 4)	(20, 0)	(30, 4)
	22.0	(12, 0)	(18, 4)	(30, 4)
	14.8	(12, 0)	(20, 0)	(32, 0)
4_a	16.0	(10, 4)	(18, 4)	(28, 8)
	23.3	(10, 4)	(18, 4)	(30, 4)
	26.2	(10, 4)	(20, 0)	(30, 4)
	19.4	(12, 0)	(18, 4)	(30, 4)
	13.9	(12, 0)	(20, 0)	(32, 0)
6_a	17.5	(10, 4)	(18, 4)	(28, 8)
	27.0	(10, 4)	(18, 4)	(30, 4)
	26.2	(10, 4)	(20, 0)	(30, 4)
	16.5	(12, 0)	(18, 4)	(30, 4)
	12.3	(12, 0)	(20, 0)	(32, 0)
8_a	21.6	(10, 4)	(18, 4)	(28, 8)
	30.1	(10, 4)	(18, 4)	(30, 4)
	23.5	(10, 4)	(20, 0)	(30, 4)
	13.7	(12, 0)	(18, 4)	(30, 4)
	10.1	(12, 0)	(20, 0)	(32, 0)

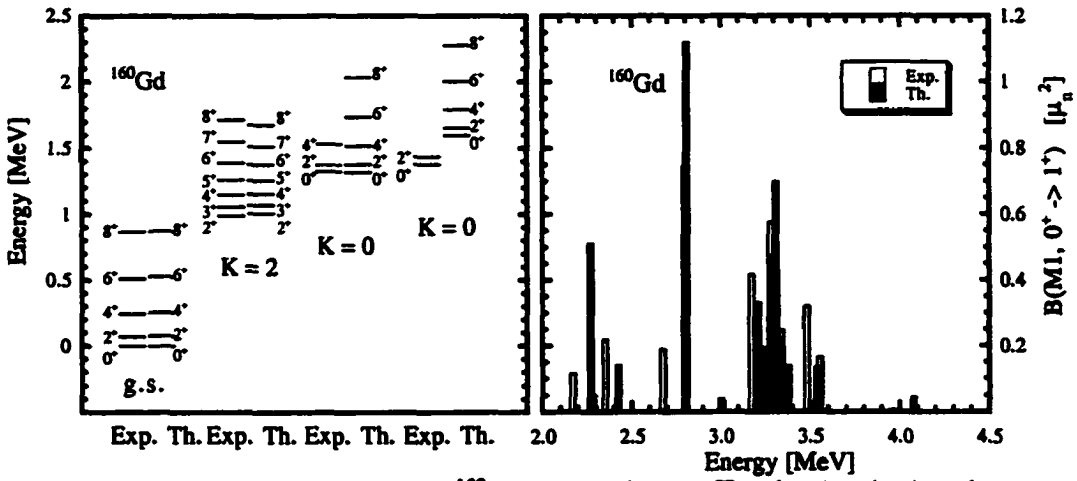

FIGURE 4.7. Energy and $M1$ spectra of ^{160}Gd obtained using Hamiltonian (4.5) with parameters from Table 4.4. 'Exp.' represents the experimental results and 'Th.' the calculated ones. The plot from the right gives the theoretical and experimental $M1$ transition strengths from the $J^\pi = 0^+$ ground-state to the various $J^\pi = 1^+$ levels. Note that in this case the strongest $M1$ transition ($1.12\ \mu_n^2$) to the 1^+ state at 2.80 MeV overlaps the experimental transition ($0.75\ \mu_n^2$) to the 2.80 MeV 1^+ state.

4.3.3 $B(E2)$ Transition Strengths and Wave Functions

Theoretical and experimental [85] $B(E2)$ transition strengths between low-lying states in ^{158}Gd are shown in Tables 4.8 and 4.9. The quadrupole operator was expressed as [36]

$$Q_\mu = e_\pi Q_\pi + e_\nu Q_\nu \approx e_\pi \frac{\eta_\pi + 1}{\eta_\pi} \tilde{Q}_\pi + e_\nu \frac{\eta_\nu + 1}{\eta_\nu} \tilde{Q}_\nu, \tag{4.12}$$

with effective charges $e_\pi = 2.25$, $e_\nu = 1.25$. These values are very similar to those used in earlier pseudo-$SU(3)$ descriptions of even-even nuclei [36, 15]. (The $(\eta+1)/\eta$ factors in this expression have the same origin as the $\langle C_2 \rangle_{\max}/\langle \tilde{C}_2 \rangle_{\max}$ renormalization of χ multiplying $Q \cdot Q$ in the Hamiltonian.) They are larger than those used in standard calculations of $B(E2)$ strengths [96] due to the passive role assigned to the nucleons in unique parity orbitals, whose contribution to the quadrupole moments is parameterized in this way.

In Table 4.8, $B(E2)$ strengths are given for transitions between members of the four low-lying bands. The results are in good agreement with the known experimental strengths. Electromagnetic

TABLE 4.7. $SU(3)$ content of calculated wavefunctions for states of the $K^\pi = 0_3^+$ band in ^{158}Gd.

J [$\hbar$]	c^2 [%]	(λ,μ)	(λ_π,μ_π)	(λ_ν,μ_ν)
0_b	3.4	(10, 4)	(18, 4)	(30, 4)
	54.0	(10, 4)	(20, 0)	(30, 4)
	40.9	(12, 0)	(18, 4)	(30, 4)
2_b	5.6	(10, 4)	(18, 4)	(30, 4)
	53.6	(10, 4)	(20, 0)	(30, 4)
	38.6	(12, 0)	(18, 4)	(30, 4)
4_b	13.0	(10, 4)	(18, 4)	(30, 4)
	52.3	(10, 4)	(20, 0)	(30, 4)
	31.0	(12, 0)	(18, 4)	(30, 4)
	2.9	(12, 0)	(20, 0)	(32, 0)
6_b	25.6	(10, 4)	(18, 4)	(30, 4)
	49.3	(10, 4)	(20, 0)	(30, 4)
	17.9	(12, 0)	(18, 4)	(30, 4)
	5.2	(12, 0)	(20, 0)	(32, 0)
8_b	33.8	(10, 4)	(18, 4)	(30, 4)
	46.6	(10, 4)	(20, 0)	(30, 4)
	7.5	(12, 0)	(18, 4)	(30, 4)
	3.3	(10, 4)	(18, 4)	(32, 0)
	7.9	(12, 0)	(20, 0)	(32, 0)

transitions from the 2_γ^+ (the band-head of the $K^\pi = 2^+$ band) to the 0^+, 2^+, and 4^+ states of the ground-state band are shown in Table 4.9. While they are about an order of magnitude larger than the measured values, the latter are very small, about 10^{-3} that of typical transitions between members of the same band, so it is difficult to attach any real significance to these differences. This strong (inter-band) and weak (intra-band) structure of the $B(E2)$ strengths underscores the significance of the assignment of the levels to K-bands.

The calculated and experimental $B(E2)$ transition strengths are given also for ^{160}Gd in Tables 4.10, 4.11, 4.12, 4.13, and 4.14. As for ^{158}Gd, the intra-band transitions are given between the energy levels of the first four bands, and for some known inter-band transitions the comparison with experimental data.

The percentage each $SU(3)$ irrep contributes to each state in the ground-state and $K^\pi = 2^+$ bands are given in Table 4.5 in ^{158}Gd. These are calculated from the wave functions, eq. (4.3), as $100 \times |C_\alpha^{JM_i}|^2$. All contributions larger than 2% are given, and in all cases, the states shown add up to at least 95% of the total wave functions. Same tables are given for first and second excited

TABLE 4.8. Theoretical and experimental intra-band $B(E2)$ transition strengths in ^{158}Gd. The subindices of the angular momentum are labeled with 'g' for ground-state, 'γ' for the gamma band ($K^\pi = 2^+$ band), 'a' for the first excited $K^\pi = 0^+$ band, and 'b' for the second excited $K^\pi = 0^+$ band.

$J^+ \to (J+2)^+$	$B(E2; J_i \to J_f)$	
	Th. (e^2b^2)	Exp. (e^2b^2)
$0^+_g \to 2^+_g$	5.06	5.02 ± 0.15
$2^+_g \to 4^+_g$	2.59	2.64 ± 0.05
$4^+_g \to 6^+_g$	2.27	
$6^+_g \to 8^+_g$	2.12	2.12 ± 0.20
$2^+_\gamma \to 4^+_\gamma$	1.04	
$4^+_\gamma \to 6^+_\gamma$	1.56	
$6^+_\gamma \to 8^+_\gamma$	1.66	
$0^+_a \to 2^+_a$	5.08	
$2^+_a \to 4^+_a$	2.57	
$4^+_a \to 6^+_a$	2.19	
$6^+_a \to 8^+_a$	2.04	
$0^+_b \to 2^+_b$	5.03	
$2^+_b \to 4^+_b$	2.52	
$4^+_b \to 6^+_b$	2.14	
$6^+_b \to 8^+_b$	2.00	
$J^+ \to (J+1)^+$	Th. (e^2b^2)	Exp. (e^2b^2)
$2^+_\gamma \to 3^+_\gamma$	2.53	
$4^+_\gamma \to 5^+_\gamma$	1.19	
$6^+_\gamma \to 7^+_\gamma$	0.61	

TABLE 4.9. Theoretical and experimental $B(E2)$ transition strengths in ^{158}Gd, between energy levels belonging to different bands. The subindices of the angular momentum follow the same convention as in Table (4.8).

$J^+_\alpha \to J^+_\beta$	$B(E2; J_i \to J_f)$	
	Th. ($\times 10^{-2} e^2b^2$)	Exp. ($\times 10^{-2} e^2b^2$)
$2^+_\gamma \to 4^+_g$	0.60	0.14 ± 0.02
$2^+_\gamma \to 2^+_g$	8.3	3.0 ± 0.4
$2^+_\gamma \to 0^+_g$	23.9	1.8 ± 0.2
$2^+_a \to 4^+_g$	0.13	0.71 ± 0.08
$2^+_a \to 0^+_g$	0.02	0.16 ± 0.02

TABLE 4.10. Theoretical and experimental intra-band $B(E2)$ transition strengths in ^{160}Gd between the energy levels belonging to the ground-state band.

$J_i^+ \rightarrow J_f^+$	$B(E2; J_i \rightarrow J_f)$ Exp. (e^2b^2)	Th. (e^2b^2)
$0_1 \rightarrow 2_1$	5.185 ± 0.041	5.163
$2_1 \rightarrow 4_1$		2.644
$4_1 \rightarrow 6_1$		2.318
$6_1 \rightarrow 8_1$		2.172

TABLE 4.11. Theoretical and experimental inter-band $B(E2)$ transition strengths in ^{160}Gd. The subindices of the angular momentum follow the same convention as in Table (4.8).

$J_i^+ \rightarrow J_f^+$	$B(E2; J_i \rightarrow J_f)$ Exp. (e^2b^2)	Th. (e^2b^2)
$2_\gamma \rightarrow 4_g$	0.1000 ± 0.0037	0.0068
$2_g \rightarrow 2_\gamma$	0.2000 ± 0.0366	0.000001
$0_g \rightarrow 2_\gamma$	0.0980 ± 0.0057	0.2546

TABLE 4.12. Calculated intra-band $B(E2)$ transition strengths in ^{160}Gd in the $K^\pi = 2^+$ band.

$J_i^+ \rightarrow J_f^+$	$B(E2; J_i \rightarrow J_f)$ Th. (e^2b^2)
$2_2 \rightarrow 3_1$	2.578
$2_2 \rightarrow 4_2$	1.081
$4_2 \rightarrow 5_1$	1.213
$4_2 \rightarrow 6_2$	1.661
$6_2 \rightarrow 7_1$	0.655
$6_2 \rightarrow 8_2$	1.739

TABLE 4.13. Calculated intra-band $B(E2)$ transition strengths in ^{160}Gd in the the first excited $K^\pi = 0_2^+$ band.

$J_i^+ \rightarrow J_f^+$	$B(E2; J_i \rightarrow J_f)$ Th. (e^2b^2)
$0_2 \rightarrow 2_3$	5.168
$2_3 \rightarrow 4_3$	2.631
$4_3 \rightarrow 6_3$	2.286
$6_3 \rightarrow 8_3$	2.115

TABLE 4.14. Calculated intra-band $B(E2)$ transition strengths in ^{160}Gd in the $K^\pi = 0_3^+$ band.

$J_i^+ \rightarrow J_f^+$	$B(E2; J_i \rightarrow J_f)$ Th. (e^2b^2)
$0_3 \rightarrow 2_4$	5.111
$2_4 \rightarrow 4_4$	2.569
$4_4 \rightarrow 6_4$	2.192
$6_4 \rightarrow 8_4$	2.042

$K^\pi = 0^+$ bands (Tables 4.6, and 4.7). While in all cases there is mixing of $SU(3)$ irreps, the mixing remains nearly the same for the states with different angular momentum belonging to the same band. In this sense the mixing is *adiabatic* within each band. This coherence explains the large $B(E2)$ transition strengths for intra-band transitions.

The components of each state belonging to the ground-state band are about 80 % $[(10,4)_\pi \times (18,4)_\nu](28,8)$, that is the leading irrep, 5% $[(10,4)_\pi \times (20,0)_\nu](30,4)$, 8% $[(12,0)_\pi \times (18,4)_\nu](30,4)$, and less from $[(10,4)_\pi \times (18,4)_\nu](30,4)$, and $[(10,4)_\pi \times (18,4)_\nu](32,0)$. These last two representations contribute less and less as angular momentum increases within the band, the last one contributes less than 2% in the $J^\pi = 8^+$ state. As angular momentum increases the leading irrep becomes more dominant. In the $K^\pi = 2^+$ band the representations that contribute the most to the states are the same as in the ground-state band. Here the leading irrep gets weaker for J^π from 2^+ to 8^+.

In the first excited $K = 0^+$ band the dominant $SU(3)$ irrep is (30,4), but unlike in the ground-state band, here the (30,4) irrep is the result of three possible combinations of proton-neutron irreps, namely 19% $[(10,4)_\pi \times (18,4)_\nu]$, 24% $[(10,4)_\pi \times (20,0)_\nu]$, and 24% $[(12,0)_\pi \times (18,4)_\nu]$. There are other two irreps that contribute with 19% $[(10,4)_\pi \times (18,4)_\nu](28,8)$, and 15% $[(12,0)_\pi \times (20,0)_\nu](32,0)$, respectively. This mixing in the wave function is the result of the single-particle and pairing interaction, since all the other terms in the Hamiltonian do not "see" the single-particle nature of the basis states. According with the $(\lambda,\mu) \leftrightarrow (\beta,\gamma)$ mapping, the last two representations correspond to different shapes of the nucleus, thus this band exhibits a superposition of shapes with the dominant shape from $(\beta,\gamma) \leftrightarrow (30,4)$. These contributions of the five configurations remain almost constant from $J^\pi = 0^+$ to $J^\pi = 8^+$, with the (28,8) getting weaker from 19% for the 0^+ state to 16% to the

8^+ state. In the same time (32,0) irrep changes from 15% for the 0^+ to 10% for the 8^+ state, and the (30,4) gets slightly stronger.

In the second excited 0^+ band the dominant irrep is (30,4) with 98% in the 0^+ state, that is actually 54% $[(10,4)_\pi \times (20,0)_\nu]$, 41% $[(12,0)_\pi \times (18,4)_\nu]$, and 4% $[(10,4)_\pi \times (18,4)_\nu]$, going down to 87% (30,4), less than 15% in the 8^+ state. At higher angular momentum some mixing occurs from the (32,2) irrep, namely 3% $[(12,0)_\pi \times (20,0)_\nu]$ in $J^\pi = 4^+$, 5% in $J^\pi = 6^+$, and 8% $[(12,0)_\pi \times (20,0)_\nu]$ and 3% $[(10,4)_\pi \times (18,4)_\nu]$ in the 8^+ state.

Mainly the interplay between the single-particle and the quadrupole-quadrupole terms in the Hamiltonian defines the $SU(3)$ mixing in the wave functions. The four bands discussed here have strong mixing and the ground-state band is dominated by the leading irrep, the one which would constitute the ground band in the pure $SU(3)$ symmetry limit. The delicate balance between these two interactions defines the gross features of the calculated energy spectra which are found to be in good agreement with experimental data.

Although the basis is strongly truncated, being built from the eighteen $SU(3)$ irreps listed in Table 4.3 for ^{158}Gd, not all of these play an important role. The low-lying states discussed above are dominated by irreps that are combination of two proton $SU(3)$ irreps, $(10,4)_\pi$ and $(12,0)_\pi$, and two neutron $SU(3)$ irreps, $(18,4)_\nu$ and $(20,0)_\nu$.

In Tables 4.15, 4.16, and 4.17 the $SU(3)$ content of the states in the first four bands of ^{160}Gd is given. As for ^{158}Gd, the low-lying energy bands are dominated by only a few $SU(3)$ irreps, namely, combinations of two proton $SU(3)$ irreps, $(10,4)_\pi$ and $(12,0)_\pi$, and two neutron $SU(3)$, irreps $(18,4)_\nu$ and $(20,0)_\nu$.

4.3.4 $M1$ Transition Strengths

The $M1$ strength distributions derived from the calculated eigenvectors are shown, along with the corresponding experimental results, in the lower plots that are a part of Figs. 4.5, 4.6, and 4.7. Key features of these distributions are easy to understand within the framework of the pseudo-$SU(3)$ model. The basic structure of the strength distribution is determined by the $SU(3)$-symmetry

TABLE 4.15. $SU(3)$ content of calculated wavefunctions in ^{160}Gd in the ground-state and $K^\pi = 2^+$ bands.

band	J [$\hbar$]	c^2 [%]	(λ_π, μ_π)	(λ_ν, μ_ν)	(λ, μ)
g.s.	0	83.3	(10, 4)	(18, 4)	(28, 8)
		3.3	(10, 4)	(18, 4)	(30, 4)
		4.3	(10, 4)	(20, 0)	(30, 4)
		6.5	(12, 0)	(18, 4)	(30, 4)
	2	83.9	(10, 4)	(18, 4)	(28, 8)
		3.1	(10, 4)	(18, 4)	(30, 4)
		4.1	(10, 4)	(20, 0)	(30, 4)
		6.3	(12, 0)	(18, 4)	(30, 4)
	4	85.3	(10, 4)	(18, 4)	(28, 8)
		2.5	(10, 4)	(18, 4)	(30, 4)
		3.7	(10, 4)	(20, 0)	(30, 4)
		5.9	(12, 0)	(18, 4)	(30, 4)
	6	87.1	(10, 4)	(18, 4)	(28, 8)
		3.1	(10, 4)	(20, 0)	(30, 4)
		5.3	(12, 0)	(18, 4)	(30, 4)
	8	89.0	(10, 4)	(18, 4)	(28, 8)
		2.5	(10, 4)	(20, 0)	(30, 4)
		4.6	(12, 0)	(18, 4)	(30, 4)
$K^\pi = 2^+$	2	95.0	(10, 4)	(18, 4)	(28, 8)
		2.8	(12, 0)	(18, 4)	(30, 4)
	3	95.0	(10, 4)	(18, 4)	(28, 8)
		2.8	(12, 0)	(18, 4)	(30, 4)
	4	94.8	(10, 4)	(18, 4)	(28, 8)
		2.8	(12, 0)	(18, 4)	(30, 4)
	5	94.7	(10, 4)	(18, 4)	(28, 8)
		2.8	(12, 0)	(18, 4)	(30, 4)
	6	94.2	(10, 4)	(18, 4)	(28, 8)
		2.7	(12, 0)	(18, 4)	(30, 4)
	7	94.2	(10, 4)	(18, 4)	(28, 8)
		2.7	(12, 0)	(18, 4)	(30, 4)
	8	93.2	(10, 4)	(18, 4)	(28, 8)
		2.6	(12, 0)	(18, 4)	(30, 4)

TABLE 4.16. $SU(3)$ content of calculated wavefunctions for states of the $K^\pi = 0_2^+$ band in ^{160}Gd.

J [$\hbar$]	c^2 [%]	(λ_π, μ_π)	(λ_ν, μ_ν)	(λ, μ)
0	14.7	(10, 4)	(18, 4)	(28, 8)
	21.4	(10, 4)	(18, 4)	(30, 4)
	24.1	(10, 4)	(20, 0)	(30, 4)
	26.6	(12, 0)	(18, 4)	(30, 4)
	13.1	(12, 0)	(20, 0)	(32, 0)
2	13.9	(10, 4)	(18, 4)	(28, 8)
	22.5	(10, 4)	(18, 4)	(30, 4)
	25.3	(10, 4)	(20, 0)	(30, 4)
	25.1	(12, 0)	(18, 4)	(30, 4)
	12.9	(12, 0)	(20, 0)	(32, 0)
4	12.1	(10, 4)	(18, 4)	(28, 8)
	25.1	(10, 4)	(18, 4)	(30, 4)
	27.5	(10, 4)	(20, 0)	(30, 4)
	22.3	(12, 0)	(18, 4)	(30, 4)
	12.3	(12, 0)	(20, 0)	(32, 0)
6	9.6	(10, 4)	(18, 4)	(28, 8)
	29.0	(10, 4)	(18, 4)	(30, 4)
	29.6	(10, 4)	(20, 0)	(30, 4)
	19.1	(12, 0)	(18, 4)	(30, 4)
	11.4	(12, 0)	(20, 0)	(32, 0)
8	6.6	(10, 4)	(18, 4)	(28, 8)
	34.4	(10, 4)	(18, 4)	(30, 4)
	30.4	(10, 4)	(20, 0)	(30, 4)
	16.3	(12, 0)	(18, 4)	(30, 4)
	10.2	(12, 0)	(20, 0)	(32, 0)

TABLE 4.17. $SU(3)$ content of calculated wavefunctions for states of the $K^\pi = 0_3^+$ band in ^{160}Gd.

J [$\hbar$]	c^2 [%]	(λ_π, μ_π)	(λ_ν, μ_ν)	(λ, μ)
0	2.3	(10, 4)	(18, 4)	(30, 4)
	55.6	(10, 4)	(20, 0)	(30, 4)
	40.6	(12, 0)	(18, 4)	(30, 4)
2	4.1	(10, 4)	(18, 4)	(30, 4)
	55.1	(10, 4)	(20, 0)	(30, 4)
	38.8	(12, 0)	(18, 4)	(30, 4)
4	10.0	(10, 4)	(18, 4)	(30, 4)
	53.8	(10, 4)	(20, 0)	(30, 4)
	32.6	(12, 0)	(18, 4)	(30, 4)
	2.3	(12, 0)	(20, 0)	(32, 0)
6	21.2	(10, 4)	(18, 4)	(30, 4)
	51.0	(10, 4)	(20, 0)	(30, 4)
	21.5	(12, 0)	(18, 4)	(30, 4)
	3.7	(12, 0)	(20, 0)	(32, 0)
8	31.0	(10, 4)	(18, 4)	(30, 4)
	48.1	(10, 4)	(20, 0)	(30, 4)
	11.1	(12, 0)	(18, 4)	(30, 4)
	5.5	(12, 0)	(20, 0)	(32, 0)

TABLE 4.18. Theoretical and experimental sumrule strengths for $M1$ transitions in ^{156,158,160}Gd from their ground-states to the respective 1^+ states.

Nucleus	$\sum B(M1)[\mu_N^2]$		
	Experiment	Pure $SU(3)$	Theory Mix
^{156}Gd	3.40	3.52	2.63
^{158}Gd	4.32	4.24	3.08
^{160}Gd	4.21	4.24	3.60

preserving part of the Hamiltonian which embodies strong $M1$ selection rules [16]. In this limit of the theory there is no coupling between different $SU(3)$ irreps and there are at most four non-zero $M1$ transitions between the 0^+ ground-state and the various 1^+ states [15, 16].

The fragmentation of the $M1$ strength that is predicted (and observed) is a result of symmetry breaking. This breaking of the symmetry is generated by the single-particle and pairing interactions that are an integral part of the Hamiltonian (4.5). For the nuclei considered, the centroids of the experimental and theoretical $M1$ strength distributions lie at about the same excitation energy, and overall there is reasonably good agreement between theory and experiment.

In ^{156}Gd the strongest calculated $M1$ strength (1.86 μ_n^2) to the 1^+ state at 3.014 MeV is only 0.065 MeV away from the strongest (1.20 μ_n^2) experimental transition at 3.070 MeV. And in ^{158}Gd the strongest predicted $M1$ transition (1.02 μ_n^2 for the 1^+ state at 3.18 MeV) almost overlaps the strongest experimental $M1$ transition (0.77 μ_n^2 to the 1^+ energy at 3.20 MeV). The best prediction for $M1$ strengths is in ^{160}Gd where the strongest $M1$ transition (1.12 μ_n^2) to the 1^+ state at 2.80 MeV overlaps the experimental transition (0.75 μ_n^2) to the 1^+ state at 2.80 MeV.

While one might like for the theory to give a slightly better reproduction of details of the $M1$ strength distributions, the fact that it does as well as it does is quite remarkable since in contrast with the quadrupole-quadrupole interaction, which is part-and-parcel of the $SU(3)$ model, a consideration of $M1$ strengths is not an integral part of the $SU(3)$ theory. As can be seen in Table 4.18, the total $M1$ strength, which for the full Hamiltonian is between 10 and 25% lower than for its pure $SU(3)$ limit, also shows reasonable agreement with the experimental results. This reduction in the strength can be traced to the symmetry mixing coupled with the fact that the model space is strongly truncated.

Also, the set of parameters used in the present calculation allows one to use a larger value for a_{sym} which pushes the centroid up in energy, closer to the experimental value.

4.4 Results for Dysprosium Isotopes and ^{168}Er

Results for energy levels of the four lowest-lying bands in ^{160,162,164}Dy and ^{168}Er, as well as $B(E2)$ transition strengths between the levels and the $B(M1)$ strength distribution of the ground-state are reported. Calculations were carried out within the framework of pseudo-$SU(3)$ model using realistic single-particle energies and quadrupole-quadrupole and pairing interaction strengths fixed from systematics, while four "rotor like" terms were adjusted nucleus-by-nucleus to obtain the best description of each energy spectrum. Comparison with experimental energies and $B(E2)$ transition strengths is in general very favorable. However, some excited bands are predicted to be too high in energy. Including other terms in the Hamiltonian would probably correct this effect. As an example, we show that scaling down the single-particle energies allows a nearly perfect description of the energy spectra. This reduction is interpreted as a mimicking of the effect of some missing two-body interactions in the Hamiltonian.

4.4.1 Parameters

In this section we apply the pseudo-$SU(3)$ model to the normal parity bands in the ^{160,162,164}Dy nuclei and ^{168}Er. These nuclei, like the Gadolinium chain, exhibit rotational ground-state bands and a few $K^\pi = 0^+$ band heads below 2 MeV. As in the calculations for the Gadolinium nuclei, approximatively twenty pseudo-$SU(3)$ irreducible representations (irreps) with the largest values of the second order Casimir operator C_2 ($Q \cdot Q = 4C_2 - 3L^2$) are used in building the basis states. For example, for ^{162}Dy the first twenty-one irreps with the largest C_2 values were used. Strengths of the quadrupole-quadrupole and pairing interactions were fixed, respectively, at values typical of those used by other authors: $\chi = 35\ A^{5/3}\ MeV$; $G_\pi = 21/A\ MeV$ and $G_\nu = 19/A\ MeV$. Calculations were carried out with the single-particle orbit-orbit (l^2) interaction strengths fixed by systematics [96],

$$D_\sigma(\sigma = \pi, \nu) = \hbar\omega\kappa_\sigma\mu_\sigma, \tag{4.13}$$

where $\hbar\omega = 41/A^{1/3}$, and κ_σ and μ_σ are assigned their usual harmonic oscillator values [96]:

$$\begin{aligned} \kappa_\pi &= 0.0637, \quad \mu_\pi = 0.60 \\ \kappa_\nu &= 0.0637, \quad \mu_\nu = 0.42. \end{aligned} \tag{4.14}$$

The other parameters were fixed as described at the beginning of the chapter. Hence, the a_3 parameter was varied to yield a best fit to the energy of the second 0^+ state; the energy of the third 0^+ was not included in the fitting procedure and as the results given below show, falls higher than the experimental number for all of the nuclei considered. As we have seen from the previous section 4.2.2, the other three parameters do not change the band-head energy of the second excited $K^\pi = 0^+$ band, but they can adjust the bands. Therefore, the a_{sym} parameter was adjusted to give a best fit to the first 1^+ state, b was fitted to the value of the band-head energy of the $K^\pi = 2^+$ band, and a was varied to get the moment of inertia of the ground-state band correct. The full set of parameters is given in Table 4.19. All of these four fitted parameters vary smoothly from one nucleus to another. Actually, all four "free" parameters decrease as the mass number "A" increases. The J^2 interaction strength decreases from 1.0×10^{-3} for ^{160}Dy to -2.1×10^{-3} for ^{168}Er, and the interaction strength of K_J^2 operator decreases from 0.10 for ^{160}Dy to 0.022 for ^{168}Er. The a_{sym} parameter that is fitted to the energy of the first 1^+ state also decreases from 1.45×10^{-3} for ^{160}Dy to 0.80×10^{-3}

TABLE 4.19. Parameters used for ^{160,162,164}Dy and ^{168}Er nuclei, in the pseudo-$SU(3)$ Hamiltonian (4.5).

parameter	^{168}Er	^{164}Dy	^{162}Dy	^{160}Dy
$\hbar\omega$	7.40	7.49	7.52	7.55
$\chi \times 10^{-3}$	6.84	7.12	7.27	7.42
D_π	-0.283	-0.286	-0.287	-0.289
D_ν	-0.198	-0.200	-0.201	-0.202
G_π	0.125	0.128	0.130	0.131
G_ν	0.101	0.104	0.105	0.106
a $\times10^{-3}$	-2.1	-2.0	0.0	1.0
b	0.022	0.00	0.08	0.10
$a_{sym} \times 10^{-3}$	0.80	1.20	1.40	1.45
$a_3 \times 10^{-4}$	0.75	0.65	1.32	1.36

for ^{168}Er. The nucleus ^{168}Er has one more pair of protons than the Dysprosium nuclei, and one more pair of neutrons than the nucleus ^{164}Dy. Since "A" is larger for ^{168}Er than for the ^{164}Dy isotopes, one might expect even smaller values for the parameters, and while this is what is observed for a and a_{sym}, the extra proton pair requires values for b and a_3 that are smaller than the ones for ^{160,162}Dy but larger than those for ^{164}Dy.

Since some excited bands are predicted to be too high in energy, other terms in the Hamiltonian might be indicated. Instead of introducing other terms, however, we show that scaling down the single-particle energies allows a nearly perfect description of the energy spectra. In this case the a_3 parameter was again allowed to vary to gain a best fit to the energies of both the second and third 0^+ states. Allowing for a scaling of the D_σ ($\sigma = \pi, \nu$) parameters, meant that a, b, a_{sym}, and a_3 had to be readjusted. The new parameter set is given in Table 4.20.

TABLE 4.20. The second set of parameters used in the pseudo-$SU(3)$ Hamiltonian corresponding to reduced one-body interaction strengths.

parameter	^{168}Er	^{162}Dy	^{160}Dy
$\chi \times 10^{-3}$	6.84	7.27	7.42
D_π	-0.153	-0.187	-0.141
D_ν	-0.107	-0.131	-0.099
G_π	0.125	0.130	0.131
G_ν	0.101	0.105	0.106
a $\times 10^{-3}$	-2.1	-1.6	-1.0
b	0.072	0.11	0.14
$a_{sym} \times 10^{-3}$	0.80	0.80	0.67
$a_3 \times 10^{-4}$	0.18	0.80	0.64

4.4.2 Energy Spectra

The experimental and calculated energies of the lowest four energy bands are compared in Figures 4.8, 4.9, 4.10, and 4.11. For illustrative purposes, the energies and $M1$ transition spectra are shown together for the two parameter sets used in the calculations, Tables 4.19 and 4.20. For both sets the calculated results are in good agreement with experiment. Likewise, the $B(E2)$ transition probabil-

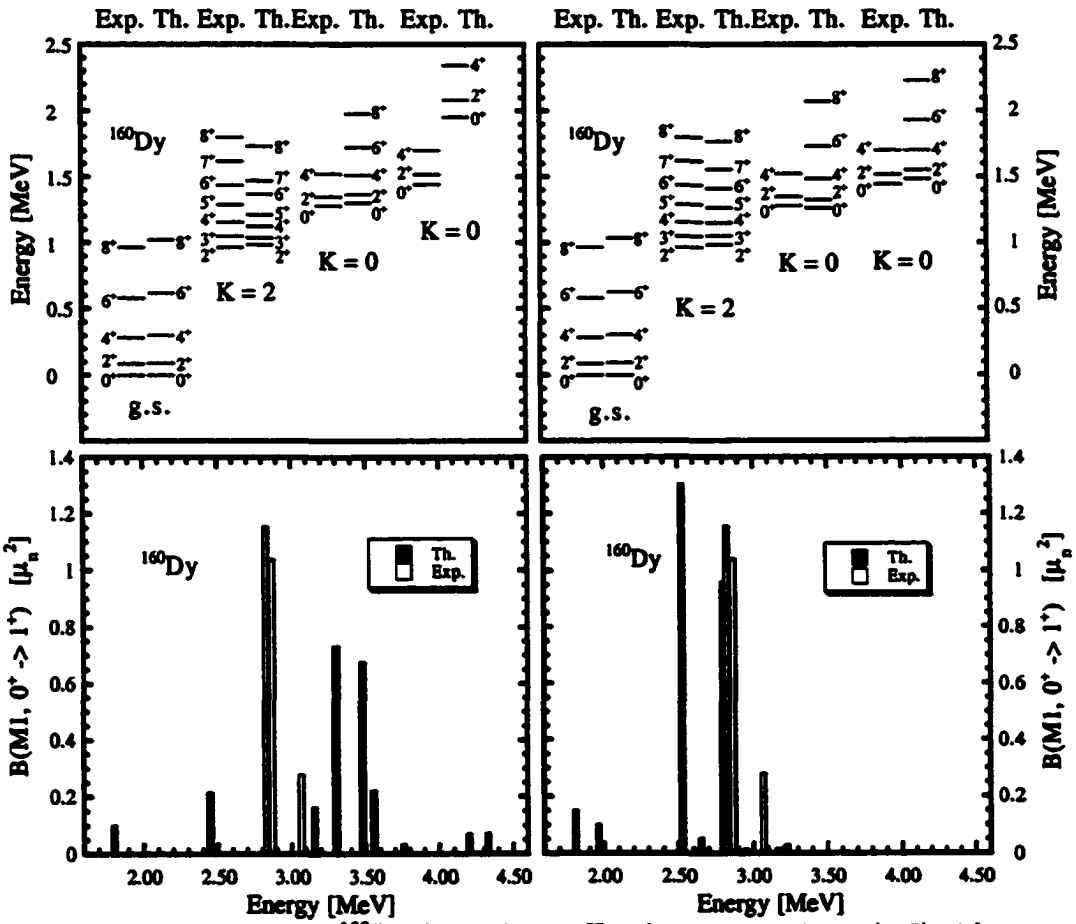

FIGURE 4.8. Energy spectra of ^{160}Dy obtained using Hamiltonian given in eq. (4.5) with parameters from Table 4.19 (left side) and from Table 4.20 (right side). 'Exp.' represents the experimental results and 'Th.' the calculated ones. The lower plot gives the theoretical and experimental $M1$ transition strengths from the $J^\pi = 0^+$ ground-state to the various $J^\pi = 1^+$ levels.

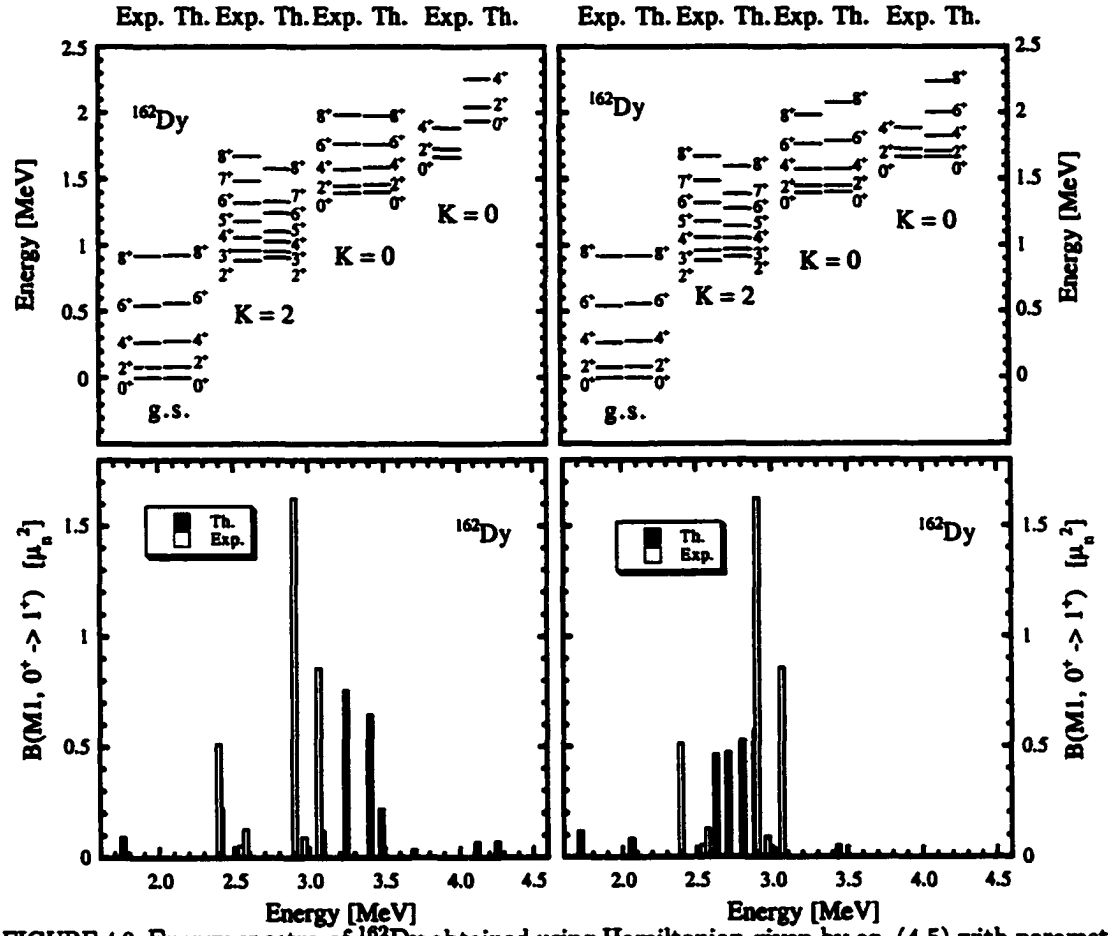

FIGURE 4.9. Energy spectra of ^{162}Dy obtained using Hamiltonian given by eq. (4.5) with parameters from Table 4.19 (left side) and from Table 4.20 (right side). 'Exp.' represents the experimental results and 'Th.' the calculated ones. The lower plot gives the theoretical and experimental $M1$ transition strengths from the $J^\pi = 0^+$ ground-state to the various $J^\pi = 1^+$ levels.

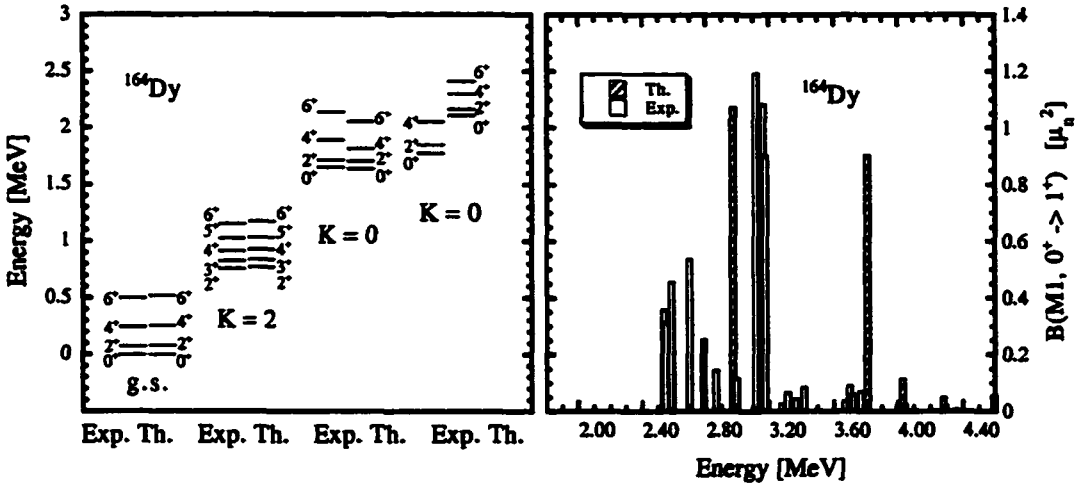

FIGURE 4.10. Energy spectra of ^{164}Dy obtained using Hamiltonian given in eq. (4.5) with parameters from Table 4.19. 'Exp.' represents the experimental results and 'Th.' the calculated ones. The plot from the right hand side gives the theoretical and experimental $M1$ transition strengths from the $J^\pi = 0^+$ ground-state to the various $J^\pi = 1^+$ levels.

ities are in excellent agreement with the experimental data. As an example the values for ^{162}Dy are given in Table 4.26.

The energy spectra calculated by diagonalizing the Hamiltonian (4.5) with parameters from Table 4.19 are in excellent agreement with the experimental data for the first three low-energy bands. These spectra are given in the left-hand-side plots of Figures 4.8, 4.9, 4.10, and 4.11. The differences between the calculated and the experimental energy values are less than 5% for the ground-state bands for all nuclei, less than 5% in the first exited $K = 0^+$ band of ^{160}Dy, ^{162}Dy, and ^{168}Er, less than 5% in the $K = 2^+$ band of ^{164}Dy, and less than 10% in the $K = 2^+$ of ^{160}Dy, ^{162}Dy, and ^{168}Er. The states in the second excited $K = 0^+$ bands are higher in values by about 0.5 MeV than the experimental ones. The moment of inertia for this band is higher than the experimental one. In ^{164}Dy good agreement with experimental levels is obtained for all four bands. Here the energies of the first excited $K = 0^+$ band are slightly compressed compare with the experimental ones.

When D_σ ($\sigma = \pi,\ \nu$) were scaled down to fit both excited 0^+ energies, the whole $K = 0_3^+$ band moved down in energy and the levels inside it were compressed such that the difference between

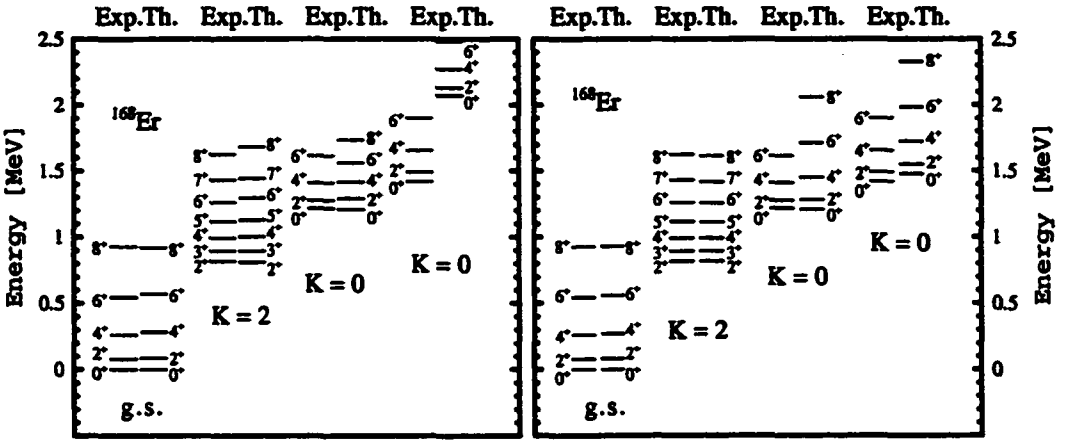

FIGURE 4.11. Energy spectra of ^{168}Er obtained using Hamiltonian given by eq. (4.5) with parameters from Table 4.19 (left side) and from Table 4.20 (right side). 'Exp.' represents the experimental results and 'Th.' the calculated ones. The lower plot gives the theoretical and experimental $M1$ transition strengths from the $J^\pi = 0^+$ ground-state to the various $J^\pi = 1^+$ levels.

these calculated energies and the experimental ones ended up being less than 7%. The description of the $K = 2^+$ band also improved. There was very little change in the ground-state band, and also the $K = 0_2^+$ band changed very little.

Left side of Figure 4.8 shows the calculated and experimental [85] $K = 0$, $K = 2$ as well as the first and second excited $K = 0$ bands for ^{160}Dy, calculated with parameters from Table 4.19. The model predicts a continuation of the first excited $K = 0$ band with two additional states of angular momentum 6 and 8 in ^{160}Dy.

The energy spectra for ^{168}Er is given in the left side of Figure 4.11. Even though this nucleus has one additional pair of protons, the calculated energy spectra exhibits the same behavior as is Dy isotopes. The ground-state, $K = 2$, and first excited $K = 0$ bands are well reproduced. An angular momentum 8 state is identified as a continuation of the first excited $K = 0$ band. The second excited $K = 0$ band is identified and lies higher than the experimental one. As Figures 4.8, 4.9, 4.10, and 4.11 show, the difference in energy between the calculated and experimental band-heads of the second excited $K = 0$ bands increases as the mass number A increases. For ^{160}Dy and ^{162}Dy the difference is about $0.3MeV$ while for ^{164}Dy it is about $0.5MeV$, and for ^{168}Er is about $0.65MeV$.

The states in the second excited $K = 0$ band are well defined. The results suggest that it may be interesting to see how the parameters change with changing proton rather than neutron number.

4.4.3 $B(E2)$ Strengths and Wave Functions

Very good agreement with experimental $B(E2)$ strengths was achieved for transitions in the ground-state band in both calculations. As an example the intra-band $B(E2)$ transition strengths are given for ^{162}Dy in Table 4.26. The intra-band transition strengths for the other three bands, calculated in the two situations with interaction strengths from Tables 4.19 and 4.20, are also given. Inter-band transition probabilities are given for a few cases where experimental numbers exist (Table 4.28). In this calculations, unlike in the ^{158}Gd, these inter-band $B(E2)$ strengths are overestimated. This must be related to the stronger single-particle interaction strengths that are used in these calculations, or some missing two-body term in the Hamiltonian.

Note that the strengths of the $B(E2)$ transition probabilities are consistent across all four bands (Tables 4.26 and 4.27). In all tables the theoretical $B(E2)$ transition probabilities are given for the two sets of calculations corresponding to the parameters from Tables 4.19 and 4.20. The differences in these values are very small, at the third digit in the ground-state and $K^\pi = 2^+$ bands, and at the second digit in the other two bands.

When reduced one-body interaction strengths are used, the calculated low-lying energy spectra are found to be in excellent agreement with experimental data for all four bands of the four nuclei considered. Eigenstates are calculated for angular momenta up to $8\hbar$. This leads to a prediction of some new levels in the $K^\pi = 2^+$ band as well as in the first and second excited $K^\pi = 0^+$ bands. In all cases these levels have strong intra-band $B(E2)$ transition probabilities.

In the previous chapter, we have shown that although the basis is strongly truncated, being built from about twenty $SU(3)$ irreps, not all of these play an important role. In the same time we have found that the $SU(3)$ content stays almost the same for all the states in a band. The $SU(3)$ content of the wave functions calculated for Dysprosium nuclei shows also that only few irreps are important. Furthermore these irreps are the same in all the states within one band, and their percentages

TABLE 4.21. $SU(3)$ content of calculated wavefunctions for states of the ground-state band in ^{162}Dy using parameters from table 4.19. Only the basis states that contribute to more than 2% are identified.

(λ_π, μ_π)	(λ_ν, μ_ν)	(λ, μ)	0	2	4	6	8
(10, 4)	(18, 4)	(28, 8)	59.3	59.3	59.4	59.6	61.9
(10, 4)	(20, 0)	(30, 4)	20.1	19.5	18.2	16.3	13.9
(10, 4)	(18, 4)	(30, 4)	6.5	6.2	5.7	4.9	4.0
(12, 0)	(18, 4)	(30, 4)	7.1	6.9	6.7	6.3	5.7
(10, 4)	(18, 4)	(32, 0)	2.7	2.6	2.3	-	-
(12, 0)	(20, 0)	(32, 0)	3.0	2.9	2.8	2.5	2.1
(10, 4)	(16, 5)	(26, 9)	-	-	-	3.2	3.5

TABLE 4.22. $SU(3)$ content of calculated wavefunctions for states of the $K^\pi = 2^+$ band in ^{162}Dy using parameters from table 4.19. Only the basis states that contribute to more than 2% are identified.

(λ_π, μ_π)	(λ_ν, μ_ν)	(λ, μ)	2	3	4	5	6	7	8
(10, 4)	(18, 4)	(28, 8)	81.4	79.1	77.5	74.1	73.9	69.6	69.7
(4, 10)	(18, 4)	(22, 14)	4.5	4.1	3.7	3.1	2.9	2.2	2.2
(10, 4)	(20, 0)	(30, 4)	5.2	4.7	4.3	3.7	3.4	2.8	2.6
(12, 0)	(18, 4)	(30, 4)	4.6	4.4	4.3	4.1	4.2	3.8	3.9
(10, 4)	(16, 5)	(26, 9)	-	3.4	4.4	7.6	6.8	11.6	8.9
(10, 4)	(18, 4)	(26, 9)	-	-	-	-	-	2.8	2.9
(10, 4)	(18, 4)	(29, 6)	-	-	-	-	-	-	2.1

vary slowly from the low angular momentum states towards the higher angular momentum states. Therefore, to support the identification of the calculated states as members of specific bands, the $SU(3)$ content is given for the ^{162}Dy nucleus in Tables 4.21-4.24. As noted by the labels in the first row, the proton, neutron, and coupled (λ, μ) values are given in the first three columns. Subsequent columns, labeled by angular momentum values, give the percentage distribution of each eigenstate across the (λ, μ) values. Only the basis states that contribute to more than 2% are identified.

The components of each state belonging to the ground-state band are about 60% $[(10,4)_\pi \times (18,4)_\nu](28,8)$, that is the leading irrep; 20% $[(10,4)_\pi \times (20,0)_\nu](30,4)$; 7% $[(12,0)_\pi \times (18,4)_\nu](30,4)$; and less from $[(10,4)_\pi \times (18,4)_\nu](30,4)$, $[(10,4)_\pi \times (18,4)_\nu](32,0)$, $[(12,0)_\pi \times (20,0)_\nu](32,0)$ and

TABLE 4.23. $SU(3)$ content of calculated wavefunctions for states of the $K^\pi = 0_2^+$ band in ^{162}Dy using parameters from table 4.19. Only the basis states that contribute to more than 2% are identified.

(λ_π, μ_π)	(λ_ν, μ_ν)	(λ, μ)	0	2	4	6	8
(4, 10)	(18, 4)	(22, 14)	91.8	89.5	87.9	87.3	86.4
(10, 4)	(20, 0)	(30, 4)	4.2	4.5	4.0	2.4	-
(7, 7)	(18, 4)	(25, 11)	-	-	2.5	5.3	8.1

TABLE 4.24. $SU(3)$ content of calculated wavefunctions for states of the $K^\pi = 0_3^+$ band in ^{162}Dy using parameters from table 4.19. Only the basis states that contribute to more than 2% are identified.

(λ_π, μ_π)	(λ_ν, μ_ν)	(λ, μ)	0	2	4	6	8
(10, 4)	(20, 0)	(30, 4)	47.0	31.7	11.0	2.7	4.0
(10, 4)	(18, 4)	(28, 8)	33.3	25.7	12.9	5.3	-
(12, 0)	(20, 0)	(32, 0)	11.0	7.1	-	-	-
(4, 10)	(18, 4)	(22, 14)	5.9	2.9	-	-	-
(10, 4)	(16, 5)	(26, 9)	-	9.6	8.7	5.1	4.1
(10, 4)	(16, 5)	(27, 7)	-	2.1	5.1	7.2	8.8
(10, 4)	(17, 3)	(27, 7)	-	17.2	52.2	67.6	64.3
(10, 4)	(18, 4)	(29, 6)	-	-	-	2.4	4.3
(10, 4)	(18, 4)	(30, 4)	-	-	-	-	3.1

$[(10,4)_\pi \times (16,5)_\nu](26,9)$. These (30,4) and (32,0) representations contribute less and less as the angular momentum increases within the band, and the last one occurs only for angular momentum 6 and 8 and contributes less than 4%. As angular momentum increases the leading irrep becomes slightly more dominant, from 59.3% to 61.9%, which is consistent with the $SU(3)$ content of the wavefunctions in Gadolinium nuclei. In the $K^\pi = 2^+$ band the representations that contribute the most to the states are the same as in the ground-state band. Here the leading irrep gets weaker for J^π from 2^+ to 8^+, which is again the same behavior as in Gadolinium nuclei.

In the first excited $K = 0^+$ band the dominant $SU(3)$ irrep is (22,14), but unlike for the Gadolinium nuclei, here the (22,14) irrep is the dominant irrep, namely, 92% $[(4,10)_\pi \times (18,4)_\nu]$ and 4% $[(10,4)_\pi \times (20,0)_\nu](30,4)$. Another basis state $[(7,7)_\pi \times (18,4)_\nu](25,11)$ appears in the wave function starting with angular momentum 4.

In the second excited 0^+ band the dominant irrep is $[(10,4)_\pi \times (20,0)_\nu](30,4)$, with 47% in the 0^+ state, and its strength is decreasing to only 4% in the 8^+ state. In the 0^+ state there are other three configurations with relatively strong percentages, 34% $[(10,4)_\pi \times (18,4)_\nu](28,8)$, 11% $[(12,0)_\pi \times (20,0)_\nu](32,0)$ and 6% $[(4,10)_\pi \times (18,4)_\nu](22,14)$, which are decreasing in strength as one moves up to the 8^+ state. Starting with angular momentum 2, some mixing occurs from (26,9), and (27,7). The latter configurations becomes stronger as one moves up to angular momentum 8. In this calculation the states in the second excited $K = 0^+$ band are higher than the experimental values,

TABLE 4.25. $SU(3)$ content of calculated four band-head states in ^{162}Dy. The percentage distributions of each state across the (λ, μ) values are given in the second and third columns for calculations in the two cases. Only the basis states that contribute to more than 2% are identified.

$J_\#$	th1.	th2.	(λ_π, μ_π)	(λ_ν, μ_ν)	(λ, μ)
0_1	59.3	64.0	(10, 4)	(18, 4)	(28, 8)
	6.5	7.4	(10, 4)	(18, 4)	(30, 4)
	20.1	7.3	(10, 4)	(20, 0)	(30, 4)
	7.1	5.1	(12, 0)	(18, 4)	(30, 4)
	2.7	3.1	(10, 4)	(18, 4)	(32, 0)
	3.0	-	(12, 0)	(20, 0)	(32, 0)
2_γ	81.4	85.9	(10, 4)	(18, 4)	(28, 8)
	5.2	4.9	(10, 4)	(20, 0)	(30, 4)
	4.6	3.0	(12, 0)	(18, 4)	(30, 4)
	4.5	2.6	(4, 10)	(18, 4)	(22, 14)
0_a	91.8	63.4	(4, 10)	(18, 4)	(22, 14)
	4.2	-	(10, 4)	(20, 0)	(30, 4)
	-	10.3	(10, 4)	(18, 4)	(28, 8)
	-	20.2	(10, 4)	(20, 0)	(30, 4)
	-	5.0	(12, 0)	(18, 4)	(30, 4)
0_b	33.3	17.6	(10, 4)	(18, 4)	(28, 8)
	47.0	40.2	(10, 4)	(20, 0)	(30, 4)
	11.0	9.7	(12, 0)	(20, 0)	(32, 0)
	5.9	27.0	(4, 10)	(18, 4)	(22, 14)
	-	3.1	(12, 0)	(18, 4)	(30, 4)

TABLE 4.26. Theoretical and experimental intra-band $B(E2)$ transition strengths in ^{162}Dy in the $K^\pi = 0_1^+$ band, calculated in the two situations. The third and fourth columns refer to calculations done using parameters from table 4.19 and 4.20, respectively.

$J_i \rightarrow J_f$	$B(E2; J_i \rightarrow J_f)$ (e^2b^2)		
	Exp.	Theory 1	Theory 2
$0_1 \rightarrow 2_1$	5.134 ± 0.155	5.134	5.133
$2_1 \rightarrow 4_1$	2.675 ± 0.102	2.635	2.634
$4_1 \rightarrow 6_1$	2.236 ± 0.127	2.325	2.321
$6_1 \rightarrow 8_1$	2.341 ± 0.115	2.201	2.193

TABLE 4.27. Calculated intra-band $B(E2)$ transition strengths in ^{162}Dy, in the $K = 2$, $K = 0_2$, and $K = 0_3$ bands, calculated in the two situations. The third and fourth columns refer to calculations done using parameters from Table 4.19 and 4.20, respectively. The energies are labeled with the subindex γ for the $K = 2$ band, a, and b for the first and second excited $K = 0$ bands.

band	$J_i \rightarrow J_f$	$B(E2; J_i \rightarrow J_f)$ (e^2b^2)	
		Theory 1	Theory 2
$K = 2$	$2_\gamma \rightarrow 3_\gamma$	2.480	2.513
	$2_\gamma \rightarrow 4_\gamma$	1.060	1.066
	$3_\gamma \rightarrow 4_\gamma$	1.630	1.655
	$4_\gamma \rightarrow 5_\gamma$	1.145	1.160
	$4_\gamma \rightarrow 6_\gamma$	1.625	1.632
	$5_\gamma \rightarrow 6_\gamma$	0.716	0.716
	$6_\gamma \rightarrow 7_\gamma$	0.607	0.615
	$6_\gamma \rightarrow 8_\gamma$	1.685	1.698
$K = 0_2$	$0_a \rightarrow 2_a$	4.193	4.581
	$2_a \rightarrow 4_a$	2.272	2.435
	$4_a \rightarrow 6_a$	2.153	2.173
	$6_a \rightarrow 8_a$	2.175	2.030
$K = 0_3$	$0_b \rightarrow 2_b$	3.517	3.780
	$2_b \rightarrow 4_b$	1.901	2.184
	$4_b \rightarrow 6_b$	2.017	2.076
	$6_b \rightarrow 8_b$	2.030	2.052

TABLE 4.28. Theoretical and experimental, inter-band $B(E2)$ transition strengths in ^{162}Dy, in the two situations. The third and fourth columns refer to calculations done using parameters from table 4.19 and 4.20, respectively. The energies are labeled with the subindex g for the ground-state and γ for the $K^\pi = 2^+$ bands.

$J_i \rightarrow J_f$	$B(E2; J_i \rightarrow J_f)$ (e^2b^2)		
	Exp.	Theory 1	Theory 2
$2_\gamma \rightarrow 4_g$	0.000017 ± 0.000001	0.006489	0.007311
$0_g \rightarrow 2_\gamma$	0.000632 ± 0.000042	0.2236	0.219120
$2_g \rightarrow 2_\gamma$	0.000210	0.0758	0.08209

and there is more mixing than in the other bands from the $SU(3)$ irreps that are not of even-even type.

When the unscaled one-body interaction strengths are used, levels of the first three energy bands are in good agreement with the experimental data. The fourth band is approximately 0.5 MeV higher in energy than observed. The percentage distribution of these eigenstates across the (λ, μ) values changes very little for the first three bands as the one-body interaction strength is scaled. These distributions are given in the second and third columns of Table (4.25), corresponding to the first and second set of parameters, for the band-head energies of the four bands considered.

TABLE 4.29. The experimental and calculated energies of the $K^\pi = 1^+$ band in ^{162}Dy using first set of parameters. The energy values of the states from the right hand side of first column are given in the second and third columns. The experimental and calculated energies of the $J = 1$ state, that is the band-head, is given in the first row. The $B(E2)$ transition probabilities are given in the last column.

$J_i \rightarrow J_f$	Energy(J_f) [MeV] Exp.	Th.	$B(E2; J_i \rightarrow J_f)$ (e^2b^2)
	1.746	1.749	
$1_1 \rightarrow 2_5$	1.783	1.797	1.312
$2_5 \rightarrow 3_3$	1.840	1.905	0.944
$2_5 \rightarrow 4_5$	1.904	1.941	1.170
$4_5 \rightarrow 5_3$	-	1.993	0.802
$4_5 \rightarrow 6_4$	-	2.066	0.648
$6_4 \rightarrow 7_2$	-	2.150	1.291
$6_4 \rightarrow 8_4$	-	2.292	1.203

As the second excited $K^\pi = 0^+$ band goes up in energy, the wavefunctions content change slightly and the first and second excited $K^\pi = 0^+$ bands switch order. Likewise, the $M1$ distribution looks $\sim 0.5MeV$ higher in value.

The first excited 1^+ state (calculated using the first set of parameters) lies very close to the experimental one. Moreover this being the band-head of the $K^\pi = 1^+$ band, the band is also well described. The calculated and experimental energies of the $K^\pi = 1^+$ band in ^{162}Dy are given in Table 4.29 together with the $B(E2)$ transition strengths. In the second and third columns of Table 4.29, the experimental and calculated energies of the states of the $K = 1^+$ band are given, which correspond to angular momentum values given in the right hand side of the first column. For example, the experimental and calculated energies of the 2_5^+ state are given in the second row, the energies of the 3_3^+ state are given in the third row, and so on, until the calculated energy of the 8_4^+, which is given in the last row. The experimental and calculated energy values of the $J = 1^+$ state is given in the first row of the table.

In these nuclei there is an experimentally known low-lying $K^\pi = 4^+$ band. Whereas this band appears in our calculations, it appears at a higher value. For completeness, a comparison between the experimental and calculated energies are given in Table 4.30 together with $B(E2)$ transition probabilities, for the same nucleus ^{162}Dy.

TABLE 4.30. The experimental and calculated energies of the $K^\pi = 4^+$ band in ^{162}Dy using the first set of parameters. The energy values of the states from the right-hand-side of the first column are given in the second and third columns. The experimental and calculated energies of the $J = 4$ state, which is the band-head, is given in the first row. The $B(E2)$ transition probabilities are given in the last column.

$J_i \rightarrow J_f$	Energy(J_f) [MeV]		$B(E2; J_i \rightarrow J_f)$
	Exp.	Th.	(e^2b^2)
	1.536	1.977	
$4_6 \rightarrow 5_4$	1.634	2.168	0.360
$4_6 \rightarrow 6_6$	1.752	2.209	0.976
$6_6 \rightarrow 7_4$	1.888	2.514	0.125
$6_6 \rightarrow 8_6$	-	2.527	1.784

4.4.4 $M1$ Transition Strengths

The basic structure of the strength distribution is determined by the $SU(3)$-preserving symmetry part of the Hamiltonian,

$$H_{SU(3)} = -\frac{1}{2}\chi\, Q\cdot Q + a_{sym}\, C_2 + a\, J^2 + b\, K_J^2, \tag{4.15}$$

which embodies strong selection rules [27], namely, there is no coupling between different $SU(3)$ irreps. In this case there are at most four $M1$ transitions between the 0^+ ground-state and the 1^+ states. Because the calculated $M1$ strengths are concentrated in only two to four states, it fails to reproduce the observed fragmentation of the strength. By including $SU(3)$-symmetry breaking terms in the Hamiltonian, namely, the one-body proton and neutron angular momentum $l^2_{\pi,\nu}$ and the two-body pairing terms $H_P^{\pi,\nu}$, this theory includes a breakup of the $M1$ strength into relatively closely packed levels centered around the sharp peaks of the pure-$SU(3)$ limit of the theory. As a consequence of the symmetry breaking we find a number of transitions close to the experimentally observed ones. However some of them have very small transition strengths.

The $M1$ transition strengths derived from the eigenvectors are given along with the experimental results in the lower part of the Figures. 4.8, 4.9, and 4.10. The centroids of the experimental and theoretical $M1$ distributions lie at about the same energy for calculations done with scaled single-particle strengths. For ^{160}Dy and ^{162}Dy, by using the parameters from Table 4.20, the first 1^+ energies

are very close to the experimental values, and the calculated and experimental $M1$ distributions span the same energy range. The fragmentation of the $M1$ strength that is predicted (and observed) is a result of symmetry breaking, which is generated by the single-particle and pairing interactions, that are a integral part of the Hamiltonian given by eq. (4.5). In the ^{160}Dy, $M1$ distribution there are two strong transitions for the energies of the 1^+ states of 1.1561 μ_N^2 at 2.8220 MeV, and of 1.0392 μ_N^2 at 2.8640 MeV. The theory predicts also two strong $M1$ transitions, one of 1.3040 μ_N^2 at 2.5229 MeV, and one of 0.96021 μ_N^2 at 2.7955 MeV. The last one is very close to the experimental counterpart. In the ^{162}Dy there are three strong $M1$ transitions, one of 0.51700 μ_N^2 at 2.3950 MeV, one of 1.6289μ_N^2 at 2.9MeV, and one of 0.85994 μ_N^2 at 3.0610 MeV. The theory predicts in this case four strong $M1$ transitions of approximative 0.5 μ_N^2 at the 1^+ energies of 2.6289 MeV, 2.7107 MeV, 2.8049 MeV, and 2.8911 MeV, that are spread over the same energy interval as the experimental transitions.

For calculations with standard single-particle energy strengths (parameters from Table 4.19), the $M1$ distribution occurs at higher energy than the experimental one, with about 0.5 MeV for both ^{160}Dy and ^{162}Dy. In the ^{164}Dy, there is one group of strong $M1$ transitions around the 1^+ state of $\simeq$ 3.00MeV, one group around the 1^+ state of $\simeq$ 2.4MeV, and a group of weaker transitions at higher energies. The calculated $M1$ strength distribution overlaps the experimental one, by few tenths of MeV to the right.

The total $M1$ strength, which for the full Hamiltonian is lower than for its pure $SU(3)$ limit due to interference generated by the mixing (Table 4.31), also shows reasonable reproduction of the experimental data, in most cases slightly underestimated. The calculated total $M1$ strength is very close to the experimental one for ^{160}Dy and ^{162}Dy in both situations, with parameters from Table 4.19 and from Table 4.20. In the pure-$SU(3)$ limit it is almost 50% larger. In ^{164}Dy, the calculated total $M1$ strength is lower than the experimental one even in the pure $SU(3)$ limit. A possible explanation for this discrepancy is the missing spin 1 admixture in the wave functions, as they are known to play an important role [51].

TABLE 4.31. Theoretical and experimental sumrule strengths for $M1$ transitions in ^{160,162,164}Dy from their ground-states to the respective 1^+ states. The calculations are done using pure $SU(3)$ Hamiltonian and a Hamiltonian that includes mixing.

Nucleus	$\sum B(M1)[\mu_N^2]$			
	Experiment	Calculated		
		Pure $SU(3)$	Theory Mix 1	Theory Mix 2
^{160}Dy	2.48	4.24	2.32	2.66
^{162}Dy	3.29	4.24	2.29	2.47
^{164}Dy	5.63	4.36	3.05	3.05

Overall, good agreement with experimental data was obtained for describing the $M1$ distributions. The strong transitions occur in the same energy range as the predicted 1^+ states, the transitions are fragmented and clustered around strong peaks, and the total $M1$ strengths for this energy range agree within the limitations of the model space.

Chapter 5. Conclusions

The pseudo-$SU(3)$ model has been used to describe the low-energy spectra as well as $E2$ and $M1$ strengths in ^{156,158,160}Gd, ^{160,162,164}Dy, and ^{168}Er. The focus has been on obtaining a consistent set of Hamiltonian parameters for describing both the low-energy spectra and electromagnetic transition properties of strongly deformed heavy nuclei. The parameters of the Hamiltonian were fixed by fitting calculated energies to the corresponding experimental numbers for low-lying states; electromagnetic transitions ($E2$ nor $M1$) were not included in the fitting procedure.

We started with a review the $SU(3)$ model, including a discussion of the basis states and the logic behind a truncation of the space to a subset of "important" represenations. We also gave algebraic expressions for matrix elements of the Hamiltonian and transition operators. After a review of fundamental tenants of the pseudo-$SU(3)$ model, which is a logical extension of the $SU(3)$ model to heavy deformed nuclei, we considered the construction of an appropriate (truncated) model space for the nuclei of interest.

The results show that pseudo-spin zero neutron and proton configurations with relatively few pseudo-$SU(3)$ irreps with largest C_2 values suffice to obtain good agreement with known experimental results. The Hamiltonian that was used included proton and neutron single-particle energies, quadrupole-quadrupole, proton and neutron pairing interactions, and four rotor-like terms with strengths that were varied to maximize agreement with observations. A consistent set of "free" parameters was determined and this set yielded a good reproduction of the first three low-lying energy bands in the even-even nuclei ^{160,162,164}Dy and ^{168}Er [40]. The interaction strengths of the quadrupole-quadrupole interaction, proton and neutron single-particle energies, and pairing interactions were fixed in these analyses. For the ^{156,158,160}Gd isotopes, good fits were obtained to members of the first four energy bands [92, 39] with the fourth being the second excited 0^+ band. In this case we scaled down the strength of the proton and neutron single-particle energies by an overall factor. The results suggest that a similar study, keeping the number of neutrons fixed and varying the proton number, may give more information on the different interaction strength. The results that

were analyzed extended beyond quantities that were used in the fitting procedure, including intra- and inter-band $B(E2)$ strengths, the $M1$ strength distribution of the ground state, and band-head energies of the first $K^\pi = 1^+$ and $K^\pi = 4^+$ bands. The C_3 interaction was found to be an important part of the story for a description of the normal parity-bands in even-even heavy deformed, unlike the situation in odd-mass nuclei. The C_3 interaction helped us fine tuning the placement of the excited 0^+ states.

The $M1$ strength distributions were not fit to the data. Nevertheless, in all cases the summed strength was found to be in good agreement with the experimental numbers. The pseudo-$SU(3)$ model therefore offers a microscopic shell-model interpretation of the "scissors" mode [15, 16], and in addition, it yields a microscopic picture for a "twist" degree of freedom that corresponds to allowed relative angular motion of the proton and/or neutron sub-distribution [98] about secondary intrinsic symmetry axes. By adding one- and two-body pairing interactions to the Hamiltonian, it was possible to describe the experimentally observed fragmentation of the $M1$ strength. The results suggest that a more detailed microscopic description of other properties of heavy deformed nuclei, such as g-factors and beta decay, may finally be within reach of a bona fide microscopic theory.

The results of this work suggest that additional applications of the pseudo-$SU(3)$ model may be warranted, including possible improvements to the basic theory. A natural first step will be to study the dependence of the interaction strengths on the single-particle energies and on the truncation. Another step would be consider the effects of integrating the intruder levels into the "active" model space. Other authors have noted [48] that nucleons in the unique parity orbitals play an important role in driving the many-particle system towards its maximum allowed deformation. In the present calculations the unique parity levels were taken into account only through a renormalization procedure. After the deformed Nilsson mean field was employed to determine the numbers of nucleons in the normal and unique (abnormal) parity orbitals, we "froze" the nucleons in the unique parity orbitals and described the dynamics under the assumption that the spectroscopically "active" nucleons resided solely in the normal parity states. This choice was further reflected through the use

of effective charges (which are larger than those usually employed in typical shell-model calculations for heavy nuclei) to describe the quadrupole electromagnetic transitions.

Another study that should be done is to explore the role of spin $S = 1$ configurations in a description of the $M1$ strength distribution, including its fragmentation. In a zeroth order theory the spin $S = 1$ configurations lie somehow higher in energies and therefore are not expected to contribute to the structure of low-lying eigenstates. Nevertheless, they may play an important role in a description of the $M1$ strength distribution since the coefficient multiplying the $S = 1$ part of the $M1$ operator is nearly an order of magnitude larger than that multiplying the $S = 0$ part.

References

[1] Y. Akiyama, A. Arima, and T. Sebe, Nucl. Phys. **A138**, 273 (1969).

[2] Y. Akiyama and J. P. Draayer, Comp. Phys. Commun. **5**, 405 (1973).

[3] A. Arima, M. Harvey, and K. Shimizu, Phys. Lett. **B30**, 517 (1969).

[4] A. Arima and F. Iachello, Phys. **99**, 253 (1976).

[5] A. Arima and F. Iachello, Ann. Phys. **111**, 201 (1978)

[6] C. Bahri, J. P. Draayer. and S.A. Moszkowski, Phys. Rev. Lett. **68**, 2133 (1992).

[7] C. Bahri and J. P. Draayer, Comp. Phys. Commun. **83**, 59 (1994).

[8] C. Bahri. Ph. D. thesis, Louisiana State University, Baton Rouge (1994).

[9] C. Bahri, J. Escher, and J. P. Draayer, Nucl. Phys. **A592**, 171 (1995); **A594**, 485 (1995).

[10] C. Bahri, J. Escher, and J. P. Draayer, Nucl. Phys. **A592**, 171 (1995).

[11] C. Bahri, J. Escher, and J. P. Draayer, Nucl. Phys. **A594**, 485 (1995).

[12] S. T. Belyaev, Dan. Mat. Fys. Medd. **31**, 11 (1959).

[13] D. R. Bes and R. A. Sorensen, Advances in Nuclear Physics **2**, 129 (1969).

[14] T. Beuschel, A. L. Blokhin, and J. P. Draayer, Nucl. Phys. **A619**, 119 (1997).

[15] T. Beuschel, J. P. Draayer, D. Rompf, and J. Hirsch, Phys. Rev. **C57**, 1233 (1998).

[16] T. Beuschel, J. G. Hirsch, and J. P. Draayer, Phys. Rev. **C61**, 054307 (2000).

[17] A. L. Blokhin, C. Bahri, and J. P. Draayer, Phys. Rev. Lett. **74**, 4149 (1995).

[18] A. L. Blokhin, C. Bahri, and J. P. Draayer, Phys. Rev. Lett. **74**, 4149 (1995).

[19] A. L. Blokhin, T. Beuschel, J. P. Draayer, and C. Bahri, Nucl. Phys. **A612**, 163 (1997).

[20] A. Bohr and B. Mottelson, Mat. Fys. Medd. Dan. Vid. Selsk. **27**, 1 (1953).

[21] A. Bohr and B. Mottelson, *Nuclear Structure, Vol. 1*, Benjamin, Reading, (1969).

[22] H. G. Börner, J. Jolie, S. J. Robinson, B. Krushe, R. Piepenbring.

[23] H. G. Börner, M. Jentschel, N. V. Zamfir, R. F. Casten, M. Krticka, and W. Andrejtscheff, Phys. Rev. **C59**, 2432 (1999).

[24] P. J. Brussard and P.M. Glaudemans, *Shell-Model Applications in Nuclear Spectroscopy*, North-Holland, Amsterdam, 1997.

[25] J. Chadwick, Proc. Roy. Soc. **A136** (1932) 692.

[26] J. P. Draayer, and K. J. Weeks, Ann. Phys. **156**, 41 (1984).

[27] O. Castaños, J. P. Draayer, and Y. Leschber, Ann. Phys. **180**, 290 (1987).

[28] O. Castaños, J. P. Draayer, and Y. Leschber, Z. Phys. **A329**, 71 (1988).

[29] O. Castaños, J. P. Draayer, and Y. Leschber, Comp. Phys. Commun. **52**, 33 (1988).

[30] O. Castaños, M. Moshinsky, and C. Quesne, Phys. Lett. **B227**, 238 (1992).

[31] R. F. Casten, J. P. Draayer, K. Heyde, P. Lipas, T. Otsuka, and D. Warner, *Algebraic Approaches to Nuclear Structure: Interacting Boson and Fermion Models*, Harcourt, Brace, and Jovanovich, New York, 436 (1993).

[32] R. F. Casten, A. Aprahamian, and J. P. Draayer, Phys. Rev. Lett. **66**, 691 (1991); **66**, 2837 (1991).

[33] F. Corminboeuf, J. Jolie, H. Lehmann, K. Köhl, F. Hoyler, H. G. Börnen, C. Doll, and P. E. Garrett, Phys. Rev. **C56**, R1201 (1997).

[34] J. F. Cornwell,*Technics in Physics 7: Group Theory in Physics, Vol. 2*, Academic Press, Orlando, (1985).

[35] J. P. Draayer, and Akiyama, J. Math. Phys. **14**, 1904 (1973).

[36] J. P. Draayer, K. J. Weeks, and K. T. Hecht, Nucl. Phys. **A381**, 1 (1982).

[37] J. P. Draayer, and K. J. Weeks, Ann. of Phys. **156**, 41 (1984).

[38] M. Dufour, and A. P. Zuker, Phys. Rev. C **54**, 1641 (1996).

[39] J. P. Draayer, G. Popa, J. G. Hirsch, and C. Vargas, Revista Mexicana De Fisica, Vol. 46, Suplemento 1, (September 2000) p.71-76.

[40] J. P. Draayer, G. Popa, and J. G. Hirsch, in *"High Spin Physics 2001" and dedicated to Zdzislaw Szymanski*, February 5-12, Poland, 2001.

[41] J. Eisenberg, and W. Greiner, *Nuclear Theory, Vol. 1, Nuclear Models* North-Holland, Amsterdam, 540 (1970).

[42] J. P. Elliott, Proc. Roy. Soc. **A245**, 128 (1958).

[43] J. P. Elliott, Proc. Roy. Soc. **A245**, 562 (1958).

[44] J. P. Elliott, Proc. Roy. Soc. London Ser. **A245**, 128 (1958); **245**, 562 (1958).

[45] J. P. Elliott, and M. Harvey, Proc. Roy. Soc. **A272**, 557 (1963).

[46] J. P. Elliott, *Proceedings of the international school of physics "Enrico Fermi"*, Academic Press, New York (1966).

[47] J. P. Elliott, and C. E. Wildon, Proc. Roy. Soc. **A302**, 509 (1968).

[48] J. Escher, J. P. Draayer, and A. Faessler, Nucl. Phys. **A586**, 73 (1995).

[49] J. Escher, C. Bahri, D. Troltenier, and J. P. Draayer, Nucl. Phys. **A633** , 662 (1998).

[50] C. Fahlander, A. Axelsson, M. Heinebrott, T. Härtlein, and D. Schwalm, Phys. Lett. **B388**, 475 (1996).

[51] D. Frekers, D. Bohle, A. Richter, R. Abegg, R. E. Azuma, A. Celler, C. Chan, T. E. Drake, K. P. Jackson, J. D King, C. A Miller, R. Schubank, J. Watson, and S. Yen, Phys. Rev. Lett. **58**, 658 (1989).

[52] J. N. Ginocchio, Phys. Rev. Lett. **78**, 436 (1997).

[53] M. Goeppert-Mayer, Phys. Rev. **75**, 1969 (1949).

[54] M. Goeppert-Mayer, Phys. Rev. **78**, 16 (1950).

[55] M. Goeppert-Mayer, Phys. Rev. **78**, 22 (1950).

[56] W. Greiner, and J. A. Maruhn, *Nuclear Models*, Springer, (1996).

[57] K. T. Hecht, Nucl. Phys. **A62**, 1 (1965).

[58] K. T. Hecht and A. Adler, Nucl. Phys. **A137**, 129 (1969).

[59] W. Heisenberg, Z. Physik **77** (1932) 1.

[60] W. Heisenberg, Z. Physik **78** (1932) 156.

[61] W. Heisenberg, Z. Physik **80** (1932) 587.

[62] K. Heyde, *Basic Ideas and Concepts in Nuclear Physics*, Second Edition, Institute of Physics Publishing, Bristol and Philadelphia,(1999).

[63] D. Ivanenko, Nature **129** (1932) 798.

[64] B. R. Judd, W. Miller Jr, J. Patera, and P. Winternitz, J. Math. Phys. **15**, 1787 (1974).

[65] U. Kneissl, J. Margraf, H. H. Pitz, P. von Brentano, R.-D. Herzberg, and A. Zilges, Prog. Part. Nucl. Phys. **34**, 285 (1995).

[66] U. Kneissl, H. H Pitz, and A. Zilges, Prog. Part. Nucl. Phys. **37**, 349 (1996).

[67] T. I. Kracíková *et al.*, Phys. Rev. **C58**, 1986 (1998).

[68] H. Lehmann *et al.*, Phys. Rev. **C57**, 569 (1998).

[69] Y. Leschber, and J. P. Draayer, Phys. Lett. **B190** (1987), 1.

[70] Y. Leschber, Hadronic Journal Supplement **3**, 1 (1987).

[71] N. Lo Iudice and F. Palumbo, Phys. Rev. Lett. **41**, 1532 (1978).

[72] N. Lo Iudice, and P. Palumbo, Nuc. Phys. **A326**, 193 (1979).

[73] N. Lo Iudice, P. Palumbo, A. Richter, and H. J. Wörtche, Phys. Rev. **42**, 241 (1990).

[74] J. Margraf, A. Degener, H. Friedrichs, R. D. Heil, A. Jung, U. Kneissl, S. Lindenstruth, H. H. Pitz, H. Schacht, U. Seemann, R. Stock, C. Wesselborg, A. Zilges, and P. von Brentano, Phys. Rev. **C42**, 771, (1990).

[75] J. Margraf, C. Wesselborg, R. D. Heil. U. Kneissl, H. H. Pitz, C. Rangacharyulu, A. Richter, H. J. Wörtche, and W. Ziegler, Phys. Rev. **C45**, R521 (1992).

[76] J. Margraf, R. T. Eckert, M. Rittner, I. Bauske, O. Beck, U. Kneissl, H. Maser, H. H. Pitz, A. Schiller, P. von Brentano, R. Fischer, R.-D. Herzberg, N. Pietralla, A. Zilges, and H. Friedrichs, Phys. Rev. **C52**, 2429 (1995).

[77] H. Maser, N. Pietrella, P. von Brentano, R.-D. Herzberg, U. Kneissl, J. Margraf, H. H. Pitz, and A. Zilges, Phys. Rev. **C54**, 2129 (1996).

[78] J. Meng, K. Sugawara-Tanabe, S. Yamaji, P. Ring, and A. Arima, Phys. Rev. **C58**, R632 (1998).

[79] A. Messiah, *Quantum Mechanics*, North Holland: Wiley and Sons (1958).

[80] D. J. Millener, J. Math. Phys. **19**, 1513 (1978).

[81] M. Moshinsky *Group Theory and the Many-Body Problem*, Gordon and Breach, Science Publishers, New York, (1968).

[82] H. A. Naqvi, and J. P. Draayer, Nuc. Phys. **A516**, 351 (1990).

[83] H. A. Naqvi and J. P. Draayer, Nucl. Phys. **A536**, 297 (1992).

[84] W. Nazarewicz, M. A. Riley, and J. D. Garrett, Nucl. Phys. **A512**, 61 (1990).

[85] National Nuclear Data Center, (http:\\bnlnd2.dne.bnl.gov).

[86] S. G. Nilsson, Dan. Videns. Selsk. Mat. Fys. Medd. **29**, No.16 (1955).

[87] M. Oshima *et al.*, Nucl. Phys. **A557**, 635c (1993).

[88] M. F. O'Reilly, J. Math. Phys. **23**, 2022 (1982).

[89] J. C. Parikh, *Group Symmetries in Nuclear Structure*, Plenum Press, New York, (1978).

[90] N. Pietralla, P. von Brentano, R.-D. Herzberg, U. Kneissl, J. Margraf, H. Maser, H. H. Pitz, and A. Zilges, Phys. Rev. **C52**, R2317 (1995).

[91] N. Pietrella, Ph. D. thesis, Inst. für Kernphysik, Universität zu Köln, Germany (1996).

[92] G. Popa, J. G. Hirsch and J. P. Draayer, Phys. Rev. **C62**, 064313 (2000).

[93] G. Popa, J. G. Hirsch, and J. P. Draayer, in *Bologna 2000 - Structure of the Nucleus at the Dawn of the Century*, May 29 -June 3, Bologna, Italy, 2000 (nucl-th/0010016).

[94] R. D. Ratna Raju, J. P. Draayer, and K. T. Hecht, Nucl. Phys. **A202**, 433 (1973).

[95] J. Retamosa, J.M. Udías, A. Poves, and E. Moya de Guerra, Nucl. Phys. **A511**, 221 (1990).

[96] P. Ring, and P. Schuck, *Nuclear many body problem*, Springer, Berlin (1979).

[97] D. Rompf, J. P. Draayer, D. Troltenier, and W. Scheid, Z. Phys. **A354**, 359 (1996).

[98] D. Rompf, T. Beuschel, J. P. Draayer, and W. Scheid, Phys. Rev. **C57**, 1703, (1998).

[99] D. J. Rowe, *Nuclear Collective Motion; Models and Theory*, Methuen and Co. Ltd., London (1970)

[100] J. J. Sakurai, *Modern Quantum Mechanics*, Addison-Wesley, (1994)

[101] V. G. Soloviev, A. V. Sushkov, N. Yu. Shirikova, and N. Lo Iudice, Nucl. Phys. **A 600**, 155 (1996).

[102] V. G. Soloviev, *et al.* , Nucl. Phys. **A613**, 47 (1996).

[103] D. Troltenier, C. Bahri, and J. P. Draayer, Nuc. Phys. **A586**, 53 (1995).

[104] D. Troltenier, C. Bahri, and J. P. Draayer, Nucl. Phys. **A586**, 53 (1995); **A589**, 75 (1995).

[105] D. Troltenier, A. L. Blokhin, J. P. Draayer, D. Rompf, and J. Hirsch, in: *Latin-American scchol of physics XXX Elaf*, edited by O. Castaños, R. Lòpez-Peña, J. Hirsch and, K. B. Wolf, AIP Conference proceedings 365, Woodbury, New York (1996).

[106] D. Troltenier, J. P. Draayer, and J. G. Hirsch, Nucl. Phys. **A601**, 89 (1996).

[107] H. Ui, Prog. Theor. Phys. **44**, 153 (1970).

[108] C. Vargas, J. G. Hirsch, P. O. Hess, and J. P. Draayer, Phys. Rev. **C58**, 1488 (1998).

[109] P. Van Isaker, and D. D. Warner, J. Phys. **G20**, 853 (1995).

[110] D.A. Varshalovich, A.N. Moskalev, and V.K. Khersonskii *Quantum Theory of Angular Momentum*, Worf Scientific, Singapore (1988).

[111] N. V. Zamfir *et al.*, Phys. Rev. **C60**, 054319 (1999).

[112] D. Zawischia, and J. Speth, Nuc. Phys. **A569**, 343c (1994).

[113] A. P. Zuker, J. Retamosa, A. Poves, and E. Caurier, Phys. Rev. **C52**, R1741 (1995).

[114] X. Wu, A. Aprahamian, S. M. Fischer, W. Reviol, G. Liu, and J. X. Saladin, Phys. Rev. **C49**, 1837 (1994).

Appendix: Basic definitions

Some basic definitions and concepts that are used throughout the text are reviewed in this appendix [34, 35, 62, 88, 89, 100]. Several group theoretical concepts such as Lie group, irreducible representations (irreps), Young diagrams and coupling of Young diagrams, group chains are given in the following few sections. Other sections are dedicated to the harmonic oscillator (HO) in different coordinate systems and to the single-particle and Nilsson models.

An important concept that is used in group theory is that of a Lie group [89]. A continuous Lie group G has an infinite number of elements that are parameterized by r variables. A well-known example is $SO(3)$, the group of rotations in three dimensions where the elements are parameterized by three angles.

The objects of interest, however, are not so much the group elements but the operators that generate infinitesimal group transformations. These operators X_α form a so-called Lie Algebra and are characterized by their commutation relationships

$$[X_\alpha, X_\beta] = C^\gamma_{\alpha,\beta} X_\gamma \,, \tag{A.1}$$

where the structure constants, $C^\gamma_{\alpha,\beta}$, define most of the group properties. The finite group transformations are then given by the generators as:

$$U(\alpha_1, \alpha_2 \ldots \alpha_s) = \exp \sum_{i=1}^{s} \alpha_i X^i \,. \tag{A.2}$$

A.1 The group $U(3)$ of the Harmonic Oscillator Hamiltonian

The Harmonic Oscillator Hamiltonian H_{OSC} can be written in terms of the position and momentum operators as

$$H_{OSC} = \frac{p^2}{2m} + \frac{1}{2} m\omega^2 r^2, \tag{A.3}$$

where the frequency parameter is $\omega = \hbar/mb^2$ and b is the oscillator length parameter. The creation (A_x, A_y, A_z) and the destruction (B_x, B_y, B_z) operators for a single oscillator quantum in the x, y, and z-direction can be expressed in terms of the position and momentum operators as

$$A_i = \frac{1}{2^{1/2}b}(r_i - \frac{ib^2 p_i}{\hbar}), \quad B_i = \frac{1}{2^{1/2}b}(r_i + \frac{ib^2 p_i}{\hbar}). \tag{A.4}$$

These operators obey the usual boson commutation relations

$$[B_i, A_i] = \delta_{ij}, \quad [A_i, A_j] = 0 = [B_i, B_j] \tag{A.5}$$

and the operator H_{OSC} becomes

$$H_{OSC} = \hbar\omega \sum_i A_i B_i \; + \; \frac{3}{2}\hbar\omega. \tag{A.6}$$

The operators $A_i(B_i)$, when acting on vacuum create (destroy) the three one-quantum states having angular momentum $l = 1$ (p states) and Cartesian components x, y, z, respectively. Let us define the three states as $\phi(r_i)$, $i = x, y, z$. Now we can apply a unitary transformation on these states by transforming the coordinates as:

$$r_i' = \sum_j U_{ij} r_j. \tag{A.7}$$

For an infinitesimal transformation $U = 1 + i\epsilon S$, where S is an arbitrary 3×3 Hermitian matrix we get

$$\begin{aligned} \phi(r_i') &= \phi(r_i + i\epsilon \sum_j S_{ij} r_j) \\ &= \phi(r_i) + i\epsilon \sum_{ij} S_{ij} \left[r_j \frac{\partial}{\partial r_i} \phi(r_i) \right] \\ &= \phi(r_i) + i\epsilon \sum_{ij} S_{ij} \left[C_{ij} \phi(r_i) \right], \end{aligned} \tag{A.8}$$

where $C_{ij} = r_i \partial/\partial r_j, i,j = x,y,z$. The change in ϕ to first order in ϵ is generated by $\sum_{ij} S_{ij} C_{ji}$. Since S is an arbitrary 3×3 matrix there are 9 such independent transformations and the corresponding infinitesimal operators can be taken as

$$C_{ij} = r_i \frac{\partial}{\partial r_j}, \quad i,j = x,y,z. \tag{A.9}$$

It is easy to check that the 9 operators $C_{\alpha\beta}$ verify the following commutation relations and can be expressed as 9 one-body operators in the occupation number formalism.

$$[C_{ij}, C_{kl}] = C_{il}\delta jk - C_{kj}\delta_{il} \tag{A.10}$$

$$C'_{\alpha\beta} = A_\alpha B_\beta \qquad (\alpha,\beta = x,y,z). \tag{A.11}$$

A.2 Representations of Lie Groups and Labeling of States

In using group theory methods to nuclear physics two problems are very important: (i) how to label irreps of a Lie Group and (ii) how to label states that belong to a given irrep. The former problem is solved using the symmetry labels for the group and the latter using the labels for states within an irrep of the group.

From the complete set of generators, one can find a maximal subset of commuting generators. For example for the group $R(3)$, no two generators commute, each commutes with itself only, and there is just one generator, usually taken as J_z, in the commuting set. On the other hand for the group $U(3)$ there are three commuting generators C_{xx}, C_{yy}, and C_{zz}. The number l of commuting generators is called the rank of the Lie group (algebra). For example the rank of $R(3)$ is 1, and that of $U(3)$ is 3. In general, for the unitary group $U(n)$ as well as the general linear group $GL(n)$ the rank is n.

The operators belonging to the commuting set can be simultaneously diagonalized. From the very definition of an irrep, we know that the group operators do not connect states belonging to two

inequivalent representations. One can choose as a basis, for a given irrep, states labeled by the eigenvalues of the commuting operators. For example for the group $R(3)$, the eigenvalue W of J_z and for $U(3)$ the numbers of oscillator quanta n_x, n_y, and n_z in the three directions can be used for labeling states of a given irrep. In general a state in the m-particle basis, can be labeled by the eigenvalues $\mathbf{W} = (W_1,\ W_2,\ \ldots, W_l)$ of the commuting operators $\{H_i,\ i = 1,\ \ldots,\ l\}$ with the simultaneous eigenfunctions U_m, where

$$H_i U_m(\mathbf{W}) = W_i U_m(\mathbf{W}) \quad (i = 1,\ \ldots,\ l). \tag{A.12}$$

The vector $\mathbf{W}$ is called the weight of the state.

One may have a group where the weight $\mathbf{W} = (W_1,\ W_2,\ \ldots, W_l)$ occurs with a multiplicity that is greater than unity. In this case, to label the basis states one finds additional operators that are functions of the infinitesimal operators of the group and that commute with $\{H_1,\ H_2,\ \ldots,\ H_l\}$. It was shown by Racah (1965) that for an r-parameter Lie group of rank l we need $[(r - 3l)/2]$ additional commuting operators. For the rotation group $R(3)$, the maximum weight $W_{max} = J$ is also the label for angular momentum eigenfunction. Also $R(3)$ is a 3-parameter Lie group of rank one, and we do not need any additional operators for labeling the states. Similarly for other groups as well, the highest weight provides group label for states of an irreducible representation. Thus an irrep for a Lie group of rank l is characterized by l quantum numbers $W_{max} = (f_1, f_2, \ldots, f_l)$.

Another important quantity is a Casimir operator. It can be shown that a Lie Group, of rank l has a set of l operators $G_i(\{X_\alpha\})$, $i = 1,\ \ldots,\ l$ called the Casimir operators which commute with all the infinitesimal operators.

$$[C, X_\alpha] = 0, \quad \alpha = 1, 2, \ldots s. \tag{A.13}$$

where s is the number of the infinitesimal operators. The maximum possible number of these so called Casimir operators in a group is given by its rank. For the different groups that will be discussed in the text, the rank and number of generators are listed in Table A.1. The generators of the rotation group

TABLE A.1. Rank and number of generators for different groups.

Group	number of generators	rank
SO($2N$)	$N(2N-1)$	N
SO($2N+1$)	$N(2N+1)$	N
U(N)	N^2	N
SU(N)	N^2-1	$N-1$

in 3 dimensions, $SO(3)$, for example, are given by the three components of the angular momentum L_x, L_y, and L_z and the Casimir operator is $L^2 = L_x^2 + L_y^2 + L_z^2$.

A.3 Young diagrams

In this appendix we assume that we are given the set of d functions of k particles distributed over N single-particle orbits. The irreducible representations may be put in one-to-one correspondence with partitions $[f] = [f_1 f_2 \dots f_s]$ such that $f_1 \geq f_2 \geq \dots \geq f_s \geq 0$ are all integers, with $f_1 + f_2 + \dots + f_s = k$. Each partition can be represented by a so-called Young shape of s rows consisting of f_1 squares in the first row, f_2 squares in the second row, and so on [89]. As an example, the group S_3 has three partitions [3], [21], and [111], which characterize the irreps. The corresponding Young shapes are given in Fig. A.1.

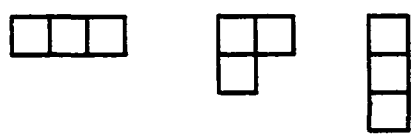

FIGURE A.1. The corresponding Young shapes for the three partitions of the group S_3.

The dimensionality of the representation is given simply by the number of ways the numbers $1, 2, \dots, k$ can be placed into the squares of the Young pattern so that they form an increasing sequence in both rows and columns. This set of numbered patterns can be used to label the various functions of an irreducible representation. Thus in the example for S_3 (see Fig. A.1) there are two one-dimensional irreducible representations, the first [3] and the third [111] irreps, and one two-dimensional irrep, [21].

A Young diagram becomes a Young tableau when particle labels are inserted into the squares. For this labeling the numbers in each row have to increase from left to right and from top to bottom. The dimension $d_{[f]}(S_k)$ of an irrep $[f_1 f_2 \dots f_s]$ of S_k, that is the number of Young tableaux possible for a specific Young diagram, is then given by

$$d_{[f_1,f_2,\dots f_s]}(S_k) = \frac{k!}{\prod_{i=1}^{s}(l_i!)} \prod_{i<j\leq s} (l_i - l_j), \tag{A.14}$$

where $l_i = f_i + s - i$.

A.4 Outer Product and Littlewood's Rules

In building up the total configuration space of protons and neutrons, it is useful to associate a Young shape for protons and one for neutrons and take their direct product. We use here an "outer product" of two representations. This is the same as finding out the possible representations when we multiply a representation $[f]$ of k_1 particles with a representation $[g]$ of k_2 particles. The representation $[f]$ is a tensor of symmetry $[f]$ under S_{k_1} and $[g]$ is a tensor of symmetry $[g]$ under S_{k_2}. When we multiply them we ask for symmetry under $S_{k_1+k_2}$. This product of two tensors for different sets of particles is called an outer product. The total number of functions in the outer product representation $[f] \otimes [g]$ of $S_{k_1+k_2}$ is the product of the number of ways of dividing $k_1 + k_2$ particles into two parts having k_1 and k_2 particles, respectively, with the number of possible functions $\psi[f]$ and $\psi[g]$ of the respective parts, i.e., d_1 and d_2.

The outer product must now be resolved into irreducible representations $[h]$ of $S_{k_1+k_2}$, which we write schematically by the equation

$$[f] \otimes [g] = \sum_h n_h [h], \tag{A.15}$$

where n_h is an integer giving the number of times the representation [h] appears in the resolution. The allowed resulting symmetries are given by the Littlewood's rules [89].

Littlewood's Rules:

1. We have Young shapes for $[f]$ and $[g]$.

2. Fill shape $[g]$ with α's in the first row, β's in the second row, and so on.

3. Add squares labeled α to $[f]$ in such a way that (a) no two letters of the same kind ($\alpha\beta$...) are in the same column, and (b) at every stage of the procedure a standard tableau is maintained.

4. Now add squares labeled β to $[f]$ with the restriction that at no stage should the total number of β's exceed the total number of α's counting from right to left and downwards.

As an application of these rules, we give an example from Ref. [89]. Let $[f] = [22]$ and $[g] = [21]$. By applying the Littlewood's rules we will obtain the irreducible representations according to the group S_7.

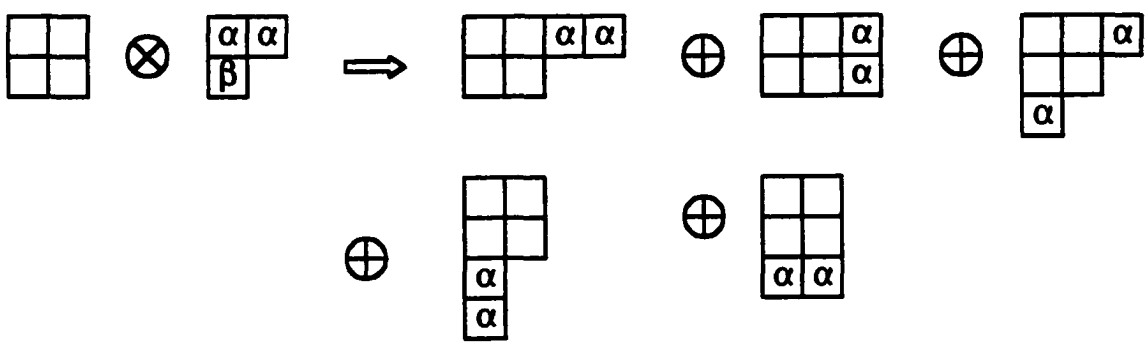

FIGURE A.2. Application of Littlewood's rules to the outer product $[22] \times [21]$, first step.

Addition of two α's is indicated in Fig. A.2. The second and fourth diagrams are not allowed because we have two α's in the same column. Adding β and following the third and fourth rules we get

$$[22] \times [21] = [43] + [421] + [331] + [322] + [3211] + [2221]. \tag{A.16}$$

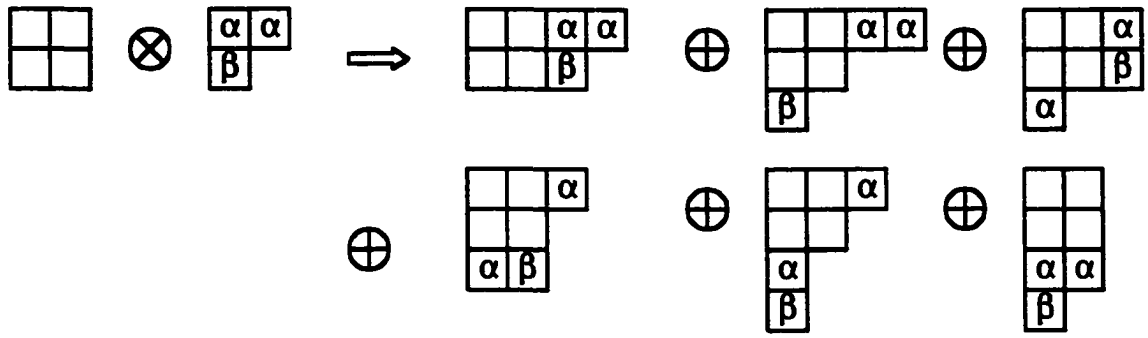

FIGURE A.3. Application of Littlewood's rules to the outer product [22] × [21], second step.

According with eq. (A.3), the dimension d_1 of [22] of S_4 is 2, and the dimension d_2 of [21] of S_3 is 2. Dimensionalities on the right-hand side are

$$14 + 35 + 21 + 21 + 35 + 14 = 140. \tag{A.17}$$

A.5 Wigner-Eckart Theorem

This section gives a review of the Wigner-Eckart theorem from the point of view of Quantum Mechanics [100] and Nuclear Physics [62], and for SU(3)-tensor operators [35]. The operators used in quantum mechanics that relate to observables can be classified according to their transformation properties, such that they are called scalar, vector, or tensor of rank k operators. If we consider the general state vector $|\psi\rangle$, under a rotation (characterized by the rotation operator U_R), the new state vector will be given by $|\psi'\rangle$, via

$$|\psi'\rangle = U_R|\psi\rangle. \tag{A.18}$$

The operator $\mathbf{A}(A_i)$ is now called a vector operator if the matrix elements transform as the components of a vector, i.e.,

$$\begin{aligned} \langle\psi'|A_i|\psi'\rangle &= \sum_j R_{i,j}\langle\psi|A_j|\psi\rangle, \text{ or} \\ \langle\psi|U_R^\dagger A_i U_R|\psi\rangle &= \sum_j R_{i,j}\langle\psi|A_j|\psi\rangle. \end{aligned} \tag{A.19}$$

Formally, for any vector $|\psi\rangle$, this can be rewritten as:

$$U_R^+ A_i U_R = \sum_j R_{i,j} A_j. \tag{A.20}$$

The $2k+1$ components $T_\kappa^{(k')}$, of a spherical tensor operator transform according to the spherical harmonics of rank k,

$$T_\kappa^{(k)\prime} = U_R T_\kappa^{(k)} U_R^+ = \sum_{\kappa'} D^{(k)}_{\kappa',\kappa}(R) T_{\kappa'}^{(k)}. \tag{A.21}$$

In calculating the matrix elements of a spherical tensor operator components $T_\kappa^{(k)}$, the Wigner-Eckart theorem allows a separation in the part that only depends on the projection quantum numbers (called the geometric part) and another part that depends on, e.g., the radial properties (and angular momentum properties) of the operator and of the state vectors (Eckart 1930).

The Wigner-Eckart Theorem. The matrix elements of tensor operators with respect to angular-momentum eigenstates satisfy:

$$\langle \alpha' j' m' | T_\kappa^{(k)} | \alpha j m \rangle = (j)^{-1} (-1)^{2k} \langle j' m', k\kappa | j m \rangle \langle \alpha' j' || T_\kappa^{(k)} || \alpha j \rangle. \tag{A.22}$$

The matrix element is written as a product of two factors. The first factor is a Clebsch-Gordan coefficient for adding j and k to get j'. It depends only on the geometry, that is, the way the system is oriented with respect to the $z-$axis. The latter, the double-bar matrix element, is called the *reduced* matrix element and is independent of m, m', and q, which specify the orientation of the physical system. The symbol (j) is a shorthand notation for $(2j+1)^{1/2}$.

This procedure can be generalized for the SU(3) case where the matrix element of a SU(3) irreducible tensor operator can be written as the product of a SU(3) Clebsch-Gordan coefficient and a so-called triple barred reduced matrix element [35]. For the SU(3) $\supset$ SU(2) chain, the Wigner-Eckart theorem takes the form

$$\langle (\lambda_3, \mu_3) \kappa_3 l_3 m_3 \,|\, T^{(\lambda_2,\mu_2)\kappa_2 l_2 m_2} \,|\, (\lambda_1, \mu_1)\, \kappa_1 l_1 m_1 \rangle$$

$$
\begin{aligned}
&= \sum_{\rho} \langle (\lambda_1,\mu_1)\,\kappa_1 l_1 m_1; (\lambda_2,\mu_2)\,\kappa_2 l_2 m_2 | (\lambda,\mu)\kappa_3 l_3 m_3 \rangle_\rho \\
&\quad \times \langle (\lambda_3,\mu_3) \,|||\, T^{(\lambda_2,\mu_2)} \,|||\, (\lambda_1,\mu_1) \rangle_\rho \\
&= \sum_{\rho} \langle l_1 m_1,\, l_2 m_2 \,|\, l_3 m_3 \rangle \langle (\lambda_1,\mu_1)\,\kappa_0 l_1;\, (\lambda_2,\mu_2)\,\kappa_2 l_2 || (\lambda_3,\mu_3)\,\kappa l_3 \rangle_\rho \\
&\quad \times \langle (\lambda_3,\mu_3) \,|||\, T^{(\lambda_2,\mu_2)} \,|||\, (\lambda_1,\mu_1) \rangle_\rho \,, \qquad \text{(A.23)}
\end{aligned}
$$

where the triple barred reduced matrix elements are of course independent from the chosen subgroup chain.

When an operator can be written as a direct product of two operators, each of them acting in a different space, the relation between the triple barred reduced matrix elements of two irreducible tensor operators $T^{(\lambda_t,\mu_t)}$ and $U^{(\lambda_u,\mu_u)}$ and the reduced matrix element of the coupled operator $[T^{(\lambda_t,\mu_t)} \otimes U^{(\lambda_u,\mu_u)}]^{\rho_0(\lambda_0\mu_0)}$ is [88]:

$$
\langle [(\lambda_1,\mu_1) \otimes (\lambda_2,\mu_2)]^{\rho(\lambda,\mu)} |||[T^{(\lambda_t,\mu_t)} \otimes U^{(\lambda_u,\mu_u)}]^{\rho_0(\lambda_0,\mu_0)} |||[(\lambda_1',\mu_1') \otimes (\lambda_2',\mu_2')]^{\rho'(\lambda',\mu')} \rangle_{\tilde{\rho}}
$$

$$
= \sum_{\rho_1\rho_2} \left\{ \begin{array}{cccc} (\lambda_1',\mu_1') & (\lambda_t,\mu_t) & (\lambda_1,\mu_1) & \rho_1 \\ (\lambda_2',\mu_2') & (\lambda_u,\mu_u) & (\lambda_2,\mu_2) & \rho_2 \\ (\lambda',\mu') & (\lambda_0,\mu_0) & (\lambda,\mu) & \tilde{\rho} \\ \rho' & \rho_0 & \rho & \end{array} \right\}
$$

$$
\langle (\lambda_1,\mu_1) |||T^{(\lambda_t,\mu_t)}|||(\lambda_1',\mu_1') \rangle_{\rho_1} \langle (\lambda_2,\mu_2) |||U^{(\lambda_u,\mu_u)}|||(\lambda_2',\mu_2') \rangle_{\rho_2} \,. \qquad \text{(A.24)}
$$

A.6 The Eigenfunctions of the Harmonic Oscillator

The Schrödinger equation of the Harmonic Oscillator (HO) can be solved in various coordinate systems, which are useful in different situations. For example, in the spherical coordinates, the spin-orbit coupling is diagonal, while deformed nuclei are often treated in the cylindrical basis. Since the procedures to solve this equation are given in many quantum-mechanics textbooks [?], only the results will be given here.

The Schrödinger equation,

$$-\frac{\hbar^2}{2m}\nabla^2\psi + \frac{1}{2}m\omega^2(x^2+y^2+z^2)\psi = E\psi, \tag{A.25}$$

can be separable in Cartesian, cylindrical or spherical coordinates. In **Cartesian coordinates**, it is written as,

$$\left[-\frac{\hbar^2}{2m}\left(\frac{\partial^2}{\partial x^2}+\frac{\partial^2}{\partial y^2}+\frac{\partial^2}{\partial z^2}\right)+\frac{\omega^2}{2}(x^2+y^2+z^2)\right]\psi(x,y,z) = E\,\psi(x,y,z). \tag{A.26}$$

The Hamiltonian in this case is simply the sum of the three one-dimensional harmonic-oscillator Hamiltonians. It can be separated in three parts using separation of variables and the solution is a product of one dimensional harmonic-oscillator wave functions

$$\phi_n(\xi) = N_n e^{-\frac{1}{2}\xi^2} H_n(\xi), \quad N_n = (\sqrt{\pi}n!2^n)^{-1/2}, \xi = x\sqrt{\frac{m\omega}{\hbar}} \tag{A.27}$$

with oscillator quantum numbers n_x, n_y, and n_z,

$$\psi_{n_x,n_y,n_z}(x,y,z) = \phi_{n_x}(x)\,\phi_{n_y}(y)\,\phi_{n_z}(z). \tag{A.28}$$

The eigenvalues of this Hamiltonian are given by:

$$E_{n_x n_y n_z} = \hbar\omega(n_x+n_y+n_z+3/2). \tag{A.29}$$

All the states with principal quantum numbers $N = n_x + n_y + n_z$ are degenerate. The $H_n(\xi)$ are Hermite polynomials, the first few of which are

$$H_0(\xi) = 1, \quad H_1(\xi) = 2\xi, \quad H_2(\xi) = -2+4\xi^2,$$
$$H_3(\xi) = -12\xi + 8\xi^3, \quad H_4(\xi) = 12 - 48\xi^2 + 16\xi^4. \tag{A.30}$$

They satisfy the differential equation:

$$\frac{d^2H_n(\xi)}{d\xi^2} - 2\xi\frac{dH_n(\xi)}{d\xi} + 2nH_n(\xi) = 0 \tag{A.31}$$

and the recurrence relation:

$$\frac{dH_n(\xi)}{d\xi} = 2nH_{n-1}(\xi). \tag{A.32}$$

For more on Hermite polynomials see any Quantum Mechanics book. From the general properties of the Hermite polynomials, the parity of the basis state ψ is

$$\pi = (-1)^{n_x+n_y+n_z} = (-1)^N. \tag{A.33}$$

For a given value of N, N can be partitioned among the integers n_x, n_y, and n_z in a total of $D_N = 1/2(N+1)(N+2)$ different ways and hence the oscillator is D_N-fold degenerate.

The Schrödinger equation in **cylindrical coordinates** is :

$$\left[-\frac{\hbar^2}{2m}\left(\frac{\partial^2}{\partial z^2} + \frac{\partial^2}{\partial \rho^2} + \frac{1}{\rho}\frac{\partial}{\partial \rho} - \frac{\partial^2}{\partial \phi^2}\right) + \frac{\omega^2}{2}(z^2+\rho^2)\right]\psi(z,\rho,\phi) = E\,\psi(z,\rho,\psi). \tag{A.34}$$

The energy as a function of the quantum numbers is given by:

$$E = \hbar\omega(n_z + 2n_\rho + |\mu| + 3/2) = \hbar\omega(2n + l + 3/2), \tag{A.35}$$

where the quantum numbers n_z and n_ρ represent the numbers of "quanta" in the z-direction and in the ρ-direction, respectively. The angular momentum projection $|\mu|$ contributes to the energy because of the centrifugal potential. The eigenfunctions of the harmonic oscillator in cylindrical coordinates are given by:

$$\psi_{n_z n_\rho \mu}(z,\rho,\phi) = N\exp\left[-\frac{1}{2}k^2(z^2+\rho^2)\right] H_{n_z}(kz)\rho^{|\mu|}L_{n_\rho}^{|\mu|}(k\rho^2)e^{i\mu\phi} \tag{A.36}$$

with $L_n^{\alpha}(x)$ being the generalized Laguerre polynomials and N an unspecified normalization constant that can be determined, and $k = m\omega/\hbar$.

For the harmonic oscillator in **spherical coordinates** the complete wave functions are given by:

$$\psi_{nlm}(r,\Omega) = \sqrt{\frac{2^{n+l+2}}{n!(2n+2l+1)!!\sqrt{\pi}x_0^3}} \times \frac{r^l}{x_0^l} L_n^{l+1/2}(r^2/x_0^2) e^{i(-r^2/2x_0^2)} Y_{lm}(\Omega), \tag{A.37}$$

with $x_0 = \sqrt{\hbar/m\omega}$. The eigenenergies are determined by the principal quantum number $N = 2(n-1)+l$ as

$$E_N = \hbar\omega\left(N + \frac{3}{2}\right). \tag{A.38}$$

Each of these state is $\frac{1}{2}(N+1)(N+2)$-fold degenerate. The oscillator constant ω is usually determined from the mean square radius of a sphere

$$\langle R^2 \rangle = \frac{1}{A}\sum_{i=1}^{A}\langle r_i^2 \rangle \tag{A.39}$$

The shells of this model contains only states of the same parity given by $\pi = (-1)^l$. The angular momentum is denoted by the letters $s, p, d, f, g, \ldots$ as in atomic physics. The spectrum for the harmonic oscillator is given in Fig. A.5. With this Hamiltonian only the first three magic numbers are reproduced.

When Goeppert-Mayer and Jensen [53] included the spin-orbit force in the single-particle Hamiltonian, the phenomenological single-particle model became a viable tool in nuclear physics. The additional term in the single-particle potential is

$$C\,\hat{l}\cdot\hat{s}, \tag{A.40}$$

and the splitting between the two levels with $j = l \pm \frac{1}{2}$ is given by:

$$E_{j=l+1/2} - E_{j=l-1/2} = C\,\hbar^2(l+\frac{1}{2}). \tag{A.41}$$

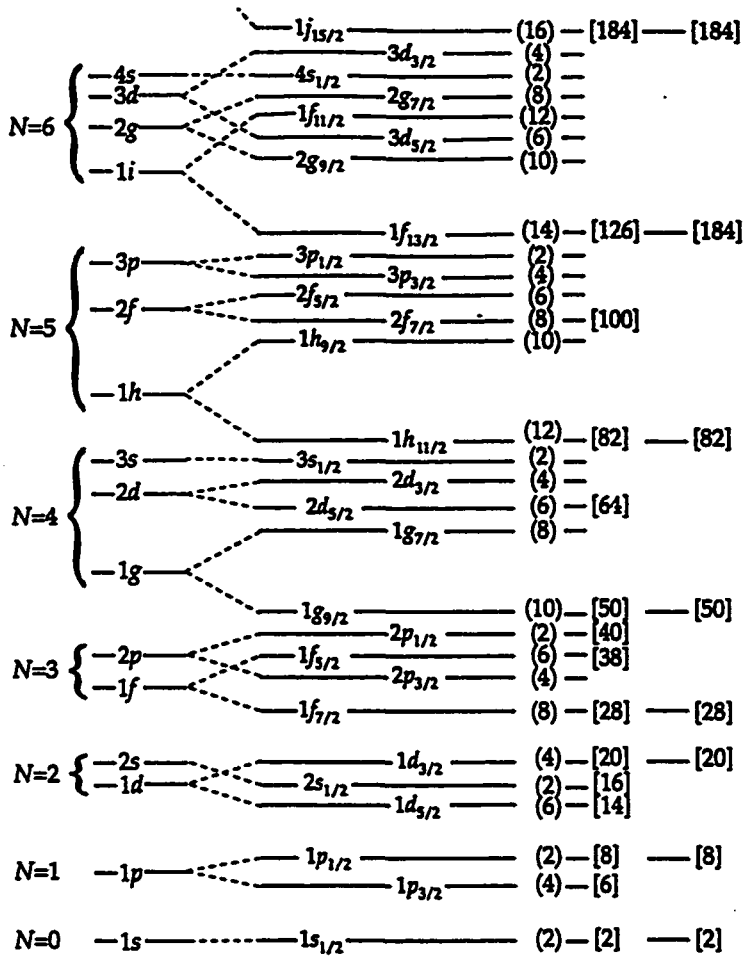

FIGURE A.4. The spectra for harmonic oscillator (far left), and harmonic oscillator plus spin-orbit coupling (right). The number of particles in each level and the total number are indicated in the right side of the states. On the extreme right the magic numbers corresponding to major shell closures are also given. Taken from [56].

Since experimentally one finds the state with $j = l + 1/2$ lower in energy, the spin-orbit coupling must have a negative sign. The typical values for $|C|$ are in the range of 0.3 to 0.6 $MeV/\hbar^2$. The spectrum for the harmonic oscillator with spin-orbit coupling is shown in Fig. A.4. The levels are labeled by the radial quantum number n, orbital angular momentum l, and total angular momentum j, as nlj. Each of these states is degenerate $2j+1$-fold with projection $\Omega = -j, \ldots, +j$. By including the spin-orbit coupling the magic numbers are correctly described.

A.7 The Deformed Shell Model

In this subsection a short review of the Deformed Shell Model is given from Ring and Schuck [96], and Greiner and Maruhn [56]. In order to apply the phenomenological shell model to deformed nuclear shapes, S. G. Nilsson [86] used a harmonic oscillator potential with different oscillator constants in the different spatial directions:

$$V(r) = \frac{m}{2}(\omega_x^2\, x^2 + \omega_y^2\, y^2 + \omega_z^2\, z^2) \tag{A.42}$$

This version of the model is often refereed to as the Nilsson model. The Hamiltonian of the model can be written as:

$$\begin{aligned} \hat{H} &= -\frac{\hbar}{2m}\nabla^2 + \frac{m\omega^2}{2}r^2 - \beta_0 m\omega_0^2 r^2 Y_{20}(\theta,\phi) \\ &\quad -\hbar\omega_0^2\kappa(2\hat{l}\cdot\hat{s} + \mu\hat{l}^2). \end{aligned} \tag{A.43}$$

The energy levels in the spherical basis, [for the spherical oscillator without spin-orbit coupling terms in the interaction], are given by:

$$E_N = \hbar\omega\left(N + \frac{3}{2}\right). \tag{A.44}$$

In the cylindrical basis they are replaced by:

$$E = \hbar\omega_z\left(n_z + \frac{1}{2}\right) + \hbar\omega_\rho\,(2n_\rho + |m| + 1) \tag{A.45}$$

where n_z is the number of quanta in the z direction, n_ρ is that of radial excitations, and m is the angular momentum projection on the z axis. For the spherical shape the levels will be grouped according to the principal quantum number N, but the behavior with the deformation depends on how much of the excitation is in the z direction. For prolate deformation, the potential becomes

shallower in this direction, and the energy contributed by n_z excitations decreases. The cylindrical quantum numbers are thus helpful in understanding the splitting for small deformations.

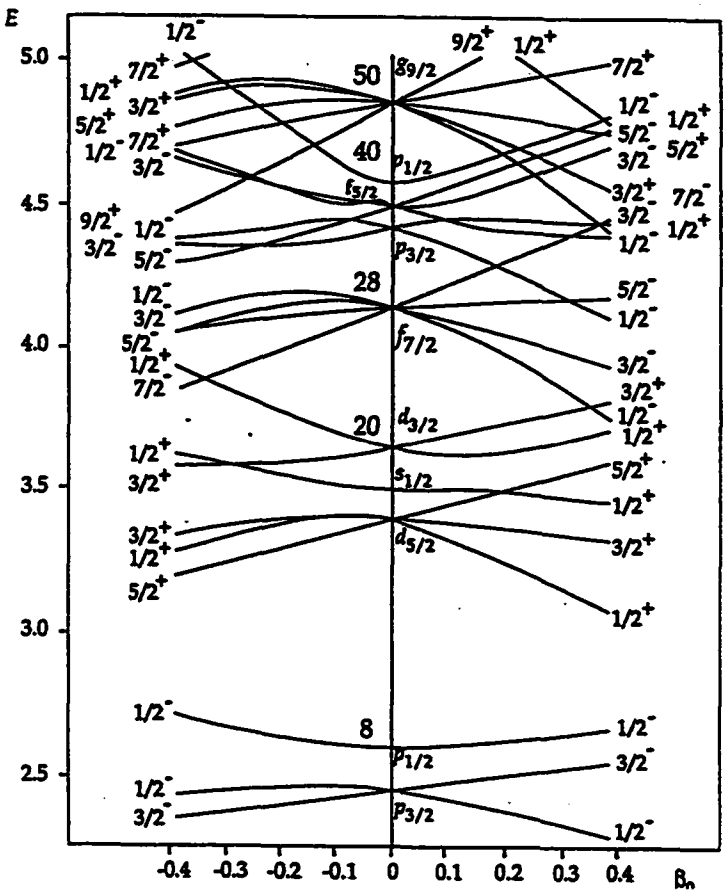

FIGURE A.5. Lowest part of the level diagram (Nilsson diagram) for the deformed shell model. The single-particle energies are plotted as functions of deformation and are given in units of $\hbar\omega_0$. The quantum numbers Ω^π for the individual levels and l_j for the spherical ones are indicated as are the magic numbers for the spherical shape. Taken from [56].

On the other hand, for very large deformation, the influence on the spin-orbit and l^2 terms becomes less important and the levels are classified according to the cylindrical quantum numbers. The single-particle levels are thus labeled with the set $\Omega^\pi[Nn_zm]$. The parity π and Ω, the projection of the total angular momentum are good quantum numbers while N, n_z, and m are only approximate and may be determined for a given level only by looking at its behavior near the spherical state.

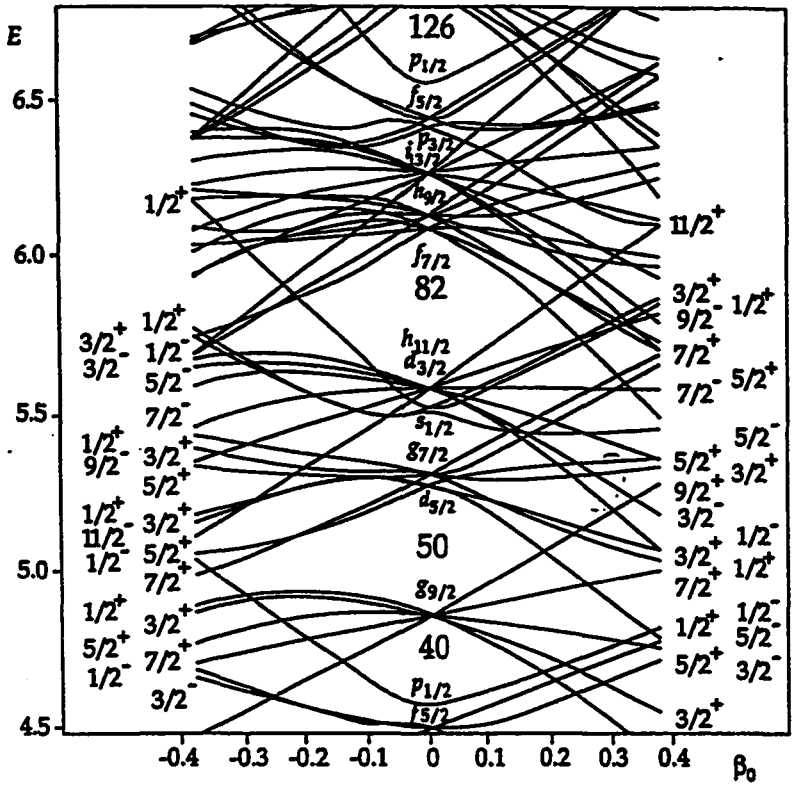

FIGURE A.6. Upper part of the Nilsson diagram. Individual quantum numbers are indicated only up to the spherical shell at magic number 82. Taken from [56].

Figures A.5 and A.6 show the resulting levels as functions of deformation. The highly degenerate spherical levels split up into the individual state pairs characterized by $\pm\Omega$ and the parity, which is determined by the orbital angular momentum in the case of a spherical shape.

Since various nuclear models are using only the nucleons in the valence shell, it is important to know exactly which levels and in what particular order they appear in the Nilsson diagram. For this reason, Fig A.7 is given to show more detail above the shell for Lead. The levels are also labeled with asymptotic quantum numbers in brackets according to $\Omega^{\pi}[Nn_z m]$, where N is spherical principal oscillator quantum number, n_z is the number of phonons in the z-direction, and m is the projection of the angular momentum. In the limit of large deformation the latter two quantum numbers become good quantum numbers.

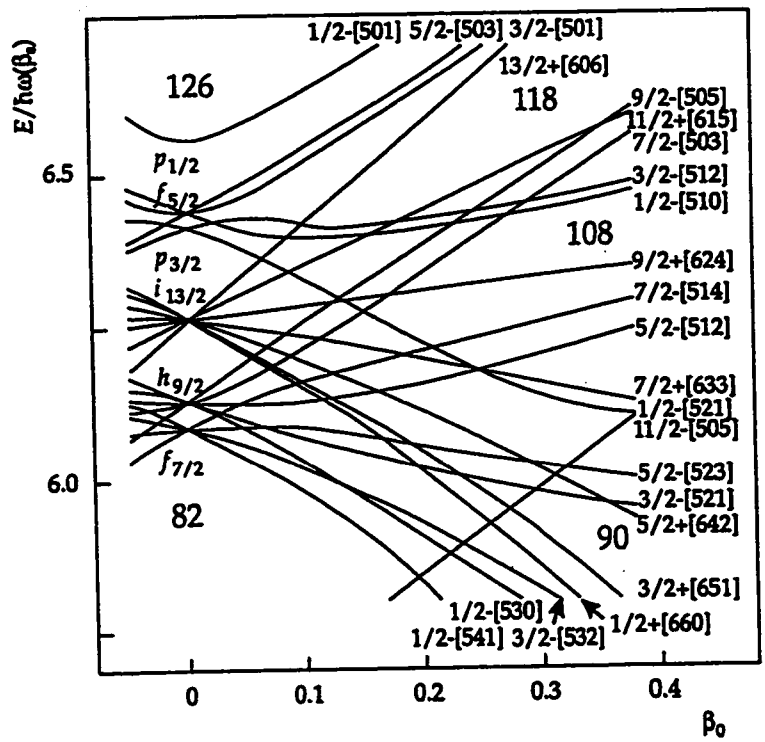

FIGURE A.7. Nilsson diagram above the shell for Lead to show more detail. Taken from [56].

Vita

Gabriela Popa was born on October 25, 1969, Corabia, Olt, Romania. She attended high school in Corabia, and studied physics at the University of Bucharest, Romania, where she received her Diploma degree in 1993. After graduation she was employed as a research-assistant at the Institute of Physics and Nuclear Engineering, Bucharest-Magurele, Romania. Her degree of Doctor of Philosophy in physics will be awarded in May of 2001.

During her graduate school years, she attended many workshops and conferences and presented her research results at the 1997 and 2000 International Symposia in Nuclear Physics at Oaxtepec, México, the Fall 1998, April 2000, and 2001 meetings of the American Physical Society, and the "Bologna 2000 - Structure of the Nucleus at the Dawn of the Century" conference, in Bologna, Italy. She was a visiting scientist at the Institute for Nuclear Theory at the University of Washington in Seattle in December 1995, and November 2000.

DOCTORAL EXAMINATION AND DISSERTATION REPORT

Candidate: Gabriela Popa

Major Field: Physics

Title of Dissertation: Shell Model Description of Normal Parity Bands In Heavy Deformed Nuclei

Approved:

Major Professor and Chairman

Dean of the Graduate School

EXAMINING COMMITTEE:

R.F. O'Connell

Date of Examination:

March 23, 2001